OCCASION

This publication has been made available to the public on the occasion of the 50th anniversary of the United Nations Industrial Development Organisation.

DISCLAIMER

FAIR USE POLICY

CONTACT

Please contact publications@unido.org for further information concerning UNIDO publications.

For more information about UNIDO, please visit us at www.unido.org

UNITED NATIONS INDUSTRIAL DEVELOPMENT ORGANIZATION
Vienna International Centre, P.O. Box 300, 1400 Vienna, Austria
Tel: (+43-1) 26026-0 · www.unido.org · unido@unido.org

Advances in Materials Technology: MONITOR

Issue Number 15 November 1989

NON-DESTRUCTIVE MATERIAL TESTING

Dear Reader,

This is number 15 of UNIDO's state-of-the-art series in the field of materials entitled Advances in Materials Technology: Monitor. This issue is devoted to one of the important problems confronting material usage: non-destructive material testing.

In each issue of this series, a selected material or group of materials is featured and an expert assessment made on the technological trends in those fields. In addition, other relevant information of interest to developing countries is provided. In this manner, over a cycle of several issues, materials relevant to developing countries could be covered and a state-of-the-art assessment made.

This issue of the Monitor covers the area of materials' testing. The detection of defects in solids is a necessary part of the control of engineering systems for their safety and successful use in practical situations. This is known variously as non-destructive testing (NDT), non-destructive evaluation (NDE), non-destructive characterization, non-destructive inspection (NDI), but also as quality control, quality technology, or as non-contact measurements. The art of non-destructive testing covers all possible measurements of properties that do not damage the solids involved, so as to determine the suitability of a part for its duty without damaging it. Test methods described in our Monitor are spread widely both in the R&D work and in manufacturing and processing of materials. The main article of this issue is written by Prof. L. Cartz, Marquette University, Milwaukee, WI, USA.

We invite our readers to share with us their knowledge and experiences related to any aspect of materials' development, production, processing and utilization. It would be a great input into strengthening a developing country's awareness to worldwide achievements in science and technology and will help them to make changes in industry and economy.

We would be grateful to receive your opinion on possible subjects for our forthcoming issues and any ideas on how to increase the value of our Monitor.

We would like to mention to our readers the possibilities of advertising in the Monitor. Advertising enables us to offer you the opportunity of giving your potential partners and customers in the developing countries more information on your products and services.

For the interest of those of our readers who may not know, UNIDO also publishes two other Monitors: Microelectronics Monitor and Genetic Engineering and Biotechnology Monitor. For those who would like to receive them, please write to the Editor, Microelectronics Monitor and Editor, Genetic Engineering and Biotechnology Monitor.

Industrial Technology Development
Division

Contents

Non-Destructive Testing; Radiography and Tomography

L. Cartz

Marquette University, Milwaukee, WI, USA

TABLE OF CONTENTS

1. Introduction

The detection of defects in solids is a necessary part of the control of engineering systems for their safe and successful use in practical situations. This is known variously as non-destructive testing (NDT), non-destructive evaluation (NDE), non-destructive characterization, non-destructive inspection (NDI), but also as quality control, quality technology, or as non-contact measurement. However, investigations go much deeper and are much vaster in scope than the detection of gross defects, and concern all aspects of the characterization of solids, their microstructure, texture, morphology, chemical constituents, physical and chemical properties, as well as their methods of preparation. There is concern for the minutest detail which may affect the future performance of the object in service, so that all properties need to be under control and all factors understood which may lead to breakdown. Nor it is appropriate to make general statements since each study and each example must be treated individually, proceeding by the use of all known properties and information about the component. Practical situations are always involved in these examinations and it is for this reason that the solid under examination should be referred to as the Engineering Component.

The art of non-destructive testing covers all possible measurements of properties that do not damage the solids involved, so as to determine the suitability of a part for its duty without damaging it. A description of the early evolution of NDT is given by Mullins (1,2) and his review still covers most of the methods presently used. The theory and practice of the established methods are well known, and it is only their use in practical situations that is developing and evolving with time. The established test methods include radiography, ultrasonics, thermography, electrical and magnetic metnods, visual testing, and microscopy. In the case of radiography, x-ray and gamma ray

are well established, but neutron, proton, and Compton scattering need also be considered and these are described in Section 2. More detail is given to recent developments than to the established aspects of the technique, and the advances in tomography are discussed in Section 3. A series of examples are listed in Section 4. Other NDT methods covering a wide spectrum are listed with references in Section 5. Organizations concerned with NDT are described in Section 6. Many of the NDT methods are highly sophisticated, yet there are a whole series of techniques that are relatively simple. One such method is visual examination, with optical aids. These methods are stressed, since it is important not to overlook the obvious in examining an engineering component. Discussions are presented in Section 6.2 concerning NDT in the developing countries.

Applications of NDT in industry concern metal, non-metals, very small to very large objects, and stationary as well as moving components. In medicine, NDT includes mammography, NMR scans, general x-radiography, and microangiography. Non-contact measurements using sensors are important in a wide range of subjects from geology, forensic studies, aerial temperatures and weather surveys, to thickness measurements and art authentication. The examinations are concerned with flaws, defects, discontinuities, imperfections, inhomogeneities, temperature and pressure variations, topography, and surface contamination.

The situation or system can vary over such a wide range that the term NDT, by itself, is not really sufficient; it is essential to add the nature of the specific product, or material. The operator of the tests is another important factor, and operator fatigue, as well as training, represents both an essential ingredient and a severe problem affecting all aspects of NDT. Since NDT is all embracing, it is most useful to have a library of as many examples

as possible, all concerned with practical situations. For this reason, a very extensive set of examples is given in Section 4, with the appropriate references.

2. Radiography

NDT by radiography has been used extensively in industry, medicine, art authentication, forensic studies, ballistics, moving parts of machinery, geological studies, as well as many other subjects. Different radiations and particle beams can be employed having different absorption characteristics in materials, and this enables the best conditions to be chosen to obtain optimum contrast in the image. X-rays, γ-rays, neutrons, protons, electrons, α-particles, and Compton scattering have all been employed. The radiography can be by Flash X-ray systems (for studies of ballistics and moving objects), laminography and tomography for views in sections of three-dimensional objects. X-ray microscopy, autoradiography and activation analyses are all closely related topics .

X-radiography is one of the earliest NDT techniques, and indeed Röntgen in 1897 reported on the observation of weights inside of a box, and of voids in a metal object (3). X-rays are generated when high energy electrons strike a solid surface (4), as synchotron radiation (5), and by very high temperature plasma (6); these methods are discussed in (7) Chapter 7. A typical x-ray system for radiography is shown in Fig. 1 when a wide range of x-ray photon energies are generated up to a maximum corresponding to the potential difference applied to the x-ray tube (4). The diverging x-ray beam is essential for radiography, though x-rays scattered by the object can remain within the diverging beam and reach the film (or detector). X-ray tubes for NDT are discussed in reference (8). These scattered x-rays will reduce the image con-

trast which is due to absorption differences within the specimen. A system of grids is sometimes employed to eliminate the scattered rays from reaching the detector; further details are given in (9).

It is useful to consider the nature of the various factors contributing to the linear absorption (attenuation) coefficient μ, defined by

$$I(x) = I(o) \exp(-\mu x) \tag{1}$$

where $I(x)$ is the x-ray intensity at a distance x, and

$$\mu = T + \tau + \sigma + k + \pi \tag{2}$$

where T is the Thomson scattering, τ is the photoelectric effect, σ is the Compton scattering consisting of $\sigma(A)$ absorption and $\sigma(S)$ scattering, k is the pair and triplet formation, and π is the photodisintegration. The relative contributions of these factors to the attenuation of the beam depend on the photon energy and absorber composition. Below 1.022 MeV, k and π are zero; τ is the dominant factor for high atomic number atoms irradiated by low energy photons; Compton scattering is important for low atomic number specimens (9). Eq. (2) can be rewritten as

$$\mu(m) = \mu/\rho = \mu(S) + \mu(\tau) \tag{3}$$

where $\mu(m)$ is the mass absorption coefficient, ρ is the density, $\mu(S)$ is the scattering component (Compton and Thomson), $\mu(\tau)$ is the photoelectric and other effects where the energy of the x-ray photon is converted into other energy forms. The regions of relative importance of $\mu(S)$ and $\mu(\tau)$ with photon

energy and atomic species are given in Fig. 2. The variation of the absorption coefficient with atomic number Z and x-ray wavelength λ are given by the approximate empirical relationships of

$$\mu/\rho \propto Z^n \propto \lambda^m \qquad (4)$$

where $n \sim 4$, and $m \sim 2.5$ except at absorption edges (4).

The detection of x-rays using films, intensifying screen, channel plates, and solid state detectors is discussed in references (7) and (9); and in an appendix of reference (10).

The quality of the radiographic image is often discussed in terms of the "unsharpness", that is the inability of a radiographic image to reproduce faithfully the boundary of a given contrast. The quality of the radiographic image is expressed also by resolving power, that is the number of lines of unit length resolved when line separation and line width are the same. This means that the unsharpness, expressed as m.m. at half-width, is inversely related to resolving power, expressed as lines per m.m.: see (9). The unsharpness of an image is made up of geometric unsharpness, screen unsharpness, and film unsharpness. The geometric unsharpness consists of effects due to the x-ray source focal spot size, motion of the object, and focal spot motion. Typical values in medical radiographs for screen unsharpness are 0.25 m.m., and film unsharpness 0.07 m.m. The geometric unsharpness depends on the focal spot size, and on the distance to the object and screen. The resulting unsharpness can be about 0.4 m.m. in typical medical radiographs.

Radiography can be contact (object close to detector), or projection (object close to x-ray source). Fresnel diffraction from sharp edges gives rise to a fringe (first maximum) at a distance x(F) in the image plane; in contact

radiography for thin specimens, about 40 μm thick, resting on the film emulsion, using x-rays of $\lambda \sim 0.1$ nm, then x(F) is about 10 nm, and similar distances apply in projection. A fringe can also occur in the image due to the total external reflection of x-rays, particularly when examination is being carried out of smooth curved surfaces (7). In general, neither Fresnel fringes nor those due to total external reflection play a role in x-radiography, and need only be considered in the case of very special x-ray microscope studies (11).

The limit of detection and contrast for projection radiography depends on the penumbra of the objects as given by simple geometry considerations from the finite size of the source. The detection limit is considered to be determined where the level of intensity between objects falls by 25%, when the resolution limit is found to be of the size of the source (11). A more precise method of consideration of the quality of radiographs uses a modulation transfer function, where Fourier analysis is used to describe the contrast boundary in the image (9). The contrast in a radiograph of an object containing different elements can be enhanced by a careful choice of λ. The contrast will depend on the differences in the mass absorption coefficients of the elements present, and these can become very large when an absorption edge change is involved. An example of this is given by Cosslett and Nixon (11) examining a specimen containing Cu and Pt, using ZnK_α radiation, which has a λ just above the K-absorption edge of Cu.

A handbook of essential x-ray and γ-ray data is given in reference (12). Reviews of methods of the interpretation and the sharpening of x-ray images are discussed in references (13), (14), and (15).

2.1 Flash Radiography

High speed flash x-radiography is carried out using an x-ray pulse of 3-100 ns duration, and Fig. 1 is a schematic of such a unit (16, 17, 18, 19). Peak voltages of 100 kV to over 2 MV are used, with a pulse generator (20). The spectrum from W or Mo targets consists of a short λ component (hard x-rays) with considerable penetration, and also longer λ radiation (soft x-rays) which can enhance the contrast of the image. At 100 kV peak voltage, the shortest λ are about 0.1 Å, and at 1 MV λ is about 0.01 Å; this is derived from λ Å = 12.4/V kV (4). Examples of Flash Radiography NDT are listed in Table III

2.2 γ-Radiography

γ-rays are emitted by many radioactive (RA) isotopes which can be used as γ-sources for radiography; γ-rays are x-rays of very high energy from RA sources. Some of the RA isotopes most frequently used are listed in Table I (21, 22, 23). The advantages of RA x-ray sources are relatively small size, low cost, independent of electricity and H_2O supplies, and can be monochromatic. The disadvantages are low intensity levels requiring long exposures, and the short life of the RA isotopes can require frequent replacement. Moreover, substantial shielding must be provided on a permanent basis when using RA sources. Examples of γ-ray NDT are given in Table III

2.3 Neutron Radiography

Neutron radiography complements x-radiography since the absorption characteristics are vastly different. Thus, while x-rays are more heavily absorbed by elements of high atomic number, neutron absorption varies

in an apparent random manner with atomic number so that hydrogen has one of the highest neutron absorption coefficients. Neutron radiography provides much more contrast for organic materials, and also for elements of neighboring atomic number; x-radiography is not suitable for observations of such materials. An example often presented is that of a thin wax string encased in a Pb block of thickness of 2", when the neutron radiograph reveals the presence of the string.

Neutrons are usually classified by energy as cold ($< 10^{-2}$ eV), thermal (< 0.3 eV), epithermal ($< 10^{4}$ eV), and fast (10-20 MeV). Thermal neutrons undergo capture by a nucleus to form a different nucleus; this is the basis of "Neutron Activation Analysis", to be discussed later. Fast neutrons have had very limited use for radiography to date.

Sources of neutrons are atomic reactors, spallation sources, and from RA isotopes. Lists of suitable RA isotopes and their characteristics are listed in (24, V.1, Chapt. 9). A portable neutron radiography system using Cf(252) is described in (25, Chapt. 7). This system is about the same size as a small portable x-ray system. The half-life of Cf(252) is 2.65 years, average neutron energy 2.3 MeV, giving a neutron yield of about 10^{12} neutron/second/gram; γ-rays are also present from the RA source. Thermal neutrons can be detected by a photographic method furnished with a converted screen converting neutrons to α, β, or γ rays. The screen can provide prompt emissions for direct exposures, though γ-rays from the source will be a problem since they affect the photographic film. The presence of γ-rays can be overcome, by using a transfer exposure method; the converter screen is exposed to the neutron beam, becoming radioactive, and is then transferred to a cassette and exposure of film (26).

In a typical direct exposure method, Cd screens are placed both in front of and behind the film, and a recommended combination is a front Cd screen 250 μm thick, and a back Cd screen 500 μm thick. A discussion of the merits of different types of converter screens is given in (26). Examples of neutron radiography are given in Table III.

2.4 Proton Radiography

The use of protons in radiography has been very limited and an extensive discussion of the method is given in (27). The great advantage of this technique is that very small density changes can be detected under suitable conditions, much smaller than for other radiations. Transmission of the monoenergetic proton beam through an object remains approximately constant for about 90% of the trajectory, after which the transmission rapidly drops to zero. It is during this last stage that a small variation in density can have a pronounced effect on transmission. Density changes as little as 0.05% can be detected. The protons can be detected by photographic or polaroid film, and measurements have been made with proton beams of several hundred MeV. Different procedures can be followed using proton absorption, proton scattering, or proton activation autoradiography (27). Applications include thickness measurements with accuracies possible of 2×10^{-3}%, the examination of welded Al sheets of 1/2 mm thickness, of foliage, and of biological specimens. Other examples are listed in Table III.

2.5 Activation Analysis

Elemental analysis of an object can be carried out by activation analysis (AA). Thermal neutron, γ, proton, and deuteron radiations in-

duce nuclear reactions to occur followed by the emission of γ-rays (28). The γ-rays can be detected using Ge (Li) semiconductor devices. The emitted γ-spectra, half-life of the radioactivity, and the type of radiation emitted can be used to identify the elements present (29, 30). In neutron activation analysis (NAA), neutrons are used to induce radiative capture reactions (n,γ), (n,p), (n,α), or (n,2n). Typical nuclear reactions are $Na^{23}(n,\gamma)Na^{24}$, $Al^{27}(n,p)Mg^{27}$, $P^{31}(n,\alpha)Al^{27}$, and $Cl^{35}(n,2n)Cl^{34}$. Quantitative analysis can be undertaken from the induced radioactivity, usually carried out by comparison with standards. Minimum amounts of elements that can be detected by NAA are listed in Table II.

For archeological purposes, the authenticity of ancient coins has been extensively studied by AA (29, 31, 32). One example uses the fact that the Ag coins are contaminated by Au and that, up to the 6th Century A.D., there was up to 1% of Au impurity in Ag coins. Subsequently, with improved methods of refinement, Ag coins contain much less Au. The γ-spectra from coins after irradiation by protons of energy 30 MeV, permit the Au concentration to be determined, which can be used to date the coins.

The age and provenance of oil paintings can be determined by AA. White lead $2PbCO_3 . Pb(OH)_2$, has been used in paintings throughout the ages, and the Pb purity has improved with the refinement process. During refinement, some of the Ra(226) from the U decay series, is removed, particularly in developments since the 18th Century. This means that the relative amounts of Ra(226), Pb(210), and Po(210) (of the U decay series) can be used to determine the age of paint specimens (33).

It is often important to determine the composition at great depths below the earth's surface. This can be carried out using a drill-hole,

typically 4" in diameter. A compact source of neutrons is inserted with a particle counter shielded from the source. The source of neutrons may consist of an α-particle emitter mixed with Be powder when a (α,n) reaction occurs. The neutrons activate the minerals and the γ-spectra is measured by the counter. Rocks bearing Fe have been identified by their characteristic γ-ray spectra (35).

Forensic studies have been carried out on the bullets fired in the assassination of President J.F. Kennedy (36). NAA showed similarities in the Ag and Sb content of several of the bullets found at the scene.

2.6 Shadow Autoradiography

A radioactive specimen in contact with a photographic emulsion will produce an image, and this technique, autoradiography, is used extensively to examine biological specimens, generally deliberately doped with a RA isotope. The RA isotope can be an α-emitter (Pu), or a β-emitter [I(131), Ru(106), Sr(90), and P(32)]. In Shadow Autoradiography, a preliminary shadowing of the specimen is carried out by a metal coating. Specimens examined by this technique are very diverse and include human skin and sputum, sheep thyroid, hung tissue, plant leaves, as well as radioactive powders (22, 30, 37).

2.7 Microangiography

Microangiography is the study by contact or projection x-radiography of the microcirculatory system of animals and humans, using the injection of an x-ray opaque solution. A colloidal solution of Ba, of particles sizes less than 0.5 μm, is typically used. Systems examined include the human eye, brain, and spinal cord (7, 37).

2.8 Thickness Measurements

Control of thickness during the production of objects is a desirable feature of quality control technology. Thickness can be measured by absorption or by back-scattering techniques of x-rays, γ-rays, α- or β-rays, or by x-ray fluorescence (22, 30). In the x-ray gauge, the absorption of a beam of x-rays is used to determine thickness of an object of known composition. A typical example is the use of additives in paper, such as the pigment kaolinite clay ($Al_2O_3 . 2SiO_2 . 2H_2O$) which has been controlled using the attenuation of a monochromatic x-ray beam (38). Similarly, the porosity of materials can be measured (39) as well as the observation of steam voids in water (40).

In the case of RA specimens, the absorption of the γ-rays emitted by the specimen itself can be used to control the thickness. An example of this, is the loading of U(235) reactor fuel elements, monitored by the γ-rays (184 keV) emitted by the U(235) specimen itself (41). The thickness of thin foils has been measured using a beam of α-particles (22) using a RA source which emits α-particles with a range of about 3.4 cm in air. The sensitivity can be adjusted to detect small changes in thickness of about 1%. A beam of β-particles has been used to determine the thickness of foils from rolling mills of Al and of steel, and in another use, to control the tobacco content of cigarettes; a radioactive isotope Sr(90) is used, which emits β-rays of energies up to about 1.35 MeV. There is an empirical relationship (22, 42) relating density, ρ, specimen thickness t, to the energy of the β-ray E_M MeV, where

$$\rho t = 0.45\ E_M - 0.16. \qquad (6)$$

The thickness of coatings on substrates can be measured using the back-scattering of x-rays, γ-rays, or β-rays. The sensitivity depends on the difference in atomic number between the substrate and coating materials (22). Typical measurements are of Sn, Zn, Cr, or brass coatings on steel, paint, or lacquer on metallic surfaces, rubber or plastics on calendering rolls, Se layers or Al, Ba coatings on photographic paper, plastic coatings on wires, glaze on porcelain. In the case of Sn plating on steel, the coatings can be controlled to about 10^{-6} cm, that is about 0.3 mg/cm^2.

X-ray fluorescence (30) has also been used to estimate surface conditions, and this is appropriate for elements of high atomic number when fluorescent yield is more important than the production of Auger electrons. Fluorescence is induced in the substrate and the reduction in intensity of the fluorescent beam leads to a calculated value of the thickness of the surface coating. When measurements are carried out in air, the longer fluorescent x-ray wavelengths are absorbed; the limit in air is the fluorescent radiation from Ti (Z = 22 with K_αx-rays, λ = 2.75 Å), when a path in air of about 10 cm will reduce the x-ray intensity by about 50%. Examples of fluorescent measurements of thickness are silver plating on Cu; Mo radiation (Mo $K_\alpha\lambda$ = 0.71 Å) is used which causes the Cu to fluorescence. In deriving the thickness of the Ag plating, allowance has to be made for the absorption in the coating of the incoming MoK_α x-radiation, as well as the attenuation of the CuK_α fluorescent radiation traversing the coating (4). Another application concerns the thickness of Zr cladding (about 0.01 cm thick) on U core nuclear fuel pins of diameter of about 0.3 cm; x-rays from a W target at 50 kV were used to excite

the ULα (λ = 0.911 Å). This enabled the identification of regions where the Zr cladding was less than 0.0075 cm thick (30, 43).

Autoradiography can also be used to measure coating thicknesses, and an example of this is the use of a flat U source on which sheets of Al, Zr, or stainless steel can be placed. The β-radiation of energies up to 2 MeV traverse the sheets, leading to accuracies of about 5% in thicknesses of metal sheets of about 0.5 mm (22, 44).

2.9 Other X-ray Methods

There are several other x-ray techniques used in the testing of solids. X-ray microscopy, or micro-focal radiography, is projection x-radiography using an x-ray source having a very fine spot size (7, 11, 45). These special x-ray generators are reviewed in Chapter 1 of reference (7). X-ray focal spot sizes down to 50 μm diameter have been obtained by special focusing techniques at 40-100 kV, with a target loading of 1 mA. This is achieved in metal-ceramic x-ray tubes with electrostatic focusing.

Various studies are in progress on x-ray optical systems. These are reviewed in references (46) and (47). Direct viewing of x-ray images can be carried out by fluoroscopy, using intensifiers of the x-ray image; these methods are reviewed in references (9) and (30).

X-ray topography is reviewed in references (34) and (48); single crystals can be examined to display dislocations, stacking faults, twinning, lattice distortions. Polycrystalline aggregates can be examined for strains, surface relief, and texture. Monochromatic x-radiation must be employed, and exposures are long, except when synchroton radiation and image intensifiers are employed.

Residual stress NDT measurements can be undertaken of polycrystalline surface layers by x-ray diffraction and the technique is reviewed in reference (49) and the principles discussed in reference (4). These measurements are very delicate, time consuming, and require extreme precision.

3. Tomography

Tomography is literally, "the picture of a slice." The differences between radiography and tomography are illustrated in Figure 3. In conventional radiography by transmission, the contrast of a defect is due to absorption differences along the total path that the x-ray traverses, as shown in Figure 3(a), and there is no attempt to determine the distance along that path of the position of the defect. Conventional radiography is by shadow projection. The position of the defect is revealed more precisely if scattered x-rays are used; see Figure 3(b). In Scattered Radiography, the region under view in the object is defined by the line of vision of the detector; this is the case using Compton scattering. Another procedure uses special motions in transmission to blur all of the object planes except the one of interest; see Figure 3(c). This is known as Laminography or Motion Tomography. A further method is Reconstructive Tomography, see Figure 3(d), where all of the planes are excluded except the one of interest, and mathematical procedures are used to reconstruct the image of the plane. In Flashing Tomosynthesis, or Multi-Radiograph Tomography, the image consists of several overlapping x-radiographs. These are unscrambled optically from the multi x-ray radiograph, see Figure 4. These methods, providing data about the 3-dimensional position of defects, are now described in more detail.

3.1 Laminography

In laminography, the x-ray source, the object, and the film are moved simultaneously, so that the projection of one particular layer of the object remains stationary relative to the film. All other layers of the object project as blurred images, since they move relative to the film (30, 50, 51, 170). The object needs to remain constant throughout the exposure, which may require a high x-radiation dose, so that this procedure is not appropriate for human beings. Different levels of the object can be viewed by adjusting the particular plane of the object in synchronism with the detector plane. Specimens examined include the variations in the wall thickness of a glass bottle (51, 170), the different levels of a complex circuit board, and the interior of a stopwatch (50).

3.2 Compton (Inelastic) Imaging

This has been applied as NDT tomography to topics as varied as microporosity in plastic explosives, and to medical studies of tumors in human tissue (52, 53). In elastic or Compton scattering results from the scattering of x-rays with a loss of energy due to recoil energy transferred to electrons. The change of wavelength $\Delta\lambda$ is given by

$$\Delta\lambda \propto (1 - \cos\phi) \tag{7}$$

where ϕ is the Compton scattering angle (42). This provides for a discrimination between the incoming x-rays and the Compton scattered x-rays of lower energy. These Compton scattered x-rays permit the monitoring of the electron density and compositional change, since the image position

is defined by the small overlap volume of the incident radiation and the scattered beam; see Figure 3(b).

Compton scattering is of sufficient intensity to be detected and differentiated from the elastically scattered radiation. The use of an industrial-type (tungsten) x-ray tube operating at 200 kV provides sufficient Compton scattered x-rays to record a suitable image on film in 2 hours of an Al casting (52). The recording time can be reduced drastically by the use of a standard x-ray image intensifier with a TV monitor when a suitable image can be obtained in less than 1 second (53). The x-ray beam in the form of a diverging fan irradiates one slice of the object; a pin-hole lens permits Compton scattered rays at 90° to enter the x-ray camera and be recorded.

With this simple system, a spatial resolution of about 1 mm is obtained of the slice of the object examined. A more advanced system has been constructed, COMSCAN (53); the x-ray tube is a standard industrial type and is operated at about 65 kV. Several collimator slits are provided, around an irradiated object, and the scattered x-rays detected by an extended array of scintillation counters of $Bi_4Ge_3O_{12}$. The volume elements of the object examined are 1 mm x 1 mm x 7 mm.

In other systems, γ-rays from RA sources have been used; e.g., Co(60) (about 200 TBq) sources, providing γ-rays of energies 1.17 and 1.33 MeV, with NaI(Te) solid state detectors. The Compton scattering can be observed at any angle, so that measurements can be carried out in an object where there is only restricted access to one side of the object.

Applications of Compton scattering tomography include examination of Al car engine components, breast cancer and its spread into surrounding tissue, examination of the human skull and jaw, the explosive charge in

shells, cooling channels in aero engine turbine blades, location of Fe bars behind 4 cm thick concrete walls, examination of the Fe base of crude oil tanks, the inspection of Fe bars and voids in concrete (52, 53).

Future developments depend on the availability of high energy x-ray sources.

3.3 Flashing Tomosynthesis

Multiple-Radiograph Tomography, or Flashing Tomosynthesis (54) requires radiographs to be taken of an object from several different angles. The reconstruction of the image of a particular layer is carried out optically, and the principle of the method is illustrated in Figure 4. The first step is the formation of a multiple image taken by flashing x-radiographs of the object using a series of x-ray sources set in the same plane, and subtending different angles at the object. A multiple image is formed, which is then decoded by projecting light through the image from a series of lenses in a pattern related to that of the x-ray sources. In Figure 4(a), and object is shown consisting of a square and a circle in different layers of the object, and illumination by three sources gives rise to a complex multiple image. Three sources of light are now projected through this complex image, in such a way that one feature of the object, here the square, superimposes in the final image; see Figure 4(b). There is a background in the image due to the non-coinciding parts of the image and this noise level can be minimized by careful selection of the pattern of the x-ray sources used, as well as the diameter of the object examined. Objects up to 60 mm in diameter have been examined, giving good images using an array of 25 x-ray tubes, when depths of 15 cm

can be portrayed in planar slices. Good images have been obtained of a phantom human head, skull,and neck (54).

3.4 Reconstructive Tomography

Mathematical procedures can be used to reconstruct the desired image plane from transmission data taken along different paths within one plane of the object, see Figure 3(d). This is known as Reconstructive Tomography (RT), Computed Tomography (CT), or Computer Assisted (axial) Tomography (CAT) (see refs. 10, 55, 56, 57, 58, 59). The various mathematical procedures are known as Iterative Least-square Technique (ILST), Algebraic Reconstructive Technique (ART), and Simultaneous Iterative Reconstruction Technique (SIRT). The data used can be x-ray transmission attenuation, but also ultrasonic (59), NMR (60), neutron transmission (59), or positron annihilation (10). The data from x-ray transmission produces a Sinogram (59), where the intensities in a sinogram are proportional to the line integral of the x-ray attenuation between the source and the detector positions.

The principle of these methods is illustrated in Figure 5; see (56). The object is considered as subdivided into an array of cells as in Figure 5(a). The contributions of the i^{th} cell in the j^{th} array are considered in the observed sinogram, so that the object is replaced by an array of cells, in each of which it is required to determine the relative density of matter. Any observation will provide the effect of the sum of the i^{th} cells along the direction of the j^{th} ray. The process to do this is illustrated in Figure 5(b), which is a simplified case of how the observations can be unraveled to arrive at the original object densities. The original object and ray measurements are shown in Figure 5(b). One

method of procedure is presented schematically using additive corrections. Starting from zero in all cells, one can correct each ray sum to approach the observed values.

Practical examples of reconstructive tomography are body scans (57), mamography (by ultra sonic transmission) (59, 61), nuclear fuel bundles inside a reactor by neutron tomography using 20 neutron radiographs (59), aerospace structures by x-ray tomography (62), and turbine blades and vanes (63).

3.5 Other Tomographic Techniques

Tomography can also be carried out by:

1. Positron Annihilation Tomography; see refs. (10, 64, 65, 66)
2. Radionuclide Tomography; see ref. (10)
3. γ-ray Tomography; see ref. (10)
4. NMR; see refs. (67, 68, 69, 70, 71)
5. Ultra-sonics; see refs. (55, 72, 73, 74, 75).

4. Examples of Radiography and Tomography

A wide range of examples of NDT are listed in Table III, covering Industrial, Medical, General Interest, and Scientific subjects.

A few special interest cases are examinations of "The Statue of Liberty", "The Liberty Bell", and forensic studies on the bullets used at the "Assassination of President Kennedy". Because of the great interest of these studies, very full details have been published, and so provide very useful, fully documented examples of NDT.

During the recent renovation of the Statue of Liberty, in the harbor of New York, USA, γ-radiographic measurements were made of crucial parts of the

original steel structural framework (76). A radioactive source of 3.7×10^{12} Bq of Ir(192) was used, when 5 min. exposures were required.

The "Liberty Bell" in Philadelphia has been γ-radiographed when the famous crack could be clearly seen (76). A source of 2.5×10^{13} Bq of Co(60) was used. The large size of the bell required the radioactive source to be placed at a considerable distance of about 5 m, to provide a full size radiograph. As a consequence, long exposures of about 36 hours were required.

Forensic studies have been carried out on the bullets fired in the assassination of President J.F. Kennedy (36). NAA showed similarities in the Ag and Sb content of several of the bullets found at the scene. This fact can be used in reviewing the number of guns involved in the assassination. The article (36) describes the complete procedure for the NAA of the bullets.

Besides the examples listed in Table III, many others are given in the published proceedings of the conferences and symposia held in recent years, and many of these are listed in ref. (77). Other review references are (24, 78, 79, 80, 81, 82, 83, 84, and 85).

A useful review of all metallurgical NDT is given in ref. (86), and in ref. (77) is given an extensive discussion of all types of metallurgical processes and the appropriate NDT. Several examples of NDT during World War II are given in ref. (87).

5. Other NDT Methods

There are a very large number of methods applied as NDT, and general reviews are given in refs. (21, 23, 77, 85, 86). These many methods are listed in Table IV with references to their description and applications.

6. Organizations Concerned With NDT

6.1 International and European Organizations

Table V gives the names and addresses of organizations closely related to NDT, concerning standardization, quality control, testing of materials, as well as NDT. Other organizations deal with radiation protection; data on radiological procedures are given in refs. (12, 88, 89, 90, 171-174). The American and the International Institutes of Welding are listed, since NDT is such an important factor in the examination of welds.

Table VI lists national societies that are members of or associated with the International Committee for Non-destructive Testing (ICNDT) which is based in Columbus, Ohio, USA.

There are many organizations concerned with standards, and indeed all countries of the world are full members or correspondent members of the International Organization for Standardization (ISO), (see Table V). A recent review of standards for NDT is given in ref. (91).

6.2 NDT in Developing Countries

Many countries, both developed and developing, of the world are members of ICNDT (see Table VI), and so are in touch with developments in NDT. The education of NDT technicians is of considerable importance, since the quality of NDT is only as reliable as that of the worker; this is discussed in several papers in ref. (85). The American Society for NDT (ASNT) has published a series of study handbooks on the training of technicians; see ref. (92). Much information is given, in review form,

in reference (77) on NDT - literature, publications, societies, technical data, examples of defects, standards, and other related matters.

Many of the NDT techniques are highly sophisticated, and these have been discussed in this review. However, there are also many of the essential NDT methods that are relatively simple, extremely effective, and can be established at low cost. A few of these methods include leak testing, liquid penetrant, acoustic, radiography, visual. Introductory texts have been published on these by ASNT (92). Elementary reviews and texts are given in refs. (21, 22, and 86). Useful periodicals are published regularly on NDT, such as ref. (168 and 169). Useful handbooks on x-ray protection and related matters are published by the National Bureau of Standards, Washington, D.C., USA (see refs. 171-174).

The developing countries listed in Table VI, which adhere to the ICNDT, are in a good position to undertake NDT under the best circumstances possible, and it would be a great advantage for any country to have a national NDT society, and to participate to the fullest extent with both ICNDT. as well as with the other international organizations; ISO, IIW, RILEM (all listed in Table V).

REFERENCES

1. L. Mullins, "Evolution of NDT," [Wiley], 5, p. 205, in ref. 2, (1961).
2. E.G. Stanford, J.H. Fearon, and W.J. McGonnagle, "Progress in Applied Materials Research," [Wiley], 5, (1964), 7, (1967), 8, (1968).
3. B. Dibner, "Röntgen and the Discovery of X-rays," [F. Watts, (New York)], (1968).
4. B.D. Cullity, "Elements of X-ray Diffraction," [Addison-Wesley], 2nd Edition, (1978).
5. A. Bienenstock and H. Winick, "Synchrotron Radiation Research," Physics Today, pp. 48-58, (1983).
6. T.N. Lee, "Solar-flare and Laboratory Plasma Phenomena," Astrophysical J., 190, pp. 467-479, (1974).
7. R.V. Ely, (Editor), "Microfocal Radiography," [Academic Press], (1980).
8. W. Hartl, D. Peter, and K. Reiber, "Metal/Ceramic X-ray Tubes for NDT," Phillips Tech. Rev., 41, pp. 24-29, (1983/1984).
9. M.M. Ter-Pogossian, "The Physical Aspects of Diagnostic Radiology," [Hoeber-Medical Division, Harper and Row], (1969).
10. K. Kouris, N.M. Spyrou, and D.F. Jackson, "Imaging with Ionizing Radiations," [Surrey University Press], (1982).
11. V.E. Cosslett and W.C. Nixon, "X-ray Microscopy," [Cambridge University Press], (1960).
12. Radiological Health Handbook, [U.S. Dept. of Health, Education and Welfare, Superintendent of Documents, U.S. Government Printing Office, Washington, D.C., USA], (1970).
13. R. Halmshaw, "Industrial X-rays Sharpen Their Image," New Scientist, No. 1477, pp. 44-46, (1985).

14. J.G. Schneeman, "Industrial X-ray Interpretation," Published by American Society of Non-Destructive Testing (ASNT), (see Ref. (92)), (1968).

15. R. Halmshaw, "Industrial Radiology," Published by ASNT, (see Ref. (92).

16. M. Held, "Flash-X-radiography in Ballistics," Materials Evaluation, 43, p. 1104, (1980).

17. F. Jamet and G. Thomer, "Flash Radiography," [Elsevier], (1976).

18. L.E. Bryand, (Editor), "Flash Radiography Symposium," American Society of Nondestructive Testing, [Houston, TX], (1976).

19. E.A. Webster and A.M. Kennedy, (Editors), "1984 Flash Radiography Symposium," Amer. Soc. NDT, (1984).

20. Anonymous, "Flash Radiography," Technical Bulletin B23, [Hewlett-Packard], (1973).

21. NASA, "Nondestructive Testing," A Survey, NASA SP-5113, (1973).

22. W.J. McGonnagle, "Nondestructive Testing," [Gordon and Breach], (1961).

23. R. Halmshaw, "Nondestructive Testing," [Arnold], (1987).

24. R.S. Sharpe, "Research Techniques in Nondestructive Testing," [Academic Press], 1 (1970), (annual publication).

25. J.J. Burke and V. Weiss, (Editors), "Nondestructive Evaluation of Materials," [Plenum], (1976).

26. H. Berger, "Neutron Radiography," [Elsevier], (1965).

27. A.M. Koehler and H. Berger, "Proton Radiography," Chapt. 1 in Vol. 2 of Ref. (24).

28. I. Kaplan, "Nuclear Physics," [Addison-Wesley], (1962).

29. B. Keisch, "The Atomic Fingerprint: Neutron Activation Analysis,"[Oak Ridge: USAEC Technical Information Center], Science, 160, pp. 413-415, (1968).

30. G.L. Clark, (Editor), "Encyclopedia of X-rays and γ-rays," [Reinhold], (1963).

31. P. Meyers, Archaeometry, 11, p. 67, (1969).

32. S.T. Fleming, "Authenticity in Art,"[Institute of Physics, United Kingdom], (1975).

33. I. Perlman, F. Asaro, and H.V. Michel, "Nuclear Applications in Art and Archeology," Ann. Rev. Nucl. Sci., p. 383, (1972).

34. R.G. Rosemeier, "Characterization of Laser Materials by Real-Time X-ray Topography," Proc. Int. Conf. Lasers, pp. 112-114, (November 1984).

35. L. Ryback, and A.H. Youmans, "New Nuclear Logging Methods," Bull. Ver. Schweiz. Petrol. Geol. u-Ing., 35, p. 34, (1968).

36. V.P. Guinn, "JFK Assassination Bullet Analysis," Ann. Chem., 51, pp. 484A-492A, (1979).

37. G.L. Clark, (Editor), "Encyclopedia of Microscopy," [Reinhold], (1961).

38. H.H. Murray and W.D. Johns, "Measurement of Coating Thickness and Weight," Tappi, 44, p. 217, (1961).

39. G.L. Clark, "Porosity Measurements by Radiation Absorption," Anal. Chem., 29, p. 1539, (1957).

40. G.E. Martin and E.W. Grohse, Proc. 9th Ann. Denver Conf. X-ray Analysis, pp. 319-334, (1969).

41. G.H. Morrison and J.F. Cosgrove, "Determination U(235) by Gamma Spectrometry," Anal. Chem., 29, p.1770, (1957).

42. R.L. Sproull, "Modern Physics,"[J. Wiley], (1967).

43. P. Lublin, Norelco Reporter, 3, pp. 58-61, (1956).

44. Anonymous, "NDE of Density Measurements," Ceram. Bull., 67, p. 1869, (1988).

45. H. Kölker, P. Henze, K.A. Schwetz, and A. Lipp, "X-ray Microfocus and Dye Penetrant Techniques for Crack Detection in Ceramics," 3rd Int. Symp. Ceramic Materials for Engines, Las Vegas, [American Ceramic Society], (in print), (1988).

46. M. Howells, et al., "Soft X-ray Microscopes," Physics Today, pp. 22-32, (August 1985).

47. J.H. Underwood and D.T. Attwood, "The Renaissance of X-ray Optics," Physics Today, pp. 44-52, (1984).

48. R.N. Pangborn, "X-ray Topography," Metal Handbook, 9th Edition, Vol. 10, [American Society of Metals], (1986).

49. P.S. Prevey, "X-ray Diffraction Residual Stress Techniques," Metals Handbook, 9th Edition, vol. 10, [American Society of Metals], (1986).

50. F.A. Hasenkamp, "Radiographic Laminography," Materials Evaluation, pp. 170-180, (August 1974).

51. A. Notea, "Film-Based Industrial Tomography," NDT International, 18, pp. 179-184, (1985); 16, pp. 263-270, (1983).

52. R.S. Holt, "Compton Imaging," Endeavour, 9, pp. 97-105,(1985).

53. G. Harding, H. Strecker, and R. Tischler, "X-ray Imaging with Compton-Scatter Radiation," Phillips Technical Review, 41, pp. 46-59, (1983/1984).

54. E. Kotz, R. Linde, U. Tiemens, and H. Weiss, Phillip Technical Review, 38, pp. 338-346, (1978/1979).

55. A. Macoviski, "Medical Imaging Systems," [Prentice Hall], (1983).

56. R.A. Brooks, and C.D. Chiro, "Theory of Image Reconstruction in Computed Tomography," Radiology, 117, pp. 561-572, (1975).

57. C.L. Morgan, "Basic Principles of Computed Tomography," [University Park Press], (1983).

58. S. Takahashi, (Editor), "Illustrated Computer Tomography," [Springer-Verlag], (1983).

59. G.T. Herman, "Image Reconstruction from Projections," [Academic Press], (1980).

60. P.R. Locher, "Proton NMR Tomography," Philips Tech. Rev., 41, pp. 73-88, (1983/1984).

61. P.D. Edmonds, "Ultrasonics," [Academic Press], (1981).

62. D.J. Hagemaier, "Aerospace Radiography - The Last Three Decades," Materials Evaluation, 43, pp. 1262-1283, (1985).

63. P. Riemers, W.B. Gilboy, and J. Goebbels, "Industrial Applications of Computerized Tomography," NDT International, 17, pp. 197-207, (1984).

64. C.F. Coleman and A.E. Hughes, "Positron Annihilation," Chapt. 11 in Vol. 3 of Ref. (24).

65. Y.K. Park, J.T. Waber, and C.L. Snead, "Positron Annihilation Methods Dislocation Densities in Fe," Materials Letters, 3, pp. 181-186, (1985).

66. M.M. Ter-Pogossian, et al., "Positron-Emission Transaxial Tomograph for Nuclear Imaging," Nuclear Medicine, pp. 79-89, (January 1975).

67. Anonymous, "NMR: A Perspective on Imaging," [G.E. Publication 5485], (1984).

68. E.R. Andrew and B.S. Worthington, "NMR Imaging," Radiology of the Skull Brain, 5, T.H. Newton and D.G. Potts, (Editors), [Mosby], (1981).

69. D. Chapman and P.D. Magnus, "High Resolution NMR," [Academic Press], (1966).

70. P. Mansfield and P.G. Morris, "NMR Imaging in Biomedicine," [Academic Press], (1982).

71. E. Fukushima and S.B.W. Roeder, "Pulse NMR," [Addison-Wesley], (1981).

72. P.N.T. Wells, "Biomedical Ultrasonics," [Academic Press], (1971).

73. O.I. Babikov, "Ultrasonics and Its Industrial Applications," [Consultants Bureau], (1960).

74. A.R. Williams, "Ultrasound: Biological Effects and Potential Hazards," [Academic Press], (1983).

75. F.W. Kremkau, "Ultrapuzzles," J. Clin. Ultrasound, 6, p. 85, (1980).

76. C.M. Berntson, "Nondestructive Testing Sheds Light on Preserving America's Past," Materials Evaluation, 43, pp. 1180-1186, (1985).

77. R.S. Sharpe, et al., (Editors), "Quality Technology Handbook," 4th Edition, [Butterworth], (1984).

78. B.B. Rath, (Editor), "Novel NDE Methods for Materials," AIME Conf. Proceed., (1982).

79. C.O. Ruud and R.E. Green, (Editors), "Nondestructive Methods for Materials Property Determination," [Plenum], (1983).

80. U.S. Dept. of Commerce, NBS, Annual Technical Activities, Office of Nondestructive Evaluation:

    1981 NBSIR 83-2741

    1982 NBSIR 82-2617

    1984 NBSIR 84-2944

    1985 NBSIR 85-3187

    1988 NISTIR 88-3839

81. Anonymous, "NDE at NASA Langley," [Langley Research Center, Hampton, VA 23665, USA], Report for 1987.

82. J.F. Bussière, P. Monchalin, C.O. Ruud, and R.E. Green, (Editors), "Nondestructive Characterization of Materials II," [Plenum], (1986).

83. E.A. Ash and C.B. Scruby, (Editors), "Novel Techniques of NDE," [Royal Society, London], (1986).

84. R.C. McMaster, (Editor), "Nondestructive Testing Handbook, Vols. 1 and 2, [The Ronald Press Co., New York], (1959).

85. D.O. Thompson and D.E. Chimenti, (Editors), "Review of Progress in Quantitative Nondestructive Evaluations," [Plenum], (1985).

86. H.E. Boyer, (Editor), "Nondestructive Inspection and Quality Control," Amer. Soc. Metals Handbook, No. 11, [Metals Park, OH], 8th Edition, (1976).

87. J.G. Crowther and R. Whiddington, "Science at War," (H.M.S.O., London, U.K.), (1948).

88. Physical Aspects of Irradiation, [NBS Handbook, No. 85, Superintendent of Documents, U.S. Government Printing Office, Washington, D.C.], (March (1964).

89. Radiation Quantities and Units, [NBS Handbook, No. 84, Superintendent of Documents, U.S. Government Printing Office, Washington, D.C.], (1962).

90. Safe Handling of Radioactive Isotopes, [NBS Handbook, No. 42, Superintendent of Documents, U.S. Government Printing Office, Washington, D.C.], (1949).

91. H. Berger, (Editor), "Nondestructive Testing Standards: A Review," [ASTM, STP 624], (1976).

92. American Society for Nondestructive Testing, (ASNT), [4153 Arlingate Plaza, #28518, Columbus, OH 43228, USA].

Self Study Handbook Series -Various Handbook Series

NDT Handbooks, 1, Leak Testing, 2, Liquid Penetrant, 3, Radiography

93. D.A. Bromley, "Neutrons in Science and Technology," Physics Today, pp. 30-39, (1983).

94. J.F. Cameron and J.R. Rhodes, Nucleonics, 19, 6, 53, (1961).

95. R.Y. Parry, "Combined β and Dielectric Gauges," J. Brit. Inst. Radio Eng., 14, pp. 427-432,(1954).

96. W.J. Richards, et al., "Neutron Tomography," Materials Evaluation, 40, pp. 1263-1267, (1982).

97. A. DeVolpi, et al., "Neutron and Gamma Ray Tomography," Materials Evaluation, 40, pp. 1273-1279, (1982).

98. F.F. Hopkins, et al., "Tomographic Image Analysis," Materials Evaluation, 40, pp. 1226-1228, (1982).

99. E. Segal, et al., "Dimensional Information from Industrial Computerized Tomography," Materials Evaluation, 40, pp. 1268-1279, (1982).

100. J.Y. Park and D. Kupperman, "U.S. Inspection Pipe Welding," ANL-84-1, NUREG/CR-3894, Argonne National Laboratory.

101. W.A. Ellingson, et al., "NDT for Structural Ceramics," FTP/A 49640, (April 1986), Argonne National Laboratory; Chemical Abstracts, 109, 214823, (1988).

102. L.J. Inglehart, et al., "Thermal-wave NDT of Composites," J. Appl. Phys., 59, pp. 234-240, (1986).

103. H. Wadley, (Editor), "NDE in the Nuclear Industry," 6th Int. Conf., ASM, (1984).

104. R.B. Pipes, (Editor), "NDE and Flaw Criticality for Composite Materials," ASTM Special Technical Publication, 696, (1979).

105. E.G. Henneke and T.S. Jones, "Detection of Damage in Composite Materials by Vibro Thermography," in Ref. (104), pp. 83-95.

106. Anonymous, "High Resolution U.S. Imaging of Damage in Composite Materials," U.S. Air Force Annual Report, p. 53, (1987).

107. K. Schneider, "New Robot Seeks Cracks in Nuclear Reactors," New York Times, pp. 22-23, (January 31, 1989).

108. J. Davies, "Cars on 3D TV," Physics World, 2, pp. 22-23, (1989).

109. V.M. Malhotra, (Editor), "NDT of Concrete," American Concrete Institute (ACI), Publication SP82, (1984); "Testing Hardened Concrete NDT," ACI Monograph No. 9, (1976)

110. A. Gilardoni, "X-rays in Art," [Como, Italy], (1977).

111. E.V. Sayre, (Editor), "Materials Issues in Art and Archeology," Materials Research Soc. Symposia Proceedings, V.123, (1988).

112. W.N. McDicken, "Diagnostic Ultrasonics: Principles and Use of Instruments," [J. Wiley], (1976).

113. M. Hussey, "Basic Physics and Technology of Medical Diagnostic Ultrasound," [Elsevier], (1984).

114. F.W. Kremkau, "Diagnostic Ultrasound," [Grune and Stratton], 2nd Edition, (1984).

115. P. Biquard, "Les Ultrasons," [Presses Universitaires de France], (1951).

116. B. Carlin, "Ultrasonics," [McGraw-Hill], (1960).

117. G. Haines, "Sound Underwater," [David & Charles, London], (1974).

118. E. Meyer and E.G. Neumann, "Physical and Applied Acoustics," [Academic Press], (1972).

119. J. Hansen, "An Ear for Detail," New Scientist, pp. 148-150, (January 1983).

120. C.F. Quate, "Acoustic Microscopy," Physics Today, pp. 34-41, (August 1985).

121. A.F. Brown, "Acoustic Wave Optics," Phys. Bull., 34, pp. 473-476, (1983).

122. A.F. Brown, "Seeing with Sound," Endeavour, 35, pp. 123-128, (1976).

123. B.A. Aulk, "Acoustic Fields and Waves in Solids," Vols. 1 and 2, [Wiley], (1973).

124. A. Vary, (Conference Chairman), "Analytical U.S. in Materials Research and Testing," NASA Conference Pub. 2383, (1984).

125. J. Szilard, "Ultrasonic Testing, Non-Conventional," [J. Wiley], (1982).

126. J.H. Krautkamer, "U.S. Testing of Materials," 2nd Ed., [Springer-Verlag], (1977).

127. A. Briggs, "Introduction to Scanning Acoustic Microscopy," [Oxford Univ. Press], (1985).

128. R.J. Urick, "Principles of Under Water Sound," [McGraw-Hill], (1975).

129. L. Filipczynski, Z. Pawlowski, and J. Wehr, "Ultrasonic Methods of Testing Materials," [Butterworth], (1965).

130. M.C. Bhardwaj, "VH Frequency U.S. in ND Characterization of Materials," Ceramic Bull., 65, p. 1461, (1986).

131. G. Bradfield, "U.S. Flaw Detection in Very Large Forgings," (Ref.(2)), 7, p. 239, (1967).

132. R.W. Astheimer, "Handbook of Infrared Radiation Measurement," [Barnes Engineering Co., Stamford, CT, USA], (1983).

133. C. Martin, P. Fauchais, and A. Borie, "Detection of Adhesion Defects by Infrared Thermography," 8th World Conference NDT, Cannes, France, Paper 3A12, (1978).

134. R. Pochaczevsky, "Assessment of Back Pain," Orthopaedic Review, 12, pp. 45-58, (1983).

135. S. Staniforth, "Colour Measurement and the Conservation of Paintings." Phys. Bull., [Inst. Phys., U.K.], pp. 302-304, (July 1985).

136. J. Cohen, "Elements of Thermography for Nondestructive Testing," NBS Tech. Note 1177, (May 1983).

137. G. Gaussorgues, "La Thermographie Infrarouge," [Librairies Lavoisier, Paris], (1980).

138. H.C. Wright, "Infrared Techniques," [Clarendon Press, Oxford], (1973).

139. J.H. Richardson, "Optical MIcroscopy for the Materials Sciences," [Marcel Dekker], (1971).

140. Tolansky, "Properties of Metallic Surfaces," Inst. Metals London, Monograph, 13, (1953).

141. R. Barer, "Lecture Notes on the Use of the Microscope," [Blackwell], (1971).

142. N.H. Hartshorne and A. Stuart, "Crystals and the Polarizing Microscope," [E. Arnold, London], (1934).

143. R.G. Greaves and H. Wrighton, "Practical Microscopical Metallography," [Chapman and Hall], (1957).

144. L.C. Martin and B.K. Johnson, "Practical Microscopy," [Blackie], (1949).

145. A.F.H. Allimond, "Manual of the Polarizing Microscope," [Cooke, Troughton, and Simms, Ltd.], (1953).

146. G.K.T. Conn, "Polarizing Light in Metallurgy," [Butterworth], (1952).

147. A.S. Kuo and H.W. Liu, Chapter 17 in "Nondestructive Evaluation of Materials," J.J. Burke and V. Weiss, (Editors), [Plenum], (1979).

148. J.P. Duncan, "Non-Coherent Optical Techniques for Surface Survey," Chapt. 8 in Vol. 2, Research Techniques in NDT, (see Ref. (24)), (1971).

149. H.L. Libby, "Introduction to Electromagnetic Nondestructive Test Methods," [Wiley], (1971).

150. C. Sutton, "Magnetic Window into Bodily Functions," New Scientist, pp. 32-37, (September 1986).

151. H.L. Libby, "Inductive Thermometry and Eddy Current NDT," (see Ref. (2)), 8, p. 121, (1968).

152. E. Downham, "Vibration Monitoring," Chapt. 9 in Vol. 2 of Ref. (24).

153. E.M. Uygur, "Nondestructive Dynamic Testing," Chapt. 6 in Vol. 4 of Ref. (24).

154. C.M. Vest, "Holographic NDE: Status and Future," NBS-GCR-81-318 - Office of Nondestructive Evaluation, NBS, Dept. of Commerce, Washington, D.C. 20234.

155. T.D. Beynon, "Neutron Holography," Phys. Bull., [Inst. Phys. U.K.], 37, pp. 129-131, (1986).

156. R.K. Erf, (Editor), "Holographic NDT," [Academic Press], (1974).

157. Fulmer Tape Abrasivity Metals, [Fulmer Research Inst., Slough, Berks, England], Phys. Bull., [Inst. Phys. U.K.], 34, p. 466, (1983).

158. G. Birnbaum and G.S. White, "Laser Techniques in NDE," Chapt. 8 in Vol. 7, Nondestructive Testing, [Academic Press], R.S. Sharpe, (Editor), (1984).

159. B. Culshaw, "Fiber Optic Sensing Techniques," Chapt.6 in Vol. 7 of Ref. (24).

160. W.J. Baxter, "Exoelectron Emission from Metals," Chapt. 12 in Vol. 3 of Ref. (24).

161. J.H. Lewis and S. Blake, "Xonics Electron Radiography in Industrial NDT Application," Chapt. 7 in vol. 3 of Ref. (24).

162. D.J. McDougall, (Editor), "Thermoluminescence of Geological Materials," [Academic Press], (1968).

163. Ometron Limited, [Park Road, Chislehurst, Kent, England], (Model SPATE 8000).

164. P. Cielo, et al., "Thermoelastic Inspection of Layered Material," Materials Evaluation, 43, pp. 1111-1116, (1985).

165. D. Graham and T. Eddie, "X-ray Techniques in Art Galleries and Museums," [A. Hilger], (1985).

166. H.H. Anderson and S.T. Picraux, (Editors), "Ion Beam Analysis in the Arts and Archaeology," Nucl. Instrum. and Methods Phys. Res., B14(1), (January 1986).

167. C.R. Heiple and S.H. Carpenter, "Acoustic Emission Produced by Deformation of Metals and Alloys: A Review," J. Acoust. Emiss., 6, pp. 177-204, (1987).

168. NDT International, [Butterworth Scientific Ltd., Guildford, Surrey, United Kingdom].

169. "Materials Evaluation," Journal of American Society of Nondestructive Testing, [Clinton, Indiana]; includes reference guide.

170. D.R. Craig and M.P. Sirkis, "Simplified Apparatus for Producing Transaxial Tomograms," Materials Evaluation, pp. 20-23, (October 1978).

171. "Permissible Dose from External Sources of Ionizing Radiations," [NBS Handbook, No. 59, Superintendent of Documents, U.S. Printing Office, Washington, D.C.], (1954).

172. "X-ray Protection Designs," [NBS Handbook, No. 50, Superintendent of Documents, U.S. Printing Office, Washington, D.C.], (1952).

173. "X-ray Protection," [NBS Handbook, No. 60, Superintendent of Documents, U.S. Printing Office, Washington, D.C.], (1955).

174. "Radiological Monitoring Methods and Instruments," [NBS Handbook, No. 51, Superintendent of Documents, U.S. Printing Office, Washington, D.C.], (1952).

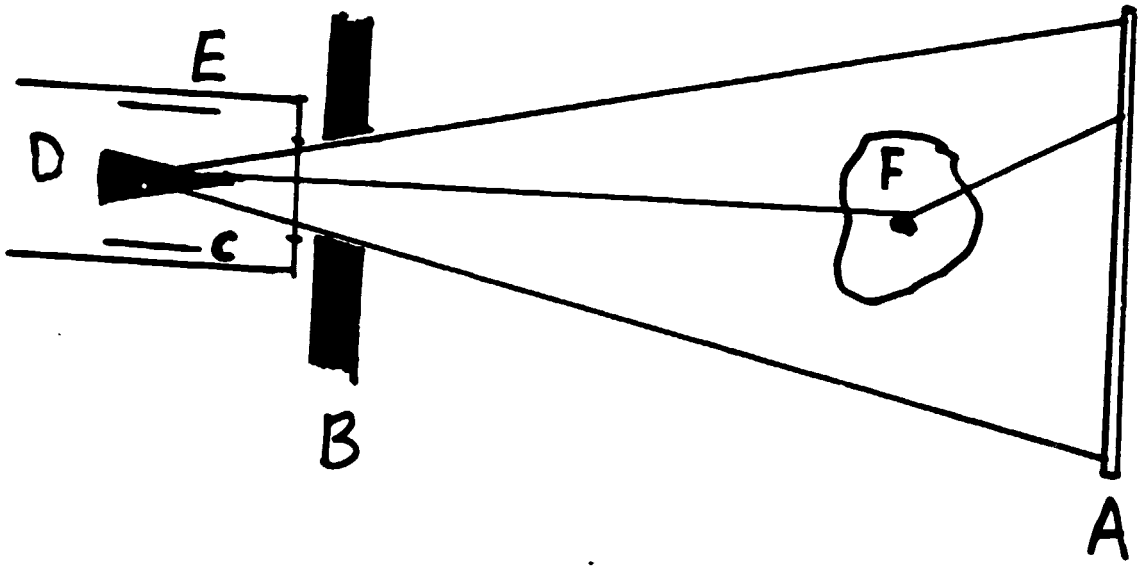

Figure 1. Schematic of X-ray Unit for Radiography. A, Detector; B, Collimator; C, Cathode; D, Target (shaped to project a small source size); E, X-ray Tube; F, object. A beam of x-rays leaves the source, D, and diverges through the defining screen, B, to the detector, A, which may consist of an intensifying screen and x-ray film. Scattered x-rays from the object, F, can attain the detector, reducing contrast in the image. The target is usually W, at a high voltage, from about 50 kV to several MV.

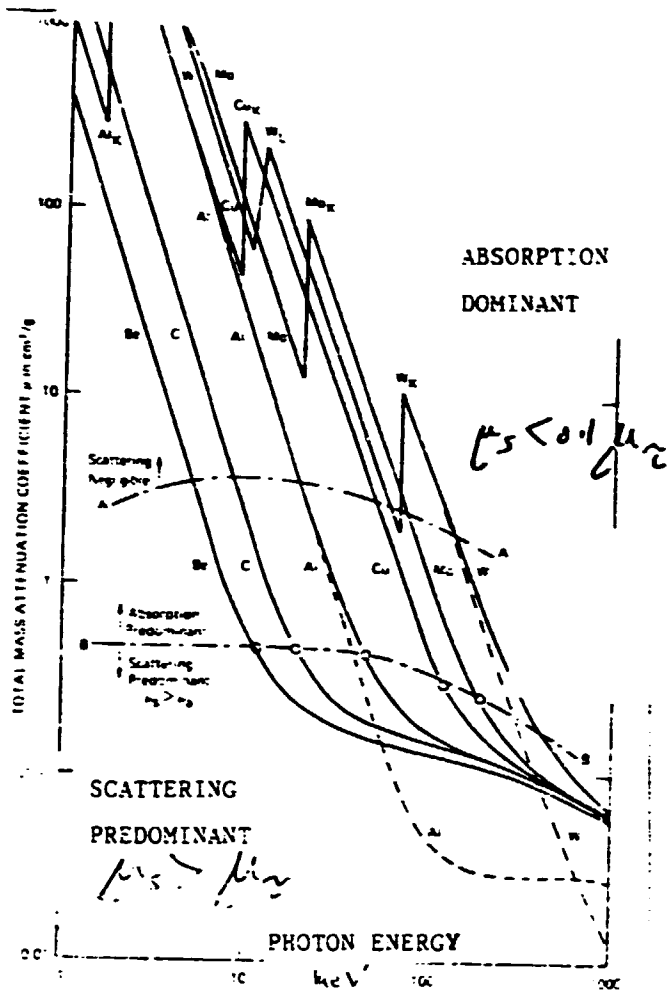

Figure 2. Absorption Processes

Relative importance of $\mu(s)$, due to all scattering processes, and $\mu(\tau)$, due to all true absorption processes, with photon energy and atomic number, where the mass absorption coefficient:

$\mu(m) = \mu(s) + \mu(\tau)$; see text, and Ref. (20).

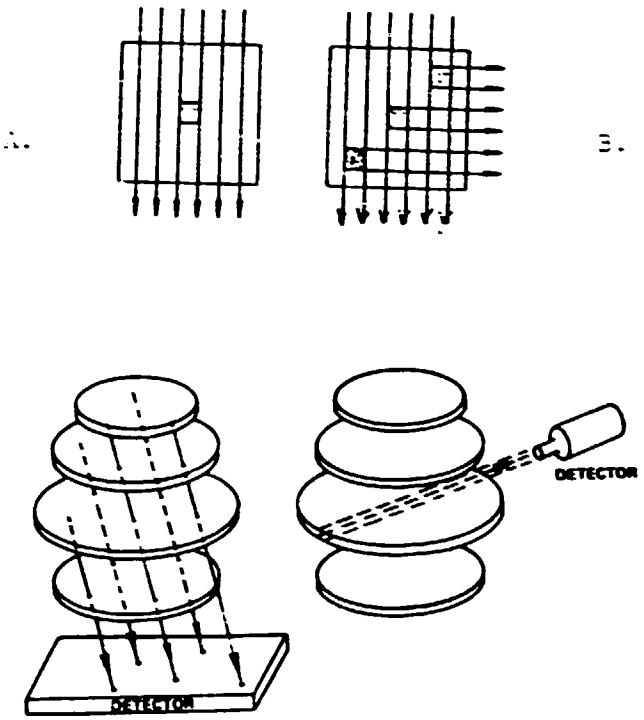

Figure 3. Diagrams Illustrating (A) Conventional Shadow Radiography by Transmission, (B) Scattered Radiography at 90° Where the Line of Vision of the Detector Will Define the Volume Under View in the Object, (C) Laminography, Where Relative Motions of Object and Detector Cause All But One Plane to be Blurred, (D) Reconstructive Tomography, Where Many Observations are Carried Out From Different Angles Within One Plane; (see Refs. 52 and 56).

A.

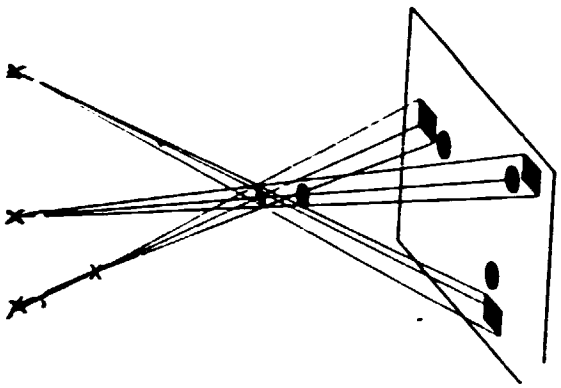

Image (1)

B.

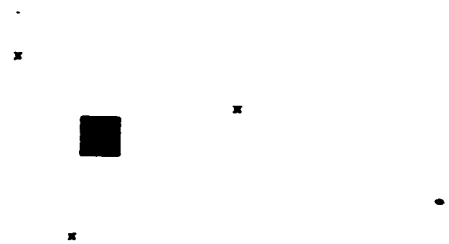

Image (2)

Figure 4. Flashing Tomosynthesis, or Multiple Radiograph Tomcgraphy

As an illustration, an object consisting of a square and a circle at different layers are illuminated by three sources resulting in a multiple image, Fig. 4A. Three light sources project image (1) so that the square part of the object is superimposed in image (2). The remainder of the image gives rise to background noise; see text and ref. '51).

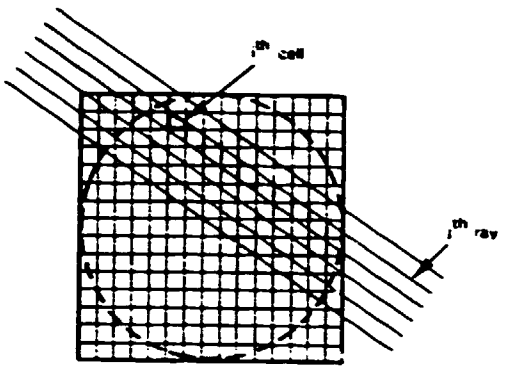

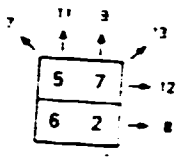

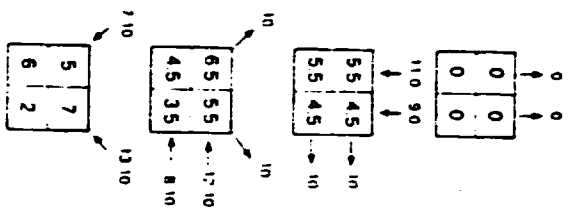

Figure 5. Illustration of Iterative Reconstruction Tomography.

A. The object is considered as an array of small volumes (voxel). The j^{th} ray sums the effects due to the voxels along its path.

B. Simple object of 4 voxel (pixel in 2D). The ray sums are given.

C. Additive Correction Scheme; see text and ref. (56).

Table I.

Radioactive Isotope	Half-Life	γ-rays (MeV)	Effective Source Size Diameter (mm)	Radioactive Source Strength $Ckg^{-1}s^{-1}Bq^{-1} \times 10^{-19}$	Steel Plate Thickness Limit (cm)
$^{60}_{27}Co$	5.3 years	1.17, 1.33	3	20	15
$^{192}_{77}Ir$	74 days	0.21-0.61	0.5	5	10
$^{169}_{70}Yb$	31 days	0.053-0.309	0.3	2	-

Radioactive Isotopes Used as Sources for γ-radiography (see Ref. (23)).

Table II.

Minimum Amounts of Some Elements Detectable by Thermal Neutron Activation Analysis, Under Normal Conditions, (see refs. 29, 30)

Element	mg	Element	mg	Element	mg
A	1	Cs	10^{2}	Ir	10^{-2}
Ag	0.1	Cu	10	K	10^{2}
Al	1	Dy	10^{-3}	Kr	10^{2}
As	10	Er	10	La	10
Au	1	Eu	10^{-2}	Mg	10
Ba	10	F	10	Mn	10^{-1}
Bi	10^{4}	Ga	1	Mo	10
Br	1	Gd	10	Na	10
Cd	100	Ge	10	Nb	1
Ce	10^{3}	Hf	10^{3}	Ni	10^{2}
Cl	1	Hg	10^{-1}	Os	10^{2}
Co	1	I	10^{-1}	P	10^{3}
Cr	10^{3}	In	10^{-2}	Pb	10^{4}

Table II, (continued)

Element	mg	Element	mg
Pd	10	Te	10
Pt	10	Ti	10^2
Rb	10	Tl	10
Re	1	V	10^{-1}
Rh	10^{-2}	W	10
S	10^4	Xe	10^2
Sb	10	Y	10^2
Sc	10^{-2}	Yb	10
Se	1	Zn	10^2
Si	10^2	Zr	10^3
Sn	10		
Sr	10		
Ta	10^2		
Tb	10^2		

Table III.

Examples of Radiography and Tomography

A. Industrial

Reference	Technique	Subject Examined
7	Projection Radiograph Microfocal X-ray Unit X-ray Microscopy	Integrated Circuit. Incomplete Interface Bonding.
93	Neutron Radiography	Combination Lock in Steel and Light Metals.
25	Neutron Radiography	Adhesive Bonded Metal Honeycomb-Plastic Structure.
25	Neutron Radiography	Explosive Train Devices. Explosive Material in Pyrotechnic Devices.
25	Neutron and X-ray Radiography	Cooling Tubes in Turbine Blades.
25	Neutron Radiography	Bolts on Aircraft Wing. Corrosion on Aircraft Wing Skin. Aircraft Fuel Tanks.
29	Neutron Activation Analysis	Traces of Metal.
35	Neutron Activation Analysis, Using Small Source.	Geological Drill-hole Analysis at Depths in the Earth's Crust.
30, 38	X-ray Gauge (Absorption)	Mass Per Unit Area of Inorganic Coatings on Paper.
39	X-ray Gauge	Porosity of Specimens.
40	X-ray Absorption	Steam Voids in H_2O.
30, 94	γ-ray Absorption	Thickness of Coatings (various)
22	γ-ray Gauge (Absorption)	Hot Steel Strip Thickness

Table III, Part A (continued)

Reference	Technique	Subject Examined
41	γ-ray Emission	Reactor Fuel U(235) Loading by Monitoring γ-radiation.
22	β-ray Absorption	Thickness Control Rolling Operation.
95	β-ray Transmission	Cigarette Industry Control of Tobacco Content.
22	Back-Scattering γ-rays	Thickness of Steel Plates.
22	Back-Scattering β-rays	Thickness: Sn, Zn coatings on steel; paint, lacquer on metallic surfaces; rubber, plastics on calendering rolls; Se on Al; Ba coating on photographic paper; Cr or brass on steel; filters in paper and plastic; porcelain glaze; plastic coatings on wire; Ni or Cr coatings on metals.
22	X-ray Back-Scattering	Thickness: electroplated metal films, evaporated coatings; pigment layers.
22, 30, 43, 94	X-ray Fluorescence	Thickness: Ag-plated Cu; Cd-plating Fe; Zr cladding of U nuclear fuel elements. Range of metal coatings on metal substrates.
51	X-ray Laminography	Wall Thickness of Glass Bottle.
50	X-ray Laminography	Different Planar Views of Printed Circuit Board, Stop-watch.
86	All Techniques	Forgings, Castings, Steel Bars and Billets, Wrought Tubular Products, Weldments, Brazed Assemblies, Soldered Joints, Adhesive Bonded Joints, Threaded Fasteners, Pressure Vessel Pipelines
59, 96, 97	Neutron Tomography	Nuclear Fuel Bundle.
62, 63	X-ray Tomography (420 kV Source)	Aerospace Structure, Turbine Blade.
63, 98, 99	γ-ray Tomography	Concrete, Timber, Steel Structures.
100, 101, 102, 103, 109	Radiography	Pipe Welding, Nuclear Industry Materials, Structural Ceramics, Concrete.

Table III, Part A (continued)

Reference	Technique	Subject Examined
19, 104, 105, 106	Vibrothermography Thermal Wave, U.S.	Composite Materials.
107	U.S. Robot Controlled	Cracks in Nuclear Reactors.
108	TV Holography	Engineering Structures; Vibrations of Car Door.
16, 17, 18, 19, 20	Flash Radiography	Ballistics. Moving Machinery, Projectiles, Phase Transformations.
44	γ-Absorption	Density Measurements.
45	X-ray Microfocus	Ceramics.
27	Proton Radiography	Thickness Al Foil, Leaves, Al Weld.
52, 53	Compton Imaging	Al Casting, Explosives.

Table III, (continued)

B. Medical

Reference	Technique	Subject Examined
7	X-radiography	Asbestos Fibers in Human Lung.
7	X-radiography	Microangiography.
55, 56, 57	X-ray Tomography (reconstructive)	Medical Examinations; Body Scan, Skull Scan, Phantom.
52, 53	Compton Scattering	Breast Cancer, Human Skull.

Table III, (continued)

C. General Interest

Reference	Technique	Subject Examined
109, 110 111, 165, 166	X-radiography	Examination of Oil Paintings and Wooden Statues.
29, 30, 33, 92, 111, 166	Activation Analysis, Ion Beam Analysis	Authenticity, Age, Provenance of Oil Paintings.
31, 32, 111	Neutron Activation Analysis	Authenticity of Ancient Coins. Au Contaminant in Ag. Ag Contaminent in Cu.
36	Activation Analysis	Forensic Studies, Assassination of President Kennedy, Ag and Sb Contents of Bullets.
76	γ-Radiography	Statue of Liberty, Crack in Liberty Bell.
27	Proton Scatter Radiography	Wristwatch.

Table III, (continued)

D. Scientific

Reference	Technique	Subject Examined
7	X-radiography	Coelocanth Scales With Denticles and Microtubes.
48	X-ray Topography	Fracture Surface Mo Single Crystal Transformation Studies, Crystal Growth Features.
49	X-ray Diffraction Residual Stress Technique	Subsurface Residual Stress, Hardness, Cold-work Effects in Steels, and Other Metals.

Table IV.

Other NDT Methods and References

Technique	References
Acoustic Emission	23, 77, 82, 167
Dynamic and Vibrational Analysis	152, 153
Electrical and Magnetic	149, 150, 151
Exo-electron Emission	160
Fiber-Optic Sensing	159
General Review of all NDT Methods	21, 22, 23, 24, 25, 77, 84, 85, 86, 92
Holography in NDT	108, 154, 155, 156
Laser Techniques	158
Liquid Penetrant	45, 86
Microwave Techniques	86
NMR	60, 67, 68, 82, 150
Positron Annihilation	65
Pressure & Leak Testing	23, 86
Surface Roughness and Abrasion	157
Thermal Methods	102, 132, 133, 134, 135, 136, 137, 138
Thermoelastic Effect	163, 164
Thermoluminescence	162
Ultra-Sonics and Acoustics	7, 23, 61, 71, 73, 75, 82, 85, 106, 112, 113, 114, 115, 116, 117, 118, 119, 120, 121, 122, 123, 124, 125, 126, 127, 128, 129, 130, 131
Visual & Microscopy	139, 140, 141, 142, 143, 144, 145, 146, 147, 148
Xonics Electron Radiography	161

Table V.

International, American and European Organizations
of Standardization, Quality Control, and NDT

1. INTERNATIONAL ORGANIZATION FOR STANDARDIZATION (ISO)
   1 rue de Varembé, case postale 56, CH-1211 Genève 20, Switzerland
   (Committee on Nondestructive Testing (ISO/TC135) - All countries of the world are full members or correspondent members of ISO.)

2. INTERNATIONAL COMMISSION ON RADIATION UNITS AND MEASUREMENTS (ICRU)
   7910 Woodmont Avenue, Suite 1016, Washington, D.C. USA

3. INTERNATIONAL COMMISSION ON RADIOLOGICAL PROTECTION (ICRP)
   Dr. F.D. Sowby, Clifton Avenue, Sutton SM2 5PU, ENGLAND

4. INTERNATIONAL INSTITUTE OF WELDING (IIW)
   54 Princess Gate, Exhibition Road, London SW7 2PG, ENGLAND

5. EUROPEAN ORGANIZATION FOR QUALITY CONTROL (EOQC)
   P.O. Box 2613, CH-3001, Berne, SWITZERLAND

6. USA NATIONAL COMMISSION ON RADIATION PROTECTION
   P.O. Box 4867, Washington, D.C. 20008, USA

7. AMERICAN SOCIETY FOR TESTING MATERIALS (ASTM)
   1916 Race Street, Philadelphia, PA 19103, USA
   (Special Technical Publications cover many aspects of NDT.)

8. AMERICAN SOCIETY OF MECHANICAL ENGINEERS (ASME)
   United Engineering Center, 345 East 47th Street, New York, NY 10017 USA
   (Special Publications cover many NDT practices.)

9. AMERICAN WELDING SOCIETY
   550 NW LeJeune Road, Miami, FL 33126 USA

Table V, (continued)

10. U.S. SOCIETY OF NONDESTRUCTIVE TESTING

    3200 Riverside Drive, Columbus, OH 43221 USA

    (Guidelines on: Supplement A - Radiographic testing method; Supplement B - Magnetic-particle method; Supplement C - Ultrasonic testing method; Supplement D - Liquid penetrant testing method; Supplement E - Eddy-current testing method.)

11. EUROTEST (International Scientific Association)

    Rue du Commerce 20-22 Bte 7, 1040 Brussels, BELGIUM
    Secretary General D. Van Elewyck

12. INTERNATIONAL UNION OF TESTING AND RESEARCH LABORATORIES FOR MATERIALS AND STRUCTURES (RILEM)

    12 rue Brancion, F-75015 Paris, FRANCE
    Secretary General Mr. M. Fickelson

13. INTERNATIONAL COMMITTEE FOR NONDESTRUCTIVE TESTING (ICNDT)

    4153 Arlingate Plaza, Caller No. 28518, Columbus, OH 43228-0518, USA

    Mr. William Widner, President, International Committee of NDT
    General Secretary, ICNDT, Ms. Beth Risinger

14. JOURNALS OF NONDESTRUCTIVE TESTING

    - "Materials Evaluation", Ref. 169
    - "NDT International", Ref. 168

Table VI

Member Societies and Associated Members
of the International Committee for Nondestructive Testing

Argentina: Centro Argentino de Ensayos No Destructivos de Materiales, Via Monte 542-3°, Buenos-Aires.

Australia: Australian Institute for NDT, 8, Windermere Crescent, Brighton, Victoria 3186.

Austria: G. Aufricht, Mittli Kommanditgesellschaft, 1030 Wien, Hegergasse 7.

Belgium: P. de Meester, Katolieke Universiteit Leuven, Guillaume de Croylaan 2, B-3030 Leuven-Heverlee.

Brazil: Miss Salete Maria Brisighello, ABENDE COBRAPI, R Fonte da Saudade, n 247/203 Rio De Janeiro.

Bulgaria: Scientific and Technical Union of Mechanical Engineering, P.O. Box 431, Rakowski 108, Sofia 1000.

Burma: U. Maung-Maung, Assistant Director, Applied Research Institute, Kanbe, Yankin PO, Rangoon.

Canada: J.G. Shewchuk, Aries Inspection Services Ltd., P.O. Box 486, Oakville, Ontario L6J 5A8

China: Institution of Non Destructive Testing, Chinese Mechanical Engineering Society, San Li Ho, Beijing.

Czechoslovakia: National Research Institute for Materials, Opletalowa 25, CS-113-12, Prague I.

Denmark: The Danish Central Welding Institute, 345 Park Alle, DK-2600 Glostrup.

Finland: Juha Sillanpaa, Technical Research Centre of Finland, Katajanokka, 00160 Helsinki 16.

France: Comité Français des Essais Non-Destructifs, 32 Bd de la Chapelle, 75880 Paris Cedex 18.

Germany: East - M. Morgner, Technische Hochschule Otto von Guericke, Boleslaw Bierut-Platz 5, 301 Magdeburg, Postschliessfach 124.
West - Herman-Josef Kopineck, The President DGZfP, Unter den Eichen 87, 1000, West Berlin 45.

Hungary: Pal Reti, Scientific Society of Mechanical Engineers, Kossuth Lajos Ter 6-8, Budapest V.

Table VI, (continued)

India: N.G. Bhagi, NDT Society of India, c/o National Test House, II/I Judges Court Road, Alipore, Calcutta 700027.

Israel: M.S. Golan, Israel Institute of Metals, Technion City, Haifa.

Italy: The Italian Society for Nondestructive Testing, 25126 Bresica, Via A Foresti 5.

Japan: Noboru Niwa, Institute of Space and Aeronautical Science, University of Tokyo, Komaba, Neguro-Ku 4 6 I, Tokyo 153.

The Netherlands: G.M. Van Dijk, Kasteel 5,6852 CM Huissen.

New Zealand: J. Drabble, Secretary NDTA, c/o Ministry of Works, P.O. Box 12041, Wellington North.

Norway: Arnfinn Jensen, A/S Kongsberg Vapenfabrikk, P.O. Box 25, N-3601 Kongsberg.

Poland: Zdislaw Pawlowski, Czeska 1 m 3,03-902 Warsaw.

South Africa: South African Association for Nondestructive Testing, P.O. Box 31548, Braamfontein 2017.

South Korea: Da Hee Rhee, Managing Director, Korea Atomic Industrial Forum Inc., Seoul Central PO Box 6583, Seoul.

Spain: A. Ruiz Rubio, CENIM, Avda Gregoria del Amo, s/n Ciudad Universitaria, Madrid-3.

Sweden: Ake Junghem, Tekniska Rontgencentralen Fack, 10405 Stockholm 50.

Switzerland: R. Hornung, Gebr Sulzer AG, Abt 1513, 8400 Winterhur.

United Kingdom: Non-Destructive Testing Centre, Atomic Energy Research Establishment, Harwell, Didcot, Oxon OX11 ORA.

USA: American Society for NDT, 4153 Arlingate Plaza, Columbus, OH 43228 USA.

USSR: President of the Scientific Council for Non-Destructive Physical Testing Methods of the USSR Academy of Sciences, 44/2 Vavilov Street, Moscow B-333, 117333.

Yugoslavia: Ahmed Sirco, President of AYUNDLS, c/o Energoinvest - OOUR IKM, Tvornicka 3, 71000, Sarajevo.

2. ELEMENTS OF THERMOGRAPHY FOR NON-DESTRUCTIVE TESTING

Julius Cohen

Radiometric Physics Division
Centre for Radiation Research
National Bureau of Standards, USA

This paper presents an elementary review of thermal imaging systems, with emphasis on the application of thermography to non-destructive testing. Topics discussed include heat radiation theory; early and contemporary thermal imaging systems; performance characteristics; effects of emissivity, background temperature, atmosphere, and field of view. Examples of various applications of thermography to non-destructive testing are given. A bibliography is included.

Key words: heat; imagery; infrared; non-destructive testing; passive; radiation; remote sensing; temperature; thermography.

1. Introduction

All objects continually emit thermal radiation from their surfaces. Usually the radiation is in the infrared portion of the spectrum, which is not visible to the unaided eye. Indeed, the radiation from an object does not become visible until its temperature exceeds 800 K.

The radiant energy emitted from a heated surface per unit time - i.e., the power radiated - depends on the nature of the surface, on its area, and on its temperature, in accordance with the Stefan-Boltzman law,

$$W = A \varepsilon \sigma T^4 ,$$

where W is the power radiated [watt]

A is the surface area [metres^2]

ε is the emissivity of the surface (sometimes called emittance)

σ is the Stefan-Boltzman constant = 5.670×10^{-8} watt.m^{-2}K^{-4}

and T is the absolute temperature.

The emissivity, ε, is a measure of the radiation efficiency of a body, compared to a perfect radiator at the same temperature; thus, ε (assumed to be wavelength independent) is a dimensionless number lying between zero and unity. For example, for a perfect radiator, termed a blackbody, $\varepsilon = 1$; for copper, $\varepsilon \simeq 0.3$.

The radiant energy is continually being emitted in the form of a mixture of electromagnetic waves of different wavelengths, and the radiant power is distributed as a continous function of wavelength. Figure 1 is a graph of the spectral distribution of the radiant power per unit area from the surfaces of several blackbodies of different uniform surface temperatures; [1] here W_λ is the radiant power density per unit wavelength at wavelength λ. Each curve is characterized by a particular wavelength λ_p, a function of temperature, for which W_λ is a maximum. The effect of increasing temperature is seen to shift λ_p to shorter wavelengths, as well as to increase the value of W_λ at each wavelength. The relationship between λ_p and temperature of the maximum W_λ is given by the approximation,

$$\lambda_p \simeq 3000/T$$

As a concrete example of spectral distribution of radiant power, a terrestrial object, commonly at ~300 K, emits in the 2 μm to 100 μm region, most of the power is in the 3 μm to 14 μm region, and the power peaks at ~10 μm. On the other hand, for an incandescent filament at ~3000 K, λ_p = 1 μm, which is in the near infrared. The filament can be seen to be glowing because of the shorter wavelengths emitted in the visible region of the spectrum (approximately 0.38 μm to 0.77 μm).

Although infrared radiation is invisible to the unaided human eye, various means have been devised for detecting and imaging an infrared scene for visualization. Infrared imaging may be classified as active or passive according to whether the scene is irradiated with an infrared source and the resultant reflected radiation is imaged, or whether the self-radiation from the scene is imaged. The latter process, which converts the temperature pattern of a scene into a corresponding contrast pattern, is termed thermography, and the viewed image is termed a thermogram.

Thermography's ability to see scenes, objects, and features otherwise invisible - sometimes even below a surface - has made it a potent means used in a variety of applications for medical, industrial, agricultural, geological, meteorological, and energy conservation purposes. For example, it is used for medical diagnosis of tumours and inflammations; for monitoring nuclear reactor steam cooling towers; for inspecting refractory linings of furnaces and

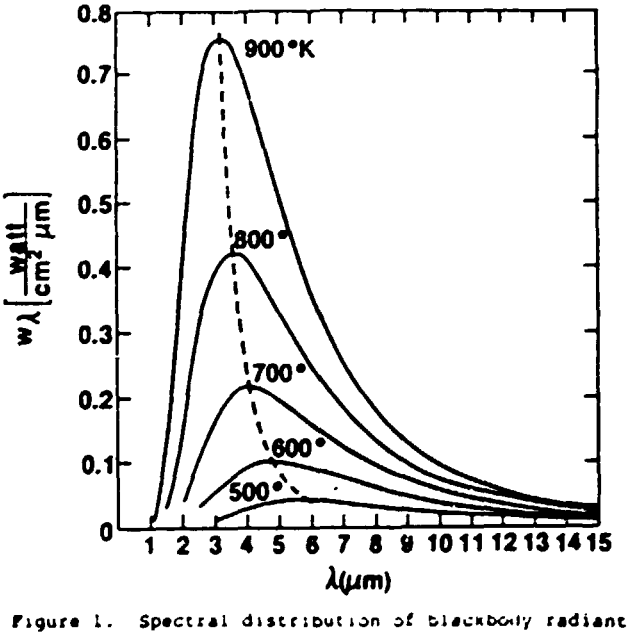

Figure 1. Spectral distribution of blackbody radiant power density at various temperatures. W_λ is the radiant power density per unit wavelength at the wavelength λ.

---

[1] These spectral distribution curves are obtained from Planck's blackbody radiation law. The area under a curve, the total power density radiated, would correspond to the Stefan-Boltzman law, with $\varepsilon = 1$.

ducts; for inspecting electrical power transformers and electrical rotating machines while under power; for studying soil moisture, crops, and vegetation decay; for studying volcanoes, glaciers, tides, and tectonic plates, and for detecting petroleum and mineral deposits; for detecting and mapping thermal effluent discharges; and for detecting heat losses from residential buildings, plants, and machinery. These are just some of the myriad ways thermography is being put to use. They are mentioned here only to suggest scope and usefulness, but will not be elaborated on, as this paper is concerned chiefly with the applications of thermography to non-destructive testing.

2. Thermal imaging systems

John W. Herschel (son of William, the discoverer of the infrared spectrum) is credited with inventing thermography in 1840, by utilizing differential evaporation of thin liquid films. This rudimentary apparatus was the prototype for the Evaporograph, as later (1929) Czerny improved on the concept by substituting thin oil films that changed colour with differential evaporation resulting from the heat of the incident infrared radiation. And in 1959, the Evaporograph was utilized for qualitative non-destructive testing of hot spots. However, this imaging device was crude and insensitive, with poor repeatability; it is much more of historical than of practical importance.

An exotic way of producing a thermal image is through the use of certain temperature-sensitive liquid crystals, applied directly to the surface to be examined. This technique is sometimes used to examine aerospace structures. However, liquid crystals exposed to the atmosphere have a short lifetime owing to contamination, and their use is rather restricted.

Thermistors, which are commonly oxidic semiconductors having a large negative temperature coefficient of resistance, also may be utilized as the detector in thermal imaging systems. But thermistors have very long time constants, high 1/f noise necessitating chopping of the radiation, and very long scan-frame times, thus making for inferior real-time display, particularly as regards resolution. For imaging systems, thermistors are of rather limited applicability. Thermistors for thermography find their chief use now in infrared microscopes where the targets are small and the image is produced on a photograph.

Most modern thermal imaging systems use either photon detectors or pyroelectrics, a type of thermal detector, as the infrared sensor which receives the radiation from the scene or the target and converts it into an electrical signal for processing and display.

Photon detectors respond to numbers of photons, hence they are wavelength dependent Owing to their electronic structure, any given detector responds to only a very narrow range of wavelengths. Photon detectors responsive to infrared radiation generally require cooling to 77 K or below, depending on the nature of the material from which the detector is made. Photon detectors fall into either of two categories, photoconductive or photovoltaic, and either may be used in a thermal imaging system. Photoconductors are homogeneous semiconductors, while photovoltaic detectors are junction or barrier devices. The advantages of the photovoltaic detectors are that they require no application of a voltage bias and do not generate a significant amount of heat as does a photoconductor, and their noise may be somewhat lower than photoconductive detectors made of the same material. However, not all materials are utilizable as photovoltaic detectors. The detectors commonly used in thermal imaging systems are indium antimonide photovoltaic detectors at 77 K, for the 3μm to 5.6μm region, and mercury cadmium telluride photoconductive and photovoltaic detectors at 77 K, for the 8μm to 14μm region. Although a single detector may be used, it is usual to use an array of detectors. In general, single detectors and linear arrays are preceded by an opto-mechanical scanner, which dissects the scene or target bit by bit for sequential reception by the detector(s). Opto-mechanical scanners generally utilize rotating or oscillating mirrors or prisms to generate a rectangular raster - i.e. a line-by-line scan of the scene or target - analagous to the formation of a picture on a television screen. On the other hand, focal-plane mosaics (square arrays of detectors) do not require scanning.

Thermal detectors respond to total radiant power, hence they are relatively wavelength independent, their response often extending to very long wavelengths, up to $\sim$ 100μm. A particularly attractive attribute of thermal detectors is that they require no cooling. This is not just a convenience; it also reduces size, weight, cost, and complexity, and does not introduce additional noise (microphonics) owing to any refrigerator vibrations. Pyroelectrics are a special class of thermal detector; unlike the others they respond only to a change in temperature, rather than to the temperature itself. Hence, pyroelectric devices need to be panned or nutated, or else the incoming radiation from the scene or target needs to be periodically interrupted, or chopped, as for example, with a rotating toothed wheel. However, pyroelectrics will produce a current, or signal, on cooling, as well as on heating, with the polarity of one opposite to that of the other, so special means are provided in the better systems to overcome the effects of changing scene polarity. The pyroelectric in a thermal-imaging system is generally a thin crystal such as triglycene sulfate (although systems employing polymeric films instead - e.g., of polyvinylidene fluoride - are being developed because of their thinness, cheapness, and superior chemical stability). Pyroelectric thermal-imaging systems are usually of the vidicon type, which means that the scene is imaged on one face of the pyroelectric, thus producing a pattern of localized charges on the poorly-conducting pyroelectric material, the magnitudes of which are read by an electron-beam scanning the opposite face of the pyroelectric, in raster fashion. Pyroelectrics, like photovoltaic detectors, do not require biasing. On the other hand, compared to photon detectors, pyroelectrics, like thermal detectors in general, have lower specific detectivities [1] and longer response times. Thus, while the performance of pyroelectric

---

1. Specific detectivity (D^*) is the signal-to-noise ratio of the detector output per unit incident power normalized to a unit sensitive detector area and a unit electrical bandwidth. D^* is defined in units of [cm $Hz^{1/2}$ / watt].

thermal imaging systems can be quite good, the performance of systems with photon detectors can be better. The main attribute of the pyroelectric system, as already mentioned, is its operability over an extensive range of wavelengths, without the necessity of cooling.

Although the heart of a thermal-imaging system is its infrared detector(s), the detector is but one of several interacting subsystems which together comprise a complex system. Figure 2 is a simplified block diagram of a scanning thermal-imaging system. The subsystems are, in general, the following, given in sequence: (1) an optical system for collecting the radiance from the scene or target, spectrally

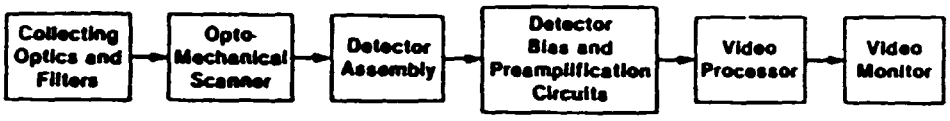

Figure 2. Simplified block diagram of a scanning thermal imaging system

filtering, and focusing it onto the detector(s); (2) a scanning system for "dissecting the scene" or a chopper for modulating the radiance; (3) a detector system including any preamplifiers and ancillary circuitry; (4) a signal processor system for receiving the low-level signal from the detector(s), amplifying it, limiting the bandwidth, extracting the information the signal contains, and delivering this information to the display system; and (5) a display system, generally a video monitor. The signal processor uses techniques similar to that used for commercial television, so (4) and (5) together may be considered as TV system. In addition to the aforementioned subsystems, there may be optical baffles, or stops, to limit field of view and a cooling system such as a dewar, pressurized gas, or heat pump, for cooling the detector(s) and baffles. Because of the complexity and sophistication of the modern thermal-imaging system, it is usually designed by a team of specialists, co-ordinated by a systems engineer. The fields which are usually represented are radiation theory and radiometry; optical design and engineering, including Fourier optics and optical scanning devices and systems; infrared physics, including detectors, noise theory, and atmospheric transmission; and television engineering.

3. System performance characteristics

Thermal images result primarily from temperature differences and/or emissivity differences in a scene or target (rather than reflections), and it is the function of a thermal-imaging system to reproduce an acceptable visible image of the scene or target from its thermal content. Thus, a thermal-imaging system is required to resolve temperature differences and emissivity differences (apparent temperature differences). Further, as temperature and emissivity are distributed spatially in the scene or target, the thermal-imaging system is required to resolve spatial differences of emissivity or temperature. A system's ability to reproduce an accurate, sharp image is given by its performance characteristics, which obviously must include measures of the system's ability to resolve (true and apparent) temperature differences and spatial variations.

Many measures have been devised for characterizing the performance of a thermal-imaging system and its subsystems, with most being of value only as an aid to the subsystem designer or systems engineer. Nevertheless, several measures relating to overall system performance may be of importance to the user of a thermographic system, depending on the application. These measures are (1) [temperature] accuracy, [1] (2) noise-equivalent temperature difference [NEΔT or NETD], (3) minimum resolvable temperature difference [MRTD] and (4) minimum detectable temperature difference [MDTD]. Item (1) is relevant to remote radiometric temperature measurements, (2) to temperature sensitivity to a broad area target, and (3) and (4) to imaging. It may be noted that measures (2), (3) and (4) are some expression of temperature difference, which certainly is not surprising. Not obvious, however, is that these temperature differences are functions of signal-to-noise ratio, which also should not be surprising as noise imposes the lower limit of radiative power which may be detected. Each of the above performance measures will now be discussed in relation to their measurement or determination and to their signficance and utility.

(1) Accuracy: For most applications of a thermal-imaging system accurate temperature measurements are not of concern, and accuracy is seldom mentioned in thermographic literature or manufacturer's specifications. Further, "highly-accurate" temperature measurements may be exceedingly difficult to make - particularly under some field conditions. Nevertheless, there appears to be a growing need for accurate radiometric temperature determinations, e.g., for process control and for research purposes. Factors which may cause inaccuracy in temperature determination include the original calibration method and inherent operational effects, and effects of atmosphere, emissivity, and reflections (discussed in subsequent sections). If accurate temperature determinations are required, it is generally advisable to make an on-site calibration using blackbody targets of known temperature.

(2) Noise-equivalent temperature difference: This is a convenient measure of an imaging system's thermal sensitivity to a broad area target whose image completely covers the area of one detector. (Such a target is referred to as an extended source.) If the target is a blackbody at temperature T, and the surrounding background, assumed to be a uniform blackbody, is at temperature T_B, the noise equivalent temperature difference NEΔT is defined as the blackbody target-to-background temperature difference in a standard test pattern which produces a peak signal-to-rms noise ratio (S/N) of unity in the reference electronic filter (used in the processing of the detector signals) when the system views the test pattern. The test pattern can be a square area of temperature greater than the background, as shown in figure 3 (a).

---

1. Some imaging systems include temperature measurement capability, other systems do not.

Expressed mathematically, noise equivalent temperature difference is given by

$$NE\Delta T = \frac{T - T_B}{S/N} = \frac{\Delta T}{S/N}$$

When S/N = 1, NEΔT = ΔT. Thus, to measure the noise-equivalent temperature difference, one finds the ΔT which just produces S/N = 1 in the reference electronic filter. Because noise-equivalent temperature difference depends on the filter and on the background temperature, usually $\sim$300 K, these should be specified along with the NEΔT value. The measurement of noise-equivalent temperature difference is not difficult; however, owing mainly to the inaccuracy in measuring rms noise levels, NEΔT is not a very accurate measure. Still, it can be used to compare the thermal sensitivities of two different systems provided the measurements conform to the same standard and the differences in NEΔT are sufficiently large. Thus, for example, if the NEΔT of system A were 0.2°C and that of system B were 0.25°C, both systems would be considered to have essentially the same thermal sensitivity. Alternatively, if the NEΔT of system A were 0.2°C and that of system B under the same conditions were 0.4°C, system A would be considered to be the more sensitive system for those conditions.

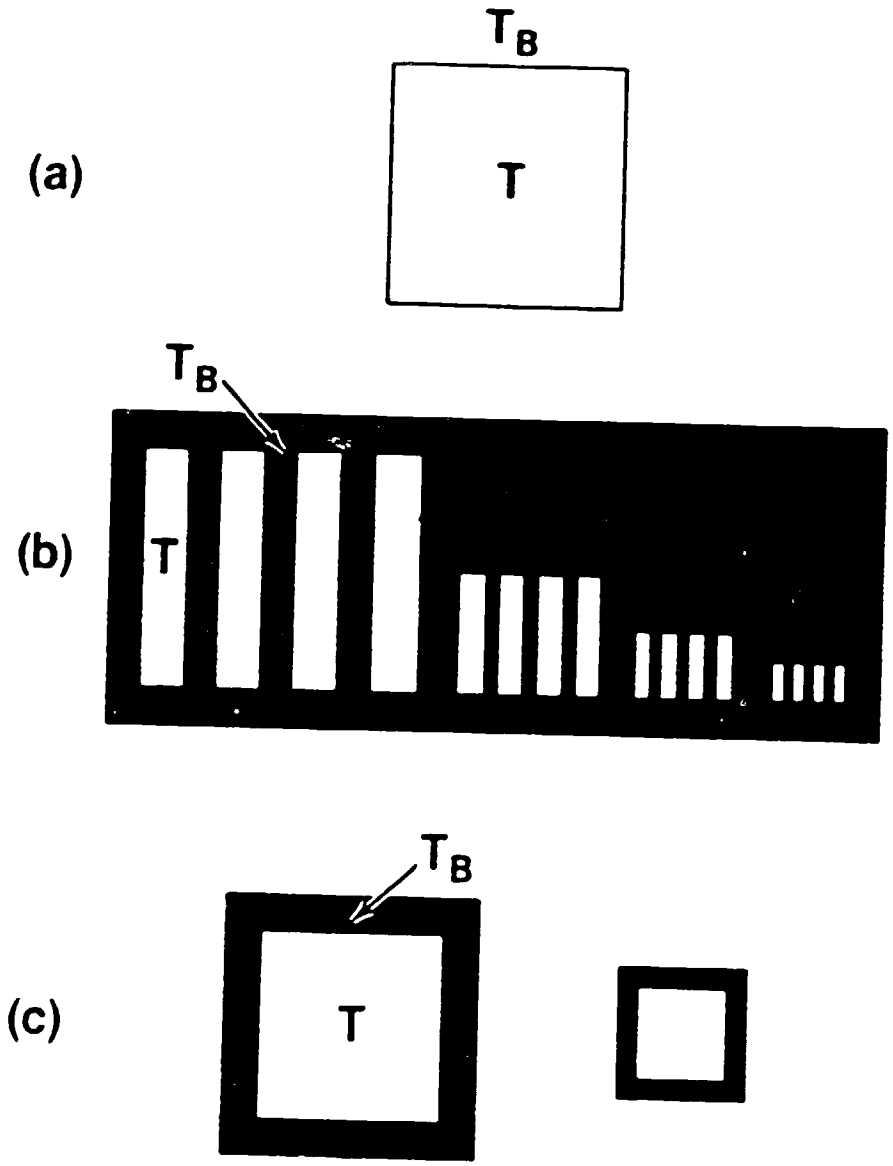

Figure 3. Targets used for measuring performance of thermal imaging systems: T is target temperature, T_B is background temperature, and $T > T_B$. (a), NEΔT. The target is an extended source of square geometry; (b), MRTD. The target is a periodic 4-bar chart of rectangular geometry, with aspect ratio of 7:1; (c), MDTD. The target is a square whose area is equal to the area of the surrounding background temperature.

Noise-equivalent temperature difference is measured at the video signal output and relates only to the thermal-imaging system exclusive of an image observer. On the other hand, where imagery itself is concerned, an observer's visualization capabilities must be included, as is done for the measures, minimum-resolvable temperature difference (MRTD) and minimum-detectable temperature difference (MDTD), discussed next.

(3) Minimum-resolvable temperature difference: MRTD is a measure of the compound system-observer capability to spatially resolve temperature differences in a standard target by observing its display on a video monitor. MRTD is a function of target geometry and it is usual practice to use a periodic 4-bar chart of rectangular geometry and aspect ratio (length:width) of 7:1. MRTD is a function also of the periodicity of the bars, or its inverse, the spatial frequency, 1/ so in practice MRTD is measured as a function of the spatial frequency and shown as a curve. Examples of targets used for these measurements are shown in figure 3 (b). The targets are blackbody radiators of different, but uniform temperatures. Further, the power of the eye-brain to resolve spatial temperature differences is a function of signal-to-noise ratio (S/N). For example, the probability of resolution with a standard target is ~50 per cent for a display S/N of roughly 3 and is ~90 per cent for S/N ≅ 5. Thus, the probability of detection should be specified along with the MRTD vs spatial frequency curves.

Qualitatively, MRTD is defined as the image S/N required for an observer to resolve a defined 4-bar pattern chart that is masked by noise, and it is expressed as the temperature difference between the bars and the background.

Analytically, the MRTD is directly proportional to the noise-equivalent temperature difference (NEΔT) of the system and inversely proportional to a mathematical quantity called the modulation transfer function (MTF); hence, MRTD can be derived or it can be measured directly. A brief discussion of the modulation transfer function will now be given in order to make clearer the significance of the minimum resolvable temperature difference.

Consider a target to be decomposed into a vast number of discrete points of various intensities or radiances - which, in fact, is precisely what the optomechanical scanner accomplishes. If an imaging system were perfect, every point in the target would be reproduced exactly in the image (with due allowance for any magnification or inversion), and the target would be reproduced exactly by the total image. In reality, perfect fidelity is a physical impossibility, owing mainly to diffraction effects from finite apertures. Examples of finite apertures in imaging systems include lenses, stops, infrared detectors (responsive areas), and the scanning electron beam spot of the display tube. Thus the image differs from the object in amplitude (it is attenuated), shape, position, or all three. The modulation transfer function (the modulus of a Fourier transform) gives a spatial description of the attenuation in amplitude; the minimum attenuation is denoted by a normalized MTF of unity.

Figure 4 (a) illustrates the effect of the finite aperture of a lens on the image of a point source. If a point source were focused through a thin (negligible refraction), aberration-free, positive lens, the image in the focal plane, parallel to the plane of the lens, would be found to be a spread-out spot of non-uniform intensity (intensity is greatest at the centrepoint) and blurred perimeter. A similar phenomenon would occur if a line source (a rectangular slit of uniform radiance or intensity) were substituted for the point source, as depicted in figure 4 (b).

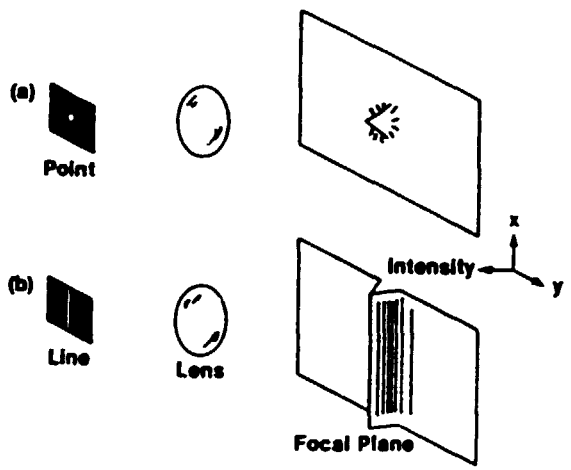

Figure 4. Effect of a finite aperture on the image of a point source (a) and a line source (b).

The MTF of the overall thermal imaging system includes the individual MTFs associated with its various apertures and it relates to the ability of the system to recreate the thermal-spatial frequency content of an object. The (system) MTF can be determined by measuring the point or line spread from a blackbody source using photometric or thermal techniques, and applying Fourier analysis. (The measurement is quite difficult - aperture dimensions and positions must be precisely determined and temperatures need to be controlled to within ± 0.05°C.)

A modulation transfer function, in general, is a sensitive function of spatial frequency, as may be noted in the example of figure 5. MTF decreases with increasing spatial frequency and in fact vanishes at sufficiently high spatial frequency; i.e., the element (aperture) blocks high spatial frequency information.

Remembering that MRTD $\propto$ NEΔT/MTF, the dependence of MRTD on spatial frequency can be graphed, as shown in the example of figure 5, where the system MTF has been included for instructive purposes. The intuitively realizable result shows that the resolution of closely-spaced lines of high spatial frequency requires greater contrast, or

---

1/ Spatial frequency may be defined in terms of the angle between an observation point and the normal distance between the centrelines of two adjacent bars. The usual units are cycles mrad or (number of) lines·picture height.

temperature difference. between a line and the background, than does widely-spaced lines of low spatial frequency.

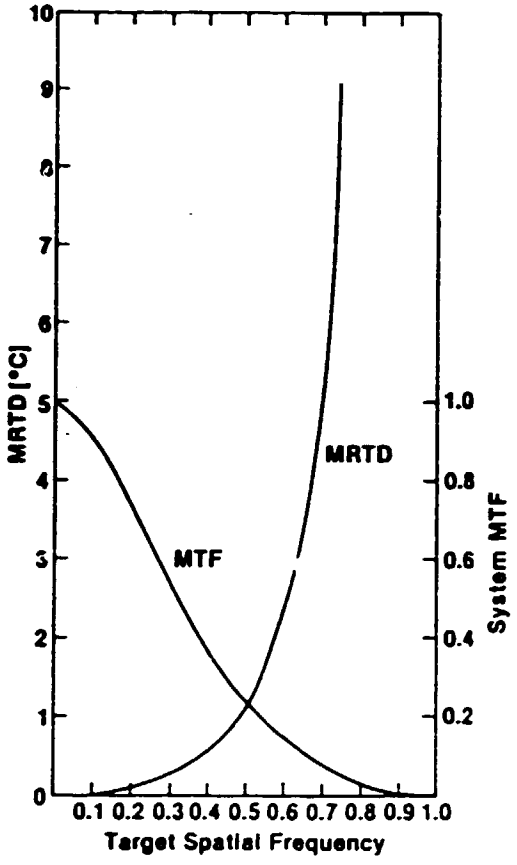

Figure 5. Example of the dependence of minimum resolvable temperature difference (MRTD) and modulation transfer function (MTF) on normalized spatial frequency.

Although MRTD is a function of noise-equivalent temperature difference, it is obvious that NEΔT alone cannot be used to compare the performance of two different systems in spatially resolving temperature differences. For example, system A can have a lower (better) NEΔT than system B, but the MTF of B may be sufficiently larger (better) than that of A, so that the MRTD of B is lower (better) than that of A.

(4) Minimum-detectable temperature difference: The minimum-detectable temperature difference (MDTD) is similar to the minimum-resolvable temperature difference, except that instead of the 4-bar pattern, the target consists of a uniformly heated square of blackbody temperature T framed by a uniform background, of specified area, at blackbody temperature T_B; this target is imaged by the system and observed under improved conditions of long search time and known target location. An MDTD target is depicted in figure 3 (c); the area of the square of temperature T is equal to the area of the surrounding background of temperature T_B. As for MRTD, curves of MDTD as a function of spatial frequency are obtained, except that spatial frequency is expressed in terms of angle of view [mrad], rather than lines picture height.

Where details in imagery are of concern, MRTD would be a more useful measure than MDTD; however, where detection of small hot spots in a wide expanse is of concern, as for many non-destructive testing applications, MDTD would be the more useful measure.

Finally, performance measures are useful indicators, and it is hoped that they will correlate with field use, so a caveat is in order. The performance measures are obtained under ideal laboratory conditions such as blackbody targets and unit transmissivity, and the temperature differences are small, $< 1°C$. Field conditions may deviate appreciably, so performance measures must be utilized cautiously or with modification.

4. The target and the image

Thermal-imaging systems act on target information and the contents of an image, including the intelligence therein, depend on characteristics of the target as well as those of the imaging system. The latter has already been treated in some detail; for optimal use of a thermal-imaging system, it is necessary to consider also the characteristics of a target. Some basic facts concerning the target are now listed:

(1) The thermal radiation from a target (radiance) emanates from its surface;

(2) A thermal-imaging system responds to irradiance at its entrance aperture (which one would like to be only radiation from the target). Thus the imaging system will perceive apparent temperatures or apparent temperature differences present at the surface of the target. If the target is a uniform blackbody, the apparent temperature will be the "true" temperature (neglecting any extraneous effects). If the target is a greybody (an object of uniform emissivity < 1), the apparent temperature will not be the "true" temperature; likewise, the system will indicate emissivity differences as temperature differences.

(3) A thermal-imaging system, no matter how good, cannot distinguish a target from its background unless there is sufficient contrast between the target and its background. Contrast is defined as the difference between the radiances of the target L and of the background L_B, divided by their sum $L + L_B$. As the ease with which an object can be identified depends on contrast, it is sometimes desirable to increase the contrast, e.g., by using spectral filters to measure over a limited spectral region, or by suppressing background radiance, a sophisticated and costly measure.

(4) Obviously the spectral response of the system's infrared detectors must include the spectral radiance of the target. Optimal detection results when the peaks of both coincide, but optimal detection is not always necessary; mismatches may be compensated by large irradiance or high spectral detectivity.

For convenience, targets may be classified according to (1) emissivity and (2) size relative to image size.

(1) If the thermal target is a perfect or near-perfect absorber of radiation over all wavelengths, it is said to be a blackbody, and the emissivity $\varepsilon \approx 1$. A target of constant emissivity < 1 is said to be a greybody.

(2) If the target fills the field of view of the detector (i.e., the image of the target is larger than the area of a single detector), the target is said to be an extended source. If the target does not fill the field of view (i.e., the image of the target is smaller than the area of a single detector), the target is said to be a non-resolvable source (and considered to be a point source).

A consideration of the foregoing will show that it is advantageous to employ targets which are blackbody extended sources:

If the target is an extended source, the radiometric quantity of concern is radiance,

$$L = \frac{W}{\pi}$$

where L is radiance [watt cm^2 sr],
W is radiant emittance [watt/cm^2].

Ignoring attenuation by the atmosphere or the optics, the irradiance at the sensor is independent of distance to the source, and is given by

$$H = L\omega$$

where H is irradiance [watt.cm^{-2}],

ω is the solid angle subtended by the detector [sr].

When two areas differ in radiance, the difference may be due to a difference in temperature or emissivity, or both, so in general,

$$\Delta L = \Delta L_T + \Delta L_\varepsilon .$$

If the source is a blackbody

$$\Delta L = \Delta L_T ,$$

and variations in radiance are due only to temperature differences. Therefore, system temperature-sensitivity performance on an actual (as opposed to test) target should correlate with the noise-equivalent temperature difference of the system (which is measured on blackbody test targets).

The noise-equivalent temperature difference may be written

$$NE\Delta T = \frac{H_o}{\omega \tau_a \Delta L} ,$$

where H_o is the noise-equivalent irradiance - i.e., the irradiance for which the signal-to-noise ratio is unity, τ_a is the atmospheric transmissivity (assuming negligible atmospheric absorption, $\tau_a \approx 1$).

It is a property of solids that any material discontinuities in an object - e.g., cracks, fractures, voids, foreign inclusions - will result in a corresponding temperature discontinuity if heat is made to flow through the object. While surface discontinuities may be discernable because of emissivity differences alone, thermal viewing of infrasurface discontinuities requires that heat flow through the target. The required heat may be developed from within the target - as with electrical components or running tires - or from without - as by heat soaking the material just prior to viewing, or by uniformly heating the surface of the material during viewing. To eliminate spurious results due to emissivity differences, it is usual practice to paint or spray the surface with a coating of highly absorbing material, thus approximating a uniform blackbody target.

The temperature discontinuities, or differences, in a heated target may originate at the surface, the subsurface, or in the interior. In any case, thermal radiation is emitted only from the surface, so infrasurface temperature differences must be transmitted to the surface if they are to be perceived by a thermal-imaging system. Whether or not an infrasurface-originating temperature difference - i.e., an infrasurface defect - can be detected depends strongly on its depth and on the thermal conductivity of the target material. If an infrasurface temperature difference is produced, heat will diffuse from the warmer to the cooler regions in all directions, including that of the surface. If the thermal conductivity of the material is low - e.g., ceramics, glass, rubber - the heat will not readily disperse, so that a temperature difference may be transferred to the surface. On the other hand, if the thermal conductivity is high - e.g., metals - heat will readily disperse and the target will soon acquire a uniform equilibrium temperature with no temperature difference manifest at the surface.

At this juncture the reader may wish to review the descriptions of the various targets used for the measurements of performance, and these have been summarized in figure 3. Additionally, recall that a quoted value of NEΔT should inlude specifications of the background temperature and the reference electronic filter in the measurement circuit, while quoted values of MRTD/MDTD should also include specifications of spatial frequency/angle of view and the probability of resolution/detection.

5. Atmospheric effects

Atmospheric effects are of great importance in airborne thermography where the source, or target, is far away. The atmosphere may attenuate the radiation from the target, as well as alter its spatial, temporal, and spectral characteristics, thus degrading the target information received. On the other hand, in non-destructive testing atmospheric effects are generally of negligible importance because the source is quite close (< 1 m) and the atmosphere is uncontaminated with vapours such as smoke, fog, etc. Occasionally, however, non-destructive testing may involve critical measurements or may have to be made under adverse conditions - e.g., the source is distant or the atmosphere is humid - such that atmospheric effects need to be considered.

Atmospheric effects arise from (1) the interaction of the atmosphere with the target radiation and (2) from inherent causes. The ways in which atmospheric effects are manifested are

1. Absorption of source radiation by various atmospheric constituents, notably water vapour, carbon dioxide, nitrous oxide and ozone, of which the first two are prominent. The absorption is selective with optical frequency, resulting in an absorption spectrum, and it is important that the system's infrared detector have spectral response within an atmospheric "window", where absorption is negligible. As noted above, atmospheric absorption (selectively) attenuates the target radiation;

2. Background thermal radiation from these same atmospheric constituents which are strong absorbers;

3. Scattering of the source radiation out of the path of the imaging optics by molecules of the permanent gases and by aerosols;

4. Scattering of unwanted background radiation into the imaging optics by these same permanent gases and aerosols;

5. Turbulence in the atmosphere, or atmospheric optical noise.

The most important of the above phenomena is atmospheric absorption, a complex subject which has received considerable study. The practicable mathematical solution of atmospheric transmission problems requires a mathematical model, of which there are many, and computer aid.

In airborne thermography, atmospheric effects may impose a handicap on good imagery which must be coped with, and mathematical methods of modelling are often used for this purpose. Although modelling is probably the best, if not the sole rational means of coping, it can only provide rough estimates because a model is based on assumptions and the implementing data are uncertain. If atmospheric absorption were a problem in non-destructive testing, it would be preferable to calibrate the system on site with the aid of a blackbody target, rather than to employ modelling.

6. Radiometric measurement of temperature

The primary function of a thermal imaging system is to obtain a visual image of a thermal target. Additionally, however, some systems may be used for remote determination of target temperature (a minority of sophisticated systems incorporate a blackbody benchmark). Such temperature measurements properly are more in the realm of radiometry than thermography. Nevertheless, the factors of concern are some of the same factors which are of concern in imagery, viz. target, background, and atmospheric effects. The manifestations of the factors differ for the two cases, but unsurprisingly the solutions are the same.

The imaging system, like any radiometric device, responds to the irradiance at its entrance aperture. If the target is unresolved, the irradiance is a function of distance to the target and its temperature is given by

$$T_u = \left[\frac{2 R^2 (\omega \Delta f)^{\frac{1}{2}}}{\sigma A_s D_o (NA)^2 D^* \tau_a \tau_o \varepsilon} \cdot \frac{S}{N}\right]^{\frac{1}{4}},$$

where T_u is temperature [K]

R is distance between target and detector [cm]

ω is solid angle subtended by detector [sr]

Δf is noise equivalent band pass [Hz]

σ is Stefan-Boltzman's constant [W/cm^2K^4]

A_s is target surface area [cm^2]

D_o is lens diameter [cm]

NA is numerical aperture [dimensionless]

D^* is specific detectivity [$cm(Hz)\ W^{-1}$]

τ_a is atmospheric transmittance [dimensionless]

τ_o is spectral transmittance of detector, including the optics [dimensionless]

ε is emissivity [dimensionless]

$\frac{S}{N}$ is signal-to-noise ratio [dimensionless].

If the target is an extended source, the irradiance is independent of the distance to the target, and its temperature T_e is given by

$$T_e = \left[\frac{2}{\sigma D_o^2 (NA)^2 D^* \tau_a \tau_o \varepsilon} \cdot \frac{S}{N} \left(\frac{\Delta f}{\omega}\right)^{\frac{1}{2}}\right]^{\frac{1}{4}}$$

Note that T_e is independent of both target distance and target area, a particularly valuable characteristic that is exploited for industrial process control and for non-destructive testing.

Assuming errors in system calibration to be negligible, the potential sources of error in temperature determination are emissivity variation atmospheric effects, and background effects. These have already been discussed in connection with imagery, and those discussions generally carry over.

Nevertheless, some additional remarks concerning background effects are worth noting here. As alluded to, above, background is not restricted to the backdrop; background in general encompasses the entire surround that interferes with the radiation being received from the target: atmospheric scattering and emission, radiation from walls and windows, etc. Background radiation which falls on a greybody target will be reflected. Assuming the target to be opaque, the reflectivity, or fraction of the impinging radiation reflected, is merely $(1-\varepsilon)$. The reflected background radiation results in errors in apparent radiance, hence temperature measurement.

On the other hand, if the target is a blackbody, it will absorb all of the impinging background radiation and none will be reflected. Thus it is practice in non-destructive testing, to coat targets such that they are rendered blackbodies. In sum, there are many advantages to working on blackbody extended sources, rather than greybodies or unresolved sources, whether for imagery or for radiometry.

7. Applications of thermography to non-destructive testing

Early on, it became apparent that the infrared radiative properties of matter were exploitable.

Thus, heat seeking devices for searching and tracking were already being proposed in 1910. The desire for new and improved capabilities, augmented by monetary support, has been the impetus and the nurture for infrared technology in general, and thermography in particular. Modern commercial imaging systems are a modified spillover.

Use of thermography for non-destructive testing dates back several decades. The main application then, as now, was the qualitative detection and location of hot spots, indicators of incipient failure. As technology advanced, however, and more sophisticated imaging systems became available, their application to non-destructive testing followed suit, and the realm of work expanded into quantiative determinations, especially important for process control and strength of materials.

It is apparent that the remote sensing capabilities of thermography and radiometry can be used effectively for automatic process control and quality control, and indeed some companies are doing so. Many accounts of such applications are not made public, however, as they are considered to be proprietary.

Finally, in the usual course of events, one is confronted by a problem for which a means of solution is then sought. With the modest background in thermography presented herein, an investigator with an appropriate knowledge of an intended target should be able to make a rational judgement concerning the feasibility of applying thermography. Some test objectives are simple and require only a simple instrument (imaging system); others are demanding and require a sophisticated instrument. Further, owing to inaccessibility of adverse targets or extraneous effects, thermographic testing may be complicated, and an alternative method of testing might be better. Usually, however, in the laboratory at least, conditions can be established favourable to the execution of simple and direct non-destructive testing by thermography. (This article was received by courtesy of Prof. L. Cartz)

3. X-RAY DIFFRACTION RESIDUAL STRESS TECHNIQUES

General uses

Macrostress measurement

- Non-destructive surface residual stress measurement for quality control
- Determination of subsurface residual stress distributions
- Measurement of residual stresses associated with failures caused by fatigue or stress corrosion

Microstress measurement

- Determination of the per cent cold work at and below the surface
- Measurement of hardness in steels in thin layers

Examples of applications

- Determination of the depth and magnitude of the compressive layer and hardness produced by carburizing steels
- Investigation of the uniformity of the surface compressive residual stresses produced by shot peening in complex geometries
- Measurement of surface residual stresses and hardness on the raceway of ball and roller bearings as functions of hours of service
- Study of the alteration of residual stress and per cent cold work distributions caused by stress-relieving heat treatment or forming
- Measurement of surface and subsurface residual stresses parallel and perpendicular to a weld fusion line as a function of distance from the weld
- Determination of the direction of maximum residual stress and per cent cold work gradient caused by machining

Samples

- Form: Polycrystalline solids, metallic or ceramic, moderate to fine grained
- Size: Various, with limitations dictated by the type of apparatus, the stress field to be examined, and X-ray optics
- Preparation: Generally, none. Large samples and inaccessible areas may require sectioning with prior strain gauging to record the resulting stress relaxation. Careful handling or protective coatings may be required to preserve surface stresses

Limitations

- Expensive, delicate apparatus generally limited to a laboratory or shop
- Only a shallow ($\leq$0.025 mm, or 0.001 in.) surface layer is measured, requiring electrolytic polishing to remove layers for subsurface measurement
- Samples must be polycrystalline, of reasonably fine grain size, and not severely textured

Estimated analysis time

- 1 minute to 1 hour per measurement, depending on the diffracted X-ray intensity and technique used. Typically, 1 hour per measurement for subsurface work, including material removal and sample repositioning

Capabilities of related techniques

- General dissection techniques: Generally good for determination of gross residual stress distributions extending over large distances or depths. Restricted to simple geometries

- Hole drilling: Applicable to a variety of samples with stress fields uniform over dimensions larger than the strain-gauge rosette and depth of the drilled hole and with magnitudes less than nominally 60 per cent of yield strength. Serious errors are possible due to local yielding for higher stresses, variation in the stress field beneath the rosettes, eccentricity of the hole, or as a result of residual stresses induced in drilling the holes

- Ultrasonic methods: Require relatively long gauge lengths and stress-free reference standards. Of limited practical application due to errors caused by transducer coupling, preferred orientation, cold work, temperature, and grain size. Sensitivity varies greatly with material

- Magnetic (Barkhausen or magnetostrictive) methods: Limited to ferromagnetic materials and subject to many of the limitations and error sources of ultrasonic methods. Highly nonlinear response with low sensitivity to tensile stresses

Introduction

In X-ray diffraction residual stress measurement, the strain in the crystal lattice is measured, and the residual stress producing the strain is calculated, assuming a linear elastic distortion of the crystal lattice. Although the term stress measurement has come into common usage, stress is an extrinsic property that is not directly measurable. All methods of stress determination require measurement of some intrinsic property, such as strain or force and area, and the calculation of the associated stress.

Mechanical methods (dissection techniques) and nonlinear elastic methods (ultrasonic and magnetic techniques) are limited in their applicability to residual stress determination. Mechanical methods are limited by assumptions concerning the nature of the residual stress field and sample geometry. Mechanical methods, being necessarily destructive, cannot be directly checked by repeat measurement. Spatial and depth resolution are orders of magnitude less than those of X-ray diffraction.

All nonlinear elastic methods are subject to major error from preferred orientation, cold work, temperature, and grain size. All require stress-free reference samples, which are otherwise identical to the sample under investigation. Nonlinear elastic methods are generally not suitable for routine residual stress determination at their current state of development. In addition, their spatial and depth resolutions are orders of magnitude less than those of X-ray diffraction.

To determine the stress, the strain in the crystal lattice must be measured for at least two precisely known orientations relative to the sample surface. Therefore, X-ray diffraction residual stress measurement is applicable to materials that are crystalline, relatively fine grained, and produce diffraction for any orientation of the sample surface. Samples may be metallic or ceramic, provided a diffraction peak of suitable intensity and free of interference from neighbouring peaks can be produced in the high back-reflection region with the radiations available. X-ray diffraction residual stress measurement is unique in that macroscopic and microscopic residual stresses can be determined non-destructively.

Macroscopic stresses, or macrostresses, which extend over distances that are large relative to the grain size of the material, are of general interest in design and failure analysis. Macrostresses are tensor quantities, with magnitudes varying with direction at a single point in a body. The macrostress for a given location and direction is determined by measuring the strain in that direction at a single point. When macrostresses are determined in at least three known directions, and a condition of plane stress is assumed, the three stresses can be combined using Mohr's circle for stress to determine the maximum and minimum residual stresses, the maximum shear stress, and their orientation relative to a reference direction. Macrostresses strain many crystals uniformly in the surface. This uniform distortion of the crystal lattice shifts the angular position of the diffraction peak selected for residual stress measurement.

Microscopic stresses, or microstresses, are scalar properties of the sample, such as per cent of cold work or hardness, that are without direction and result from imperfections in the crystal lattice. Microstresses are associated with strains within the crystal lattice that traverse distances on the order of or less than the dimensions of the crystals. Microstresses vary from point to point within the crystal lattice, altering the lattice spacing and broadening the diffraction peak. Macrostresses and microstresses can be determined separately from the diffraction-peak position and breadth.

Principles of X-ray diffraction stress measurement

Figure 1 shows the diffraction of a monochromatic beam of X-rays at a high diffraction angle (2θ) from the surface of a stressed sample for two orientations of the sample relative to the X-ray beam. The angle ψ, defining the orientation of the sample surface, is the angle between the normal of the surface and the incident and diffracted beam bisector, which is also the angle between the normal to the diffracting lattice planes and the sample surface.

Diffraction occurs at an angle 2θ, defined by Bragg's Law: $n\lambda = 2d \sin\theta$, where n is an integer denoting the order of diffraction, λ is the X-ray wavelength, d is the lattice spacing of crystal planes, and θ is the diffraction angle. For the monochromatic X-rays produced by the metallic target of an X-ray tube, the wavelength is known to 1 part in 10^5. Any change in the lattice spacing, d, results in a corresponding shift in the diffraction angle 2θ.

Figure 1(a) shows the sample in the $\psi = 0$ orientation. The presence of a tensile stress in the sample results in a Poisson's ratio contraction, reducing the lattice spacing and slightly increasing the diffraction angle, 2θ. If the sample is then rotated through some known angle ψ (Fig. 1b), the tensile stress present in the surface increases the lattice spacing over the stress-free state and decreases 2θ. Measuring the change in the angular position of the diffraction peak for at least two orientations of the sample defined by the angle ψ enables calculation of the stress present in the

sample surface lying in the plane of diffraction, which contains the incident and diffracted X-ray beams. To measure the stress in different directions at the same point, the sample is rotated about its surface normal to coincide the direction of interest with the diffraction plane.

Because only the elastic strain changes the mean lattice spacing, only elastic strains are measured using X-ray diffraction for the determination of macrostresses. When the elastic limit is exceeded, further strain results in dislocation motion, disruption of the crystal lattice, and the formation of microstresses, but no additional increase in macroscopic stress. Although residual stresses result from nonuniform plastic deformation, all residual macrostresses remaining after deformation are necessarily elastic.

The residual stress determined using X-ray diffraction is the arithmetic average stress in a volume of material defined by the irradiated area, which may vary from square centimetres to square millimetres, and the depth of penetration of the X-ray beam. The linear absorption coefficient of the material for the radiation used governs the depth of penetration, which can vary considerably. However, in iron-, nickel-, and aluminium-base alloys, 50 per cent of the radiation is diffracted from a layer approximately 0.005 mm (0.0002 in.) deep for the radiations generally used for stress measurement. This shallow depth of penetration allows determination of macro- and microscopic residual stresses as functions of depth, with depth resolution approximately 10 to 100 times that possible using other methods.

Although in principle virtually any interplanar spacing may be used to measure strain in the crystal lattice, availability of the wavelengths produced by commercial X-ray tubes limits the choice to a few possible planes. The choice of a diffraction peak selected for residual stress measurement impacts significantly on the precision of the method. The higher the diffraction angle, the greater the precision. Practical techniques generally require diffraction angles, 2θ, greater than 120°.

Table 1 lists recommended diffraction techniques for various alloys. The relative sensitivity is shown by the value of K_{45}, the magnitude of the stress necessary to cause an apparent shift in diffraction-peak position of 1° for a 45° ψ tilt. As K_{45} increases, sensitivity decreases.

Basic procedure

Sample preparation. If the geometry of the sample does not interfere with the incident or diffracted X-ray beams, is generally minimal. Preparation of the sample surface depends on the nature of the residual stresses to be determined. If the stresses of interest are produced by such surface treatments as machining, grinding, or shot peening, the residual stress distribution is usually limited to less than 500 µm of the sample surface. Therefore, the sample surface must be carefully protected from secondary abrasion, corrosion, or etching. Samples should be oiled to prevent corrosion and packed to protect the surface during handling. Secondary abrasive treatment, such as wire brushing or sand blasting, radically alters the surface residual stresses, generally producing a shallow, highly compressive layer over the original residual stress distribution.

Fig. 1 Principles of x-ray diffraction stress measurement

(a) $\psi = 0$. (b) $\psi = \psi$ (sample rotated through some known angle ψ). D, x-ray detector; S, x-ray source; N, normal to the surface

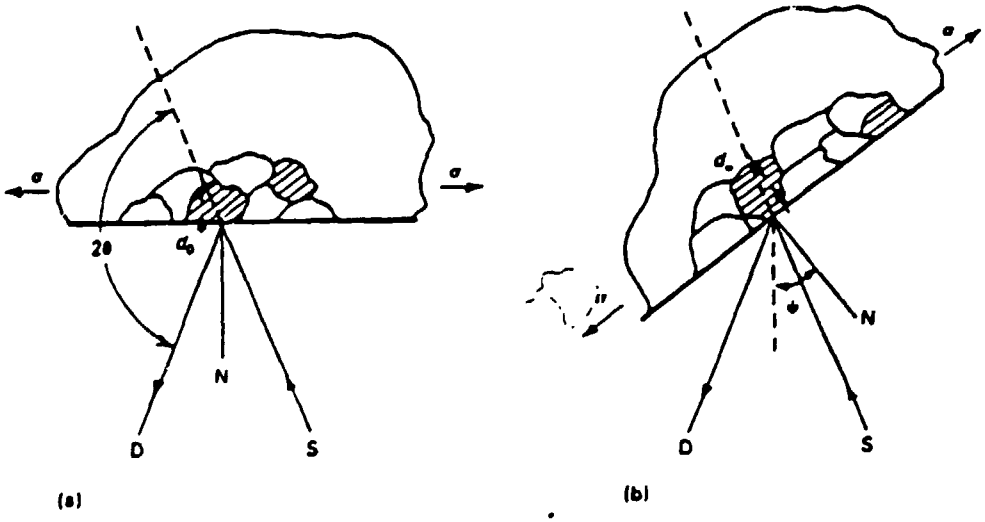

If the stresses of interest are those produced by carburizing or heat treatment, it may be advisable to electropolish the surface of the sample, which may have undergone finish grinding or sand blasting after heat treatment. Electropolishing eliminates the shallow, highly stressed surface layer, exposing the subsurface stresses before measurement.

To measure the inside surface of tubing, in bolt holes, between gear teeth, and other restrictive geometries, the sample must be sectioned to provide clearance for the incident and diffracted X-ray beams. Unless prior experience with the sample under investigation indicates that no significant stress relaxation occurs upon sectioning, electrical resistance strain-gauge rosettes should be applied to the measurement area to record the strain relaxation that occurs during sectioning. Unless the geometry of the sample clearly defines the minimum and maximum directions of stress relaxation, a full rectangular strain-gauge rosette should be used to calculate the true stress relaxation in the direction of interest from the measured strain relaxation.

Following X-ray diffraction residual stress measurements, the total stress before sectioning can be calculated by subtracting algebraically the sectioning stress relaxation from the X-ray diffraction results. If only near-surface layers are examined on a massive sample, a constant relaxation correction can be applied to all depths examined. If a significant volume of material is removed, as in determination of the stress distribution through the carburized case of a thin bearing race, a more accurate representation of sectioning relaxation can be achieved by applying strain-gauge rosettes to the inner and outer surfaces and by assuming a linear relaxation of stress through the sample.

Sample positioning. Because the diffraction angles must be determined to accuracies of approximately $\pm 0.01°$, the sample must be positioned in the X-ray beam at the true centre of rotation of the ψ and 2θ axes, and the angle ψ must be constant throughout the irradiated area. Therefore, extremely precise positioning of the sample to accuracies of approximately 0.025 mm (0.001 in.) is critical. Further, the size of the irradiated area must be limited to an essentially flat region on the sample surface. Small-diameter samples or such sample geometries as small-radius fillets, the roots of threads, and fine-pitched gears may contribute to major sources of error if the X-ray beam is not confined to an essentially flat region at a known ψ tilt on the curved surface. If the irradiated area is allowed to span a curved surface, ψ will not be constant during determination of lattice spacing. These restrictions imposed by the sample geometry may prohibit X-ray diffraction residual stress measurement in many areas of primary concern, such as the roots of notches.

Table 1 Recommended diffraction techniques, x-ray elastic constants, and bulk values for various ferrous and nonferrous alloys

Alloy	Radiation	Lattice plane (hkl)	Diffraction angle (2θ), degrees	Elastic constants (E/(1 + ν), GPa (10⁶ psi) (hkl)	Bulk	Bulk anisotropy, %	E_{bulk}, MPa	E_{bulk}, ksi	Linear absorption coefficient (μ), mm⁻¹	Linear absorption coefficient (μ), in.⁻¹
Aluminum-base alloys										
2014 T6	Cr Kα	(311)	139.0	59.4 ± 0.76 (8.62 ± 0.11)	54.5 (7.9)	−8.3	387	56.2	442	1124
2024 T351	Cr Kα	(311)	139.3	53.8 ± 0.55 (7.81 ± 0.08)	54.5 (7.9)	+1.1	348	50.5	435	1105
7075 T6	Cr Kα	(311)	139.0	60.9 ± 0.48 (8.83 ± 0.07)	53.8 (7.8)	−11.4	397	57.6		
7050 T6	Cr Kα	(311)	139.0	57.1 ± 0.41 (8.28 ± 0.06)	53.8 (7.8)	−5.8	372	54.0	443	1126
Iron-base alloys										
Incoloy 800	Cu Kα	(420)	147.2	148.2 ± 2.8 (21.5 ± 0.4)	147.5 (21.4)	−0.4	758	110.0	1656	4205
Steel	Cu Kα	(420)	147.0	157.2 ± 2.8 (22.8 ± 0.4)	151.0 (21.9)	−3.9	814	118.0	2096	5321
316	Cu Kα	(420)	146.5	132.4 ± 1.4 (19.2 ± 0.2)	153.8 (22.3)	+16.0	696	101.0	2086	5245
Inconel	Cu Kα	(420)	147.0	118.2 ± 4.1 (17.1 ± 0.6)	112.4 (16.3)	−3.8	560	81.2	1916	4130
410 (22 HRC)	Cr Kα	(211)	155.1	176.5 ± 0.7 (25.6 ± 0.1)	155.8 (22.6)	−11.7	680	98.5	840	2129
410 (42 HRC)	Cr Kα	(211)	155.1	173.1 ± 1.4 (25.1 ± 0.2)	155.8 (22.6)	−9.9	667	96.7	840	2129
1050 (56 HRC)	Cr Kα	(211)	156.0	184.1 ± 2.1 (26.7 ± 0.3)	148.2 (21.5)	−19.4	683	99.0	885	2244
4340 (50 HRC)	Cr Kα	(211)	156.0	168.9 ± 2.8 (24.5 ± 0.4)	156.5 (22.7)	−7.3	627	90.9	939	2307
8200	Cr Kα	(211)	155.5	169.6 ± 2.8 (24.6 ± 0.4)	158.9 (23.0)	−6.5	643	93.2	894	2271
9310	Cr Kα	(211)	155.5	172.4 ± 2.8 (25.0 ± 0.4)	160.0 (23.2)	−7.2	653	94.7	894	2271
52100	Cr Kα	(211)	156.0	173.7 ± 2.1 (25.2 ± 0.3)	153.8 (22.3)	−11.5	645	93.5	716	1807
M50 (62 HRC)	Cr Kα	(211)	154.0	179.3 ± 2.1 (26.0 ± 0.3)	157.9 (22.9)	−11.9	724	105.0	1000	2490
17-4PH	Cr Kα	(211)	155.0	180.0 ± 0.7 (26.1 ± 0.1)	158.9 (23.0)	−11.9	696	101.0	888	2254
Nickel-base alloys										
Inconel 600	Cu Kα	(420)	150.8	159.3 ± 0.7 (23.1 ± 0.1)	165.5 (24.0)	+3.9	724	105.0	896	2275
Inconel 718	Cu Kα	(420)	145.0	140.0 ± 2.1 (20.3 ± 0.3)	156.5 (22.7)	−8.9	772	112.0	1232	3127
Inconel X 750	Cu Kα	(420)	151.0	160.6 ± 1.4 (23.3 ± 0.2)	160.6 (24.0)	+5.0	724	105.0	813	2062
Incoloy 901	Cu Kα	(420)	146.0	134.4 ± 3.4 (19.5 ± 0.5)	158.6 (23.0)	+17.9	717	104.0	1408	3569
René 95	Cu Kα	(420)	146.7	168.9 ± 0.7 (24.5 ± 0.1)	164.1 (23.8)	−2.8	882	128.0	935	2370
Titanium-base alloys										
Commercially pure Ti	Cu Kα	(213)	139.5	90.3 ± 1.4 (13.1 ± 0.2)	84.8 (12.3)	−6.1	581	84.3	917	2320
Ti-6Al-4V	Cu Kα	(213)	141.7	84.1 ± 0.7 (12.2 ± 0.1)	84.8 (12.3)	+0.8	509	73.9	867	2203
Ti-6Al-2Sn-4Zr-2Mo	Cu Kα	(213)	141.5	102.0 ± 1.4 (14.8 ± 0.2)	86.2 (12.5)	−15.5	622	90.2	866	2200

(a) Constants determined from load-plane-bending tests; the magnitude of the stress necessary to cause an apparent shift in diffraction peak position of 1° for a 45° angle hk

Irradiated area and measurement time. The residual stress determined by X-ray diffraction is the arithmetic average stress in the area defined by the dimensions of the X-ray beam. Consideration must be given to an appropriate beam size for the nature of the stress to be investigated. If average stresses over significant areas are of interest, the maximum beam size allowed by the geometry of the sample would be an appropriate choice. If local variations in residual stress, such as those produced by individual passes of a grinding wheel, are of interest, a smaller irradiated area with a geometry appropriate for the investigation should be selected. Practical dimensions of the irradiated area may range from circular zones 1.25 mm (0.050 in.)in diameter to a range of rectangular geometries from approximately 0.5 to 13 mm (0.020 to 0.5 in.). The maximum irradiated area generally feasible is approximately 13 X 8 mm (0.5 X 0.3 in.).

As the irradiated area is increased, the data collection time necessary to achieve adequate precision for residual stress measurement diminishes. The precision with which the diffracted intensity can be determined varies as the inverse of the square root of the number of X-rays collected. To determine the intensity to an accuracy of 1 per cent at a single point on the diffraction peak, 10^4 X-rays must be counted, regardless of the time required. With diffracted intensities typically available on the fixed slit diffractometer system, this may require collection times of approximately 30 seconds for each point on the diffraction peak. If seven data points are collected on each diffraction peak for a two-angle technique, total measurement time may be 10 to 15 minutes. Reducing the irradiated area sufficiently to decrease the diffracted intensity by an order of magnitude increases the data collection time proportionally for the same precision in measurement. If fluorescence is not a problem, position-sensitive detectors can be used to collect data simultaneously at numerous points across the diffraction peak, with some sacrifice in angular precision, reducing data collection time by an order of magnitude.

Diffraction-peak location. The transition metal target X-ray tubes used for stress measurement produce a continuous spectrum of white radiation and three monochromatic high-intensity lines. The three lines are the $K\alpha_1$, $K\alpha_2$, and $K\beta$ characteristic radiations with wavelengths known to high precision. The $K\alpha_1$ and $K\alpha_2$ lines differ too little in wavelength to allow separation of the diffraction peaks produced. The $K\alpha_1$ line, the highest intensity, is nominally twice that of the $K\alpha_2$ line. The $K\beta$ line is produced at a substantially shorter wavelength and can generally be separated from the $K\alpha$ lines by filtration, the use of high-energy resolution detectors, or crystal monochromators. The $K\beta$ line and is typically one fifth the intensity of the $K\alpha_1$ line and is generally too weak for practical X-ray diffraction residual stress measurement on plastically deformed surfaces.

Because the K doublet is generally used for residual stress measurement, the diffraction peaks produced consist of a superimposed pair of peaks, as shown in figure 2, for four cases, indicating the various degrees of broadening that may be encountered. The variable blending of the $K\alpha$ doublet typical of an annealed sample is indicated by curve A; a fully hardened or cold-worked sample, curve D. Because the accuracy of X-ray diffraction residual stress measurement depends on the precision with which the diffraction peak can be located, the method used to locate broadened doublet peaks is of primary importance.

Precise determination of the position of the diffraction peak at each ψ tilt begins with collection of raw intensity data at several points on the peak. The diffracted intensity (X-rays counted per unit time) or inverse intensity (time for a fixed number of X-rays to be counted) is determined to a precision exceeding 1 per cent at several fixed diffraction angles, 2θ, spanning the diffraction peak. Depending on the method to be used for peak location, 3 to 15 individual data points and 2 background points are measured using standard diffractometer techniques. If data are collected using a position-sensitive detector, the diffracted intensity can be determined at dozens of data points spanning the diffraction peak. Sharp diffraction peaks, such as those shown in curve A in figure 2, may be located using intensity data of lower precision than that required for broad peaks, as shown in curve D. The number of X-rays to be collected, and therefore the time required for stress measurement to a fixed precision, increases as the diffraction peaks broaden.

Before determining a diffraction-peak position, the raw measured intensities must be corrected for Lorentz polarization and absorption. A sloping background intensity is then corrected by subtracting the background, assuming a linear variation beneath the diffraction peak. Various numerical methods are available to calculate the position of the diffraction peak. The simplest method, incorporated in early automated diffraction equipment, is to locate 2θ positions on either side of the peak at which the intensity is equal and assume the peak position to be at the midpoint. A straight line can be fitted to the opposing sides of the diffraction peak and the point of intersection of the two lines taken as a peak position.

A, fully annealed, B and C, intermediate hardness; D, fully hardened

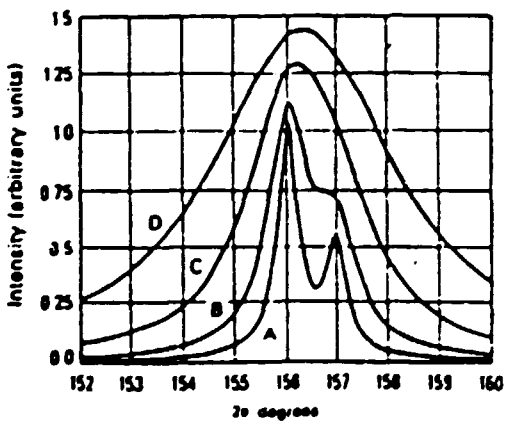

Figure 2. Range of $K\alpha$ doublet blending for a simulated steel (211) Cr K peak at 156.0°.

A significant improvement in precision can be achieved, approaching the 0.01° resolution of most diffractometers, by collecting 5 to 15 data points in the top 15 per cent and fitting a parabola by least squares regression before calculation of the peak vertex.

If the intensity is measured at many points ranging across the entire K_α doublet, the peak position can be calculated as the centroid of the area above the background or by autocorrelation. Both of these area integration methods are independent of the peak shape, but are extremely sensitive to the precision with which the tails of the diffraction peak can be determined.

All the above methods are effective, regression-fit parabola being superior, if applied to a single symmetrical diffraction-peak profile, such as the simple K_{α_1} peak shown in curve A in figure 2 or the fully combined doublet shown in curve D. All can lead to significant error in the event of partial separation of the doublet, as shown in curve B (figure 2). Partial separation commonly results from defocusing as the sample is tilted through a range of ψ angles. If residual stresses are measured as a function of depth, diffraction peaks can vary from breadths similar to curve D (figure 2) at the cold-worked surface through a continuous range of blending to complete separation beneath the cold-work layer, as shown in curve A. All the techniques of peak location discussed can lead to significant error in stress measurement as the degree of doublet separation varies.

The Rachinger correction can be applied to separate the K_α doublet before fitting parabolas, but the precision of the correction diminishes on the K_{α_2} side of the combined profile and is generally inadequate for precise residual stress measurement. Fitting Pearson VII distribution functions (Cauchy to Gaussian bell-shaped) separately to the K_{α_1} and K_{α_2} diffraction peaks, assuming a doublet separation based on the difference in wavelength, provides a method of peak location that overcomes most of the problems outlined above.

Figures 3 and 4 show the effect of the peak-location method on the results obtained. Figure 3 illustrates comparison of the same data reduced using Pearson VII distribution functions and a five-point least squares parabolic fit for ground Ti-6Al-4V using the (21.3) planes for residual stress measurement. Apparent nonlinearities in d versus $\sin^2 \psi$ for the parabola fit are due to inaccurate diffraction-peak location in the presence of partial blending of the K_α doublet. Figure 4 shows the errors in stress measurement by the two methods of peak location applied to the identical data for the entire stress profile. The errors for the distribution function fit are smaller than the plotting symbols at all depths.

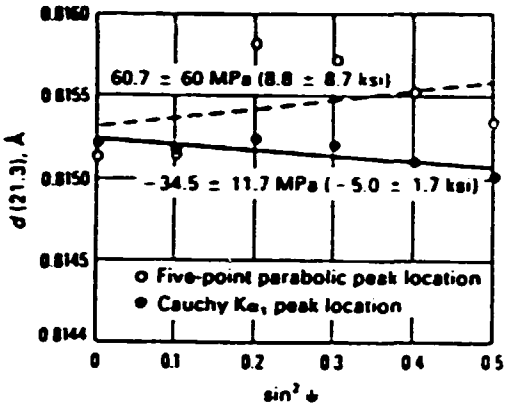

Figure 3. Comparison of d (21.3) versus $\sin^2 \psi$ data taken 0.176 mm (0.0069 in.) below the surface for a ground Ti-6Al-4V sample using two diffraction-peak location methods

Fig. 4. Comparison of residual stress patterns derived using Cauchy and parabolic peak location for a ground Ti-6Al-4V sample using a six-angle $\sin^2 \psi$ technique

Errors in stress measurement by two methods of diffraction-peak location are shown.

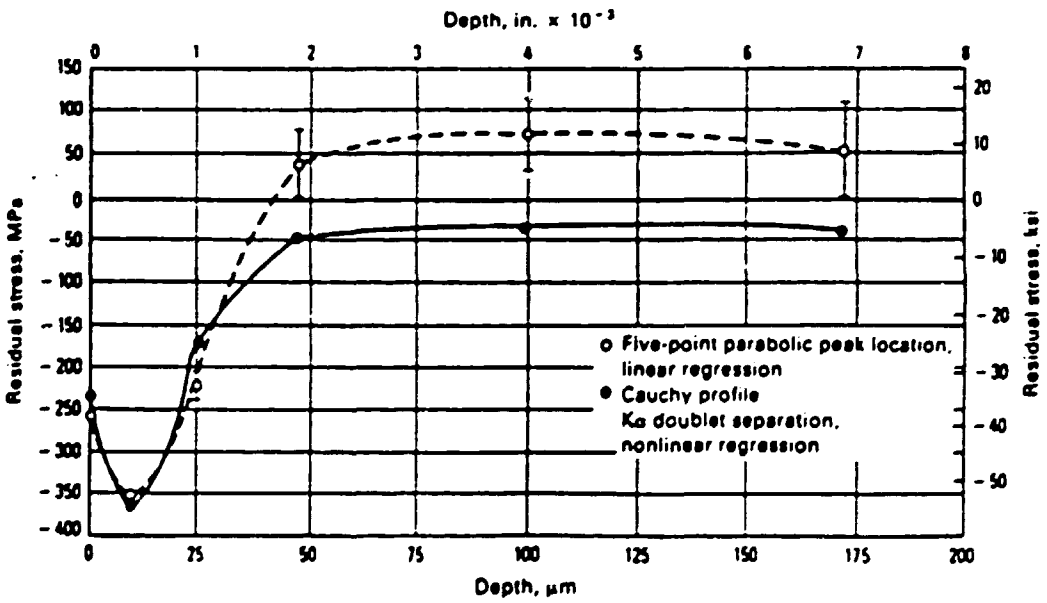

Microstress determination and line broadening. Diffraction peak broadening caused by microstresses in the crystal lattice can be separated into components due to strain in the crystal lattice and crystallite size. Separation of the broadening, which is of instrumental origin, from that due to lattice strain and crystallite size is performed using Fourier analysis of the diffraction-peak profile and data collection sufficient to define precisely the shape of the entire diffraction peak. Analysis of the Fourier series terms allows separation of the components of the broadening attributable to lattice strain from that caused by reduction in the crystallite size. However, this method requires extensive data collection and depends on the precision with which the tails of the diffraction peak can be separated from the background intensity.

For most routine analyses of microstresses associated with cold working or heat treatment for which separation of the strain and size components is not necessary, much simpler determinations of diffraction-peak breadth are adequate. The diffraction-peak width can be quantified precisely as the integral breadth (total area under the peak divided by diffraction-peak height) or the width at half the height of the diffraction peak. The width of the diffraction peak can be measured directly from strip-chart recordings or calculated from the width of the function fitted to the diffraction-peak profile during macrostress measurement. Microstresses and macrostresses can then be determined simultaneously from the peak breadth and position.

Sample fluorescence complicates the selection of radiation to be used for residual stress measurement. The radiation necessary for the highest precision techniques may cause fluorescence of the elements present in the sample under investigation. The use of Cu K_α radiation for residual stress measurement in alloys containing iron, chromium, or titanium can result in fluorescent background intensities many times as intense as the diffracted radiation, greatly reducing the signal-to-noise ratio. Problems with fluorescence may be overcome in some cases by use of metal foil filters, but generally require use of a crystal monochromator or high energy resolution solid-state detector. Failure to eliminate fluorescence can degrade severely the precision with which the diffraction peak can be located accurately, increasing random experimental error significantly. Diffracted-beam monochromators and solid-state detectors can be used only on standard laboratory diffractometers. The position-sensitive detectors available for residual stress measurement are the gas-filled proportional counter or fluorescence screen type and have insufficient energy resolution to overcome fluorescence.

Sources of error

Instrumental and positioning errors. The principal sources of error in X-ray diffraction residual stress measurement are related to the high precision with which the diffraction-peak position must be located. Errors of approximately 0.025 mm (0.001 in.) in alignment of the diffraction apparatus or positioning of the sample result in errors in stress measurement of approximately 14 MPa (2 ksi) for high diffraction angle techniques and increase rapidly as the diffraction angle is reduced.

Instrument alignment requires coincidence of the θ and Ψ axes of rotation and positioning of the sample such that the diffracting volume is centred on these coincident axes. If a focusing diffractometer is used, the receiving slit must move along a true radial line centered on the axes of rotation. All these features of alignment can be checked readily using a stress-free powder sample. If the diffraction apparatus is property aligned for residual stress measurement, a loosely compacted powder sample producing diffraction at approximately the Bragg angle to be used for residual stress measurement should indicate not more than $\pm$14 MPa ($\pm$2 ksi) apparent stress. Alignment and positioning errors result in systematic additive error in residual stress measurement.

Effect of sample geometry. Excessive sample surface roughness or pitting, curvature of the surface within the irradiated area, or interference of the sample geometry with the diffracted X-ray beam can result in systematic error similar to sample displacement. Coarse grain size, often encountered in cast materials, can lessen the number of crystals contributing to the diffraction peak such that the peaks become asymmetrical, resulting in random error in diffraction-peak location and residual stress measurement. Rocking of coarse-grained samples about the ψ axis through a range of a few degrees during measurement can be used to increase the number of crystals contributing to the diffraction peak in coarse-grained samples to allow residual stress measurement on samples with a grain size as large as ASTM No. 1. Residual stress generally cannot be measured reliably using X-ray diffraction in samples with coarser grain sizes.

X-ray elastic constants. A major source of potential systematic proportional error arises in determination of the X-ray elastic constants $(E/1 + \nu)_{(hkl)}$. The residual stress measured is proportional to the value of the X-ray elastic constants, which may differ by as much as 40 per cent from the bulk value due to elastic anisotropy. The X-ray elastic constant must be determined empirically by loading a sample of the material to known stress levels and measuring the change in the lattice spacing as a function of applied stress and Ψ tilt. The X-ray elastic constant can then be calculated from the slope of a line fitted by least squares regression through the plot of the change in lattice spacing for the Ψ tilt used as a function of applied stress.

Table 1 lists elastic constants determined in four-point bending for various alloys along with the bulk elastic constants and the potential systematic proportional error that could result from use of the bulk values. X-ray elastic constants should be determined whenever possible to minimize systematic proportional error.

Subsurface measurement and required corrections

Measuring residual stress distributions as functions of depth into the sample surface necessitates electropolishing layers of material to expose the subsurface layers. Electropolishing is preferred for layer removal because no residual stresses are induced, and if properly performed, preferential etching of the grain boundaries does not occur. Any mechanical method of removal, regardless of how fine the abrasive or machining method, deforms the surface and induces residual

stresses, altering severely the state of stress present in the sample. Such methods must be avoided. Thick layers can be removed using a combined machining or grinding procedure, followed by electropolishing to remove at least 0.2 mm (0.008 in.) of material to eliminate the machining or grinding residual stresses.

Subsurface stress gradients. Although the X-ray beam penetrates only to shallow depths (approximately 0.005 mm, or 0.0002 in.) beneath the exposed surface, the residual stress distributions produced by machining and grinding may vary significantly over depths of this order. Because the X-ray beam is attenuated exponentially as it passes into and out of the sample, stress measurements conducted in the presence of such a subsurface stress gradient yield an exponentially weighted average of the stress at the exposed surface and in the layers below. The intensity of the radiation penetrating to a depth χ is:

$$I(x) = I_0 e^{-\mu x}$$

where I_0 is the initial intensity, μ is the linear absorption coefficient, and e is the natural logarithm base (2.71828...). If the linear absorption coefficient is known, this exponential weighting can be unfolded provided measurements have been conducted at a sufficient number of closely spaced depths to define the stress gradient adequately. Correction for penetration of the radiation into the subsurface stress gradient requires calculating the derivative of the lattice spacing at each ψ tilt as a function of depth. The linear absorption coefficient is calculated from the chemical composition, mass absorption coefficients for the elemental constituents of the alloy, density of the alloy, and radiation used. Failure to correct for penetration of the radiation into the stress gradient can lead to errors as large as 345 MPa (50 ksi).

Significant relaxation of stress in the surface exposed by layer removal can occur in determination of subsurface residual stresses. If the sample geometry and nature of the residual stress distribution conform to the simple symmetries of flat plates or cylindrical bodies, closed-form solutions are available to correct the results obtained on the surfaces exposed by electropolishing for removal of the stressed layers above. These corrections involve integration over the residual stress measured in the layers removed from the exposed layer back to the original surface. The accuracy of these corrections depends on the depth resolution with which the stress distribution is measured. Correction for layer removal can be combined with correction for sectioning to determine the total state of residual stress before dissection of the sample.

The magnitude of the layer-removal stress-relaxation correction, which depends on the stress in the layers removed and the sample geometry, increases with the total strain energy released. For massive samples from which only thin layers have been removed or for any sample geometry in which no significant stresses are present, correction will be insignificant. However, the correction can be large for some combinations of stress distribution and geometry.

Many components, such as gear teeth and turbine blades, do not conform to the simple geometries and assumed stress fields to which the closed-form layer-removal corrections apply. For these geometries, electropolishing in a confined pocket to minimize stress relaxation, which is assumed to be negligible, is the only practical approach.

Applications

The following examples result from investigations performed on horizontal laboratory diffractometers modified for stress measurement and instrumented with a lithium-doped silicon solid-state detector for suppression of sample fluorescence. The examples implement the two-angle technique and the fitting of a parabola to the top 15 per cent or a Cauchy profile of the entire diffraction peak, as appropriate for the symmetry of the diffraction peaks produced. Results were corrected for Lorentz polarization and absorption as well as a sloping background intensity. Subsurface results were corrected for penetration of the radiation into the subsurface stress gradient and for sectioning and layer removal stress relaxation, as appropriate.

The elastic constants used to calculate macroscopic stress from strain in the crystal lattice were obtained empirically by loading an instrumented beam of the alloy under investigation in four-point bending. The samples were positioned to the centre of the diffractometer using a feeler gauge capable of repeat positioning precision of $\pm$ 0.05 mm ($\pm$0.002 in.). The alignment of the diffractometers was established and checked using nickel or iron powder in accordance with ASTM E 915.

Example 1: Subsurface residual stress and hardness distributions in an induction-hardened steel shaft. The longitudinal residual stress and hardness distributions through the case produced by induction hardening of a 1070 carbon steel shaft were investigated to qualify a modification of the induction-hardening procedure. The sample consisted of a nominally 205 mm (8 in.) long shaft of complex geometry; a 16 mm (5/8 in.) diameter induction-hardened bearing surface was the region of interest.

The sample was first sectioned to approximately 100 mm (4 in.) in length to facilitate positioning on the diffractometer. Because the sample was cut a distance of several diameters from the area of interest, no attempt was made to monitor sectioning stress relaxation, assumed to be negligible. X-ray diffraction macroscopic residual stress measurements were performed using the two-angle Cr K_α (211) technique in the longitudinal direction as a function of depth to approximately 4 mm (0.16 in.) beneath the original surface, fully removing the hardened case. The material was removed by electropolishing complete cylindrical shells as necessary to correct for layer removal stress relaxation using closed-form solutions. Simultaneous determinations of the breadth of the Cauchy diffraction-peak profile fitted to the K_{α_1} peak were used to calculate the hardness of the material using an empirical relationship.

Example 2: Residual stress and per cent cold work distribution in belt-polished and formed Inconel 600 tubing. Inconel 600 tubing of the type used for steam generators subject to potential stress corrosion cracking is fabricated by cross roll straightening and belt polishing of the outer

diameter surface. Belt polishing induces subsurface residual stress and cold-work distributions, which can impact on the state of residual stress present in the tubing when it is formed into U-bends.

A single sample of mill-annealed and belt-polished straight tubing was investigated to determine the longitudinal subsurface residual stress and per cent plastic strain distribution as functions of depth produced by belt polishing. X-ray diffraction macro- and microstress measurements were performed using a Cu K_α (420) two-angle technique. The $K_{\alpha 1}$ diffraction peak was separated from the doublet by fitting a Cauchy diffraction-peak profile. The X-ray elastic constant required had been determined previously by loading a sample of the alloy in four-point bending. An empirical relationship was established by annealing, then drawing samples of tubing to plastic strain levels in excess of 20 per cent, generating an empirical relationship.

The subsurface longitudinal residual stress and percent plastic strain distributions were determined by electropolishing thin layers of material in complete cylindrical shells from around the circumference of the 16 mm (0.625 in.) nominal diameter tubing. Layer removal began with 0.005 mm (0.0002 in.) thick layers near the sample surface, the increment between layers increasing with depth to nominally 0.4 mm (0.017 in.) beneath the original surface. Corrections were applied for the stress gradient and layer removal.

A 63 mm (2.5 in.) U-bend manufactured from Inconel 600 tubing was strain gauged at the apex and sectioned to remove approximately a 50 mm (2 in.) arc length. This portion of the U-bend was mounted in a special fixture providing precision orientation around the circumference of the tubing to an accuracy of 0.1°. X-ray diffraction residual macrostress measurements were made on the existing surface as a function of angle θ around the circumference of the tubing.

Example 3: Local variations in residual stress produced by surface grinding. The high spatial resolution of X-ray diffraction residual stress measurement was applied to determine the longitudinal surface and subsurface residual stress variation near grinder burns produced by traverse grinding of a sample of 4340 steel with a hardness of 50 HRC. Three samples were initially investigated: two were ground abusively to produce grinder burn, and one was ground gently using adequate coolant. X-ray diffraction residual stress measurements were performed initially on only the surfaces of the three samples using a Cr K_α (211) two-angle technique. The diffraction-peak positions were located using a five-point parabolic regression procedure, assuming the K_α doublet to be completely blended into a single symmetrical peak for all measurements performed in the hardened material. The irradiated area was 0.5 by 6.4 mm (0.020 by 0.250 in.), with the long axis aligned in the grinding direction. Measurements were conducted using the narrow irradiated area as a function of distance across the surface of each sample. A single measurement using a 12.5 by 6.4 mm (0.5 by 0.250 in.) irradiated area spanning nearly the entire region covered by the series of measurements made with the smaller irradiated zone was then performed on each sample.

The residual stresses produced by many grinding and machining operations can vary significantly over local distances, particularly if there is significant heat input, loss of coolant, or tool dulling. Further, use of a non-destructive surface measurement of residual stress or a nital etch to reveal grinder burn may not reveal subsurface tensile residual stresses that could degrade fatigue performance severely.

Example 4: Longitudinal residual stress distribution in welded railroad rail. Continuously welded railroad rail may be subject to high tensile or compressive applied stresses resulting from thermal contraction and expansion in the field. The presence of significant residual stresses in the flash butt welded joints of such rail could contribute to failure near the welds.

To determine the longitudinal residual stresses in the hardened head of welded rail near the weld, a nominally 200 mm (8 in.) portion of rail containing the weld was band sawed from a section of continuous rail after welding. Sectioning stress relaxation was assumed to be negligible.

The surface of the rail head was prepared by electropolishing to a nominal depth of 0.25 mm (0.010 in.) to remove any surface residual stresses that may have originated from sources other than welding. X-ray diffraction longitudinal residual stress measurements were then conducted using the two-angle technique at a series of positions across the centre line of the weld, which was located by etching with nital before electropolishing. A Cr K_α (211) technique was used, locating the diffraction peak using a parabolic regression procedure. The rail head was induction hardened, and the K_α doublet was completely blended and symmetrical throughout the hardened head portion of the rail.

The analytical methods for predicting the residual stresses produced by welding generally predict a symmetrical residual stress distribution around the weld fusion line; however, the actual stress distributions revealed by measurement are often substantially more complex than those predicted.

Example 5: Determination of the magnitude and direction of the maximum residual stress produced by machining. The direction of maximum residual stress, that is, most tensile or least compressive, is assumed to occur in the cutting or grinding direction during most machining operations. This is frequently the case, but the maximum stress often occurs at significant angles to the cutting direction. Furthermore, the residual stress distributions produced by many cutting operations, such as turning, may be highly eccentric, producing a highly tensile maximum stress and a highly compressive minimum stress.

The residual stress field at a point, assuming a condition of plane stress, can be described by the minimum and maximum normal principal residual stresses, the maximum shear stress, and the orientation of the maximum stress relative to some reference direction. The minimum stress is always perpendicular to the maximum. The maximum and minimum normal residual stresses, and their orientation relative to a reference direction, can be calculated along with the maximum shear stress using Mohr's circle for stress if the stress σ_θ is determined for three different values of θ.

To investigate the minimum and maximum normal residual stresses and their orientation produced by turning an Inconel 718 cylinder, X-ray diffraction residual stress measurements were performed in the longitudinal, 45°, and circumferential directions at the surface and at subsurface layers to a nominal depth of 0.1 mm (0.004 in.), exposing the subsurface depths by electropolishing complete cylindrical shells around the cylinder. The cylinder was nominally 19 mm (0.75 in.) in diameter and uniformly turned along a length of several inches. The irradiated area was limited to a nominal height of 1 mm (0.05 in.) around the circumference by 2.5 mm (0.10 in.) along the length. Measurements were conducted using a Cu $K\alpha$(420) two-angle technique, separating the $K\alpha_1$ peak from the doublet using a Cauchy peak profile.

The measurements performed independently in the three directions were combined using Mohr's circle for stress at each depth to calculate the minimum and maximum normal residual stresses and their orientation defined by the angle ϕ, which was taken to be a positive angle counterclockwise from the longitudinal axis of the cylinder. (Extracted from an article written by Paul S. Prevey, Lambda Research, Inc. Article courtesy Prof. L. Cartz)

4. X-RAY TOPOGRAPHY

General uses

- Imaging of individual lattice defects, such as dislocations, twins, and stacking faults, in near-perfect crystals
- Non-destructive characterization of surface relief, texture, lattice distortion, and strain fields due to defects and defect accumulations in imperfect single crystals and polycrystalline aggregates
- Measurement of crystal defect densities as well as crystallite subgrain sizes and shapes
- Evaluation of tilt angles across subgrain boundaries, interfacial defects and strains, domain structures, and other substructural entities

Examples of applications

- Study of crystal growth, recrystallization, and phase transformations, focusing on crystal perfection and attendant defects
- Characterization of deformation processes and fracture behaviour
- Correlation between crystal defects and electronic properties in solid-state device materials
- Synchrotron radiation extends the use of topography to permit the study of dynamic processes, such as magnetic domain motion, in situ transformations (solidification, polymerization, recrystallization), radiation damage, and yielding

Samples

- Form: For defect imaging (transmission or reflection case), flat, relatively perfect ($<10^6$ dislocations/cm^2) single crystals with uniform thickness or wedge shape. Evaluation of lattice distortions, texture, substructure, and surface relief in monocrystals, polycrystalline aggregates, ceramic or metal alloys, or composites
- Size: 1 X 1 cm (0.4 X 0.4 in.), 1 µm to several millimeters thick, up to 5 cm (2 in.) diameter or larger wafers; thin films 100 nm and thicker
- Preparation: Usually desirable to remove surface damage due to cutting, abrading, and so on, from virgin material by chemical or electrolytic polishing

Limitations

- Sample must be crystalline
- Relatively defect-free crystals required for defect imaging techniques
- Thickness of single-crystal or polycrystalline samples that can be studied in transmission arrangement is limited by intensity and wavelength of incident radiation used as well as absorption by the sample
- Direct images are actual size. Further magnification must be obtained optically; that is, grain size of photographic plate emulsion must be small enough to allow substantial enlargement

Estimated analysis time

- Several minutes to hours exposure time for conventional photographic (plate or film) methods, in addition to developing/enlarging time
- Milliseconds to several seconds using synchrotron radiation and/or electronic or electro-optical imaging systems

Capabilities of related techniques

- Optical metallography: Characterization of grain size and shape, subgrains, phase morphology, and slip traces using suitable etchants; estimation of low dislocation densities and determination of slip systems by etch pit techniques
- Scanning electron microscopy: Observation of irregular surfaces, surface relief, and various features induced by deformation, such as slip bands and rumpling; examination of fracture surfaces to evaluate crack initiation and propagation
- Electron channeling: Qualitative evaluation of crystal perfection over shallow surface layer of crystals with high symmetry orientations
- Transmission electron microscopy: Imaging of line and planar defects and estimation of defect densities; substructural and morphological characterization of thin foils prepared from bulk sample or replicas taken from the surface

- Neutron diffraction and topography: Study of very thick or heavy metals in transmission arrangement and of magnetic domain structure

Introduction

X-ray topography is a technique that comprises topography and X-ray diffraction. The term topography refers to a detailed description and mapping of physical features in a region. In the context of X-ray diffraction, topographic methods are used to survey the lattice structure and imperfections in crystalline materials. The method and procedure used depend largely on the density of defects present and the nature of the crystalline material to be examined, but all methods share the capability for non-destructive application. Research in the semiconductor/device and structural/ mechanical materials industries, both of which use topographic techniques extensively, is focused on the study of similar features of the crystal lattice, but on different levels.

For large, nearly perfect crystals, images of individual defects may be obtained and recorded on photographic plates or film. Defects near the surface can be completely characterized and defined using reflection topography (the Bragg case); defects in the bulk can be probed using transmission techniques (the Laue case) (figure 1). For relatively imperfect crystals, reflection topography can be applied to evaluate surface relief, small changes in crystallographic orientation, and the strains associated with the accumulation and or interaction of various types of lattice defects in the near surface layer. X-ray topography can also be used to study the microstructural changes, lattice defects, strain distribution, and texture induced by thermal and deformation processing and during the service of polycrystalline aggregates, including metal alloys, ceramics, and composites.

(a) Reflection topography (the Bragg case)
(b) Transmission topography (the Laue case) P, primary beam; R, diffracted beam; n, normal to diffraction planes; θ_B, Bragg angle

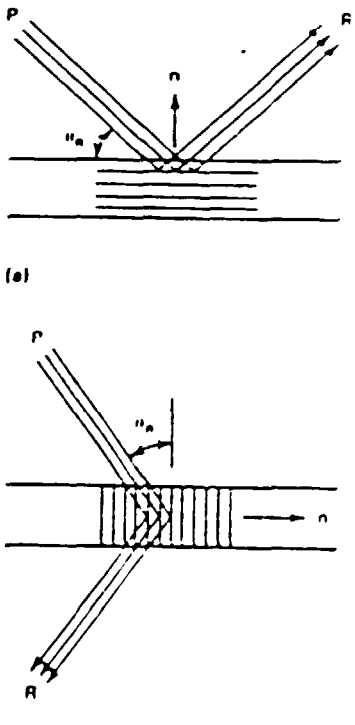

Figure 1. Arrangements for X-ray topography.

Kinematical theory of diffraction. Many X-ray diffraction techniques, such as those used for crystal structure determination, rely on uniformity in the sample, and any incidental nonuniformity in the diffraction spot is intentionally averaged using a suitable method. However, in X-ray topography, this intensity variation within the diffraction spot is of interest. The various topographic methods depend on the capability to record the microstructural detail of the diffraction spot as a diffraction profile or in a photographic image.

In theory, the diffracted intensities are attributed to a combination of kinematical and dynamical effects. The kinematical theory of diffraction accounts for the intensities reflected by ideally imperfect crystals. Such crystals are mosaic in structure, consisting of many small misaligned blocks. Only a single Bragg reflection takes place in the crystal, with waves scattered by each block interacting no further with each other or with the lattice. This readily explains the origin of contrast in a reflection topograph of a highly distorted crystal. For example, if a white (polychromatic) beam of X-rays from a point source impinges on a crystal surface, any imperfections that introduce tilts between adjacent regions cause the reflected rays to overlap partially (figure 2(a)).

(a) Polychromatic x-rays from a point source. The misoriented crystal domains are numbered 1 to 3 and separated by tilt boundaries I and II. (b) Top and side views of the line source of characteristic x-rays

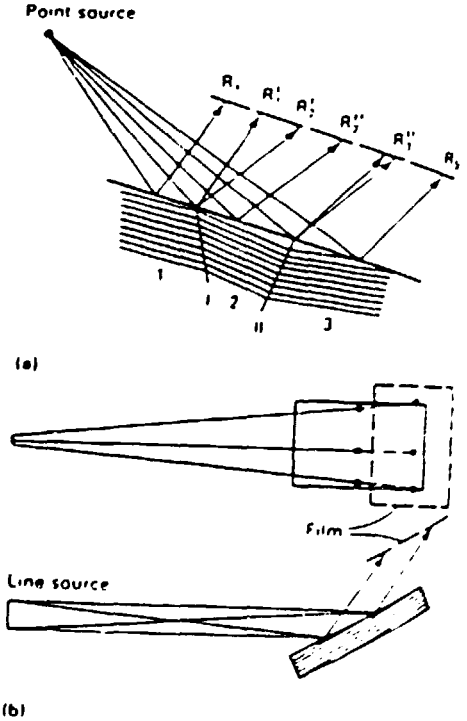

Figure 2. Two methods for obtaining reflection topographs.

A line source of monochromatic radiation used as shown in figure 2(b) produces much the same result. The primary beam has some divergence, and the deviations from a parallel lattice cause nonuniformity in the reflected intensity.

Many topographic characterizations involving metal alloys and other mechanical/structural materials require only consideration of kinematical diffraction. Rather than imaging materials on the basis of differences in X-ray absorption, as in X-ray radiography, the topographic techniques applied to polycrystals exploit the elastically (diffracted) and inelastically scattered X-rays. This allows diverse structural features, usually associated with the particular crystal structure and orientation, to be imaged in materials exhibiting only minor variations in X-ray absorption.

The dynamical theory of diffraction treats the stronger wave interaction present in near-perfect crystals, for which multiple diffraction occurs. This contribution to X-ray diffraction phenomena enables the imaging of individual crystal defects, making X-ray diffraction topography a useful tool for characterizing and evaluating solid-state device materials.

The first predictions based on dynamical theory, and later observed experimentally using double-crystal diffractometry, were that the angular range of reflection for a perfect crystal would be narrow (seconds of arc) and that the integrated intensity would be orders of magnitude less than that for a similar but imperfect crystal (figure 3(a)). The latter phenomenon was rationalized by accounting for the attenuation of the incident beam due to the normal photoelectric absorption and to coherent scattering and multiple diffraction - the so-called primary extinction effect associated with successive reflections by many perfectly parallel places (figure 3(b)).

The two- and many-beam cases considered the refraction, absorption, and propagation directions of the wave fields. Several significant consequences are evident regarding the flow of X-ray energy in and through perfect crystals. In the two-beam case (only the incident and reflected waves were considered), the portion of the primary beam entering, or accepted by, the crystal when set an angle satisfying the Bragg condition consists of a wave bundle with a small divergence (limited to several seconds of arc). By virtue of dynnamical interaction, the forward (O) and reflected (h) waves generate four wave fields within the perfect crystal - two wave fields for the σ and π polariza- tion modes, respectively. The angular spread of the wave fields, termed the Borrmann fan, extends through the angle of $2\theta_B$ (figure 4(a)). For thin crystals, that is, $\mu t < 1$, where μ is the linear absorption coefficient and t is the crystal thickness, the energy flows through the entire Borrmann fan. Because each wave field propagates through the crystal with different phase velocity, a periodic exchange of energy takes place between the O and h waves. The minimum distance required to convert completely the energy of the incident O-beam into the reflected h-beam is the extinction distance. The intensities pertaining to the beams emerging from the exit surface of the crystal, designated R_O and R_h, depend on the extinction distance and crystal thickness.

(a) Reflected intensity distribution (rocking curve) for a near-perfect absorptionless crystal rotated through its angle for Bragg reflection, θ_B. (b) Attenuation of the incident beam by simple (R_h) and multiple (R_O) reflection. R_O' is 180° out of phase with R_O.

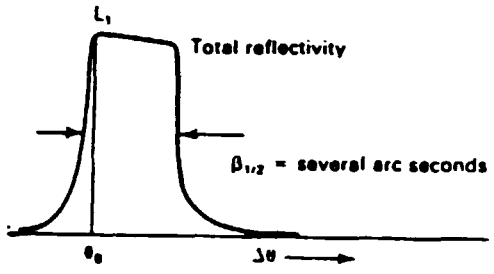

(a)

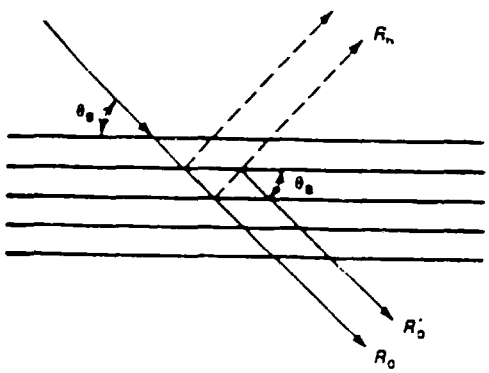

(b)

Fig. 3. Diffraction in a near-perfect crystal.

Anomalous transmission. For sufficiently thick crystals, that is $\mu t \geq 10$, the X-ray energy is confined to a much narrower fan situated about the reflecting plane half-way between k_O and k_h, as if the wave were being diffracted repeatedly by two adjacent lattice planes (figure 4(b)). Further, of the four wave fields in the crystal, those with maximum field intensity (antinodes) at the atomic planes are absorbed strongly, but those with intensity minima (nodes) at these planes suffer substantially less attenuation. As a result of the reduced effective absorption, the transmitted beam emerges from the crystal with nearly the same intensity as the reflected beam, a phenomenon known as anomalous transmission, or the Borrmann effect.

Defect imaging. If crystals are considered thin relative to the photoelectric penetration distance $1/\mu$, but thick relative to extinction distance, the capability to visualize defects derives primarily from kinematical contrast, but is made possible only through the dynamical effects associated with diffraction. In reflection topography (the Bragg case), the coupling of the incident and reflected waves as a wave field,

typical of dynamical interaction, is destroyed by the severe lattice distortion associated with the defect. Thus, the primary extinction effect is suppressed in this vicinity, and kinematic diffraction prevails. Only an incident wave bundle with a narrow angular divergence is accepted into the wave fields constituting the Borrmann fan. In practice, the primary beam has a considerably larger divergence of several minutes of arc. Distorted areas of the crystal, such as the dislocation core, can reflect some portion of this substantial intensity, producing dark contrast where normally only weak diffracted intensities would be measured. Thus, this direct image has a kinematic origin.

(a) Borrmann fan in a thin crystal. (b) Fan with reduced effective width in a thick crystal. P is the primary beam defined by slits S; k_0 and k_h are the outermost wave vectors; R_0 and R_h, the transmitted and reflected directions (toward the reciprocal lattice origin and the reciprocal lattice point $n(hkl)$). Reduced effective absorption in (b) results in anomalous transmission.

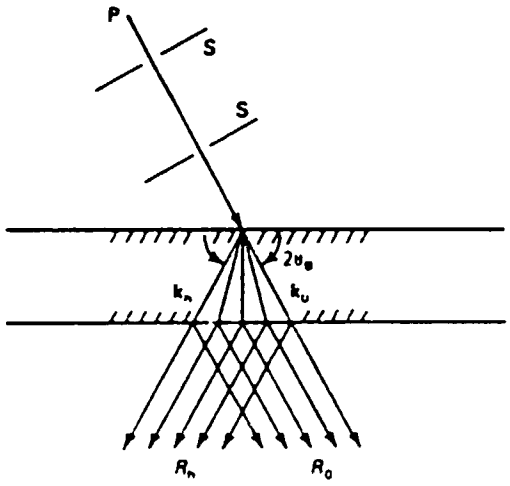

(a)

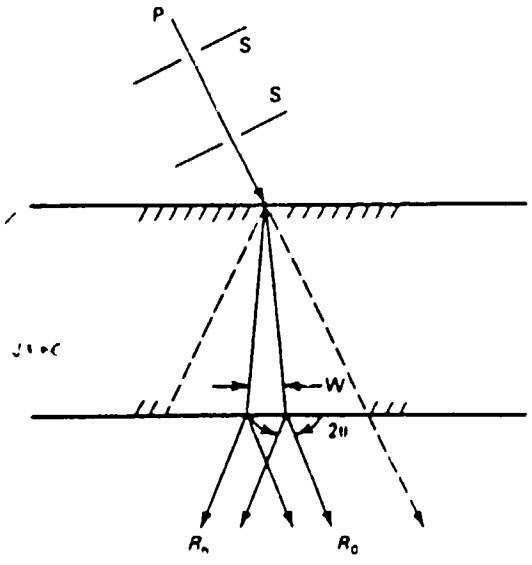

(b)

Fig. 4. The flow of X-ray energy in crystals of different thicknesses.

Contrast is also affected by the particular orientation of the defect and its strain field. The reflecting planes incurring the maximum contrast will lie perpendicular to the displacement due to strain. Therefore, for a dislocation, the plane with reciprocal vector parallel to the Burgers vector provides the greatest contrast. Because some atomic displacement also occurs perpendicular to the slip plane, planes with lattice normal in this direction contribute to the contrast. Only those lattice planes having reciprocal vectors lying normal to the plane containing the Burgers vector and the slip plane normal are devoid of contrast due to the dislocation.

A similar kinematic origin accounts for the direct image of a defect in transmission topography (the Laue case), as illustrated for a dislocation in figure 5. Passage of the dislocation through the Borrmann fan contributes to the contrast in two other ways. First, changes in the beam path and absorption caused by the strains about the dislocation weaken the wave field at a point such as C in figure 5. The wave is diverted to either side of its original direction PC. Second, interaction of the wave fields caused by the larger strains near the dislocation core result in the excitation of a new wave in the direction PC' and further attenuates the wave field at C. The resultant shadow in the reflected beam from C is the dynamic image; the enhanced intensity from C' associated with the new wave path produces the intermediate image.

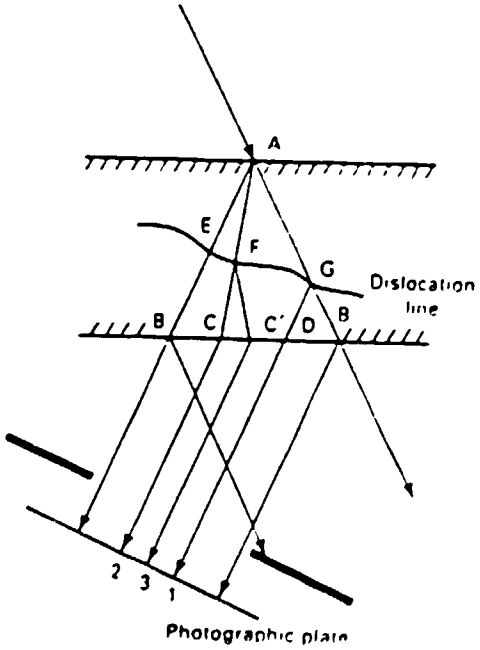

Fig. 5. Origin of direct (1), dynamical (2), and intermediate (3) image contrast for a dislocation.

Pendellösung fringes. Energy transfer between the two running waves in the crystal, k_0 and k_h, and the thickness of the crystal control the intensities of the reflections R_0 and R_h. When a photographic plate or film intercepts the reflected beam from a wedge-shaped crystal, interference, or Pendellösung fringes are recorded, lying parallel to the edge of the crystal. Pendellösung fringes can also be obtained for crystals of uniform thickness by using Lang section topography (in traverse topographs of crystals with rectangular cross section, superposition of the fringes cause smearing of the intensity contrast, preventing their disclosure). The fringes are sensitive to lattice distortion; small elastic strains bend and/or alter the fringe spacing in traverse topographs of wedge-shaped crystals, and additional fringes may appear in section topographs upon introduction of elastic strain fields to a crystal. However, plastic deformation destroys the dynamical interaction, and the fringe patterns disapear.

In thick crystals, fringe patterns are absent, because only waves subject to reduced effective absorption traverse the crystal. However, should a fault plane, such as those associated with a stacking fault or twin, lie near the surface, excitation of new waves can occur. Fringes are produced in the Borrmann fan at the exit surface due to the interference between newly scattered waves (II) and between waves that maintain the propagation directions from the original crystal orientation (I) (figure 6). Superposition of the two sets of fringes produces a pattern, or image, characteristic of the fault.

Fig. 6 Origin of fringes caused by a fault plane between crystals I and II

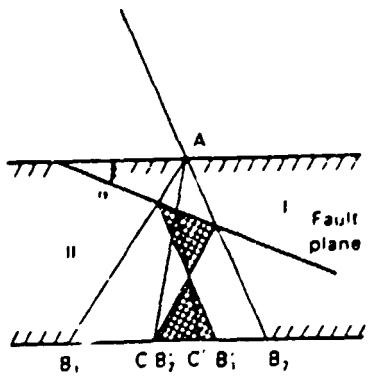

Another pattern, the X-ray analogue to bend contours in transmission electron microscopy, can be exploited to characterize strain fields in a crystal. A band(s) of enhanced intensity is typically obtained for a distorted crystal when irradiated with a monochromatic beam, owing to the limited region of the crystal that is oriented for diffraction. These equi-inclination contours occur in different locations when the crystal is rotated to a new angular position. Rotating the crystal in discrete angular increments and recording successive positions of a band in a multiple exposure produces a mapping of the contour with angle of rotation. The patterns are particularly useful for studying crystals deformed to a level at or above the macroscopic yield point, for which the dislocation density generally is too high ($> 10^{4}$ cm^{-1}) for imaging individual dislocations by conventional topography.

Methods and instrumentation

Topographic methods are employed for two primary reasons. Some methods are intended principally for use in characterizing defects in single crystals and are applied routinely in studying semiconductor substrates, thin films, and other device materials. Other techniques are useful in studying a broader spectrum of engineering materials. Appropriate selection of technique, procedure and instrumentation affords disclosure of surface relief; topological and deformation features, such as slip lines and subgrains; grain morphology; crystallographic texture; and various combinations of lattice distortion and plastic strain/cold work. These techniques can be applied non-destructively, require little or no preparation of the sample, and often permit easy and rapid scanning of relatively large areas.

Reflection topography. The most widely used reflection arrangements for X-ray topography are the Schulz and Berg-Barrett methods. These techniques are suited to the evaluation of substructure in all crystalline materials, particularly as associated with cold work, recovery, recrystallization, and precipitation hardening.

In the Schulz method, the white radiation from a fine-focus X-ray tube or microfocus generator impinges on the sample (figure 2(a)). The sample is angled approximately 25° to the direction of the diverging X-ray beam. Uniform magnification in the horizontal and vertical directions is achieved if the photographic plate is placed parallel to the crystal surface. The technique has numerous applications in crystal growth and recrystallization studies for evaluation of subgrain size and misorientations.

The Berg-Barrett method uses monochromatic radiation and a line source increases the observation range (figure 2(b)). Attainment of optimum resolution requires a narrow line width as well as maintenance of a long source-to-monochromator distance and a short sample-to-photographic plate distance. If the reflecting planes are inclined to the surface such that the angle of X-ray incidence is small and the angle of reflection approximately of 90°, the plate can be as close as 0.1 mm (0.004 in.) to the surface. In addition, penetration of the X-rays is minimized with the asymmetrical reflection, providing a sharper image. Figure 7 illustrates the reflection camera. The reduction in primary extinction caused by the strains about dislocations can be studied by observing the contrast effects for various crystallographic planes. The distribution of dislocations and the strains due to intersecting slip systems can be investigated by preparing topographs from several different reflections from the same family of planes. Another contribution to

the contrast in the image derives from surface relief inherent in the sample. Any departure from a perfectly smooth surface, such as that caused by cleavage steps, leads to shadowing.

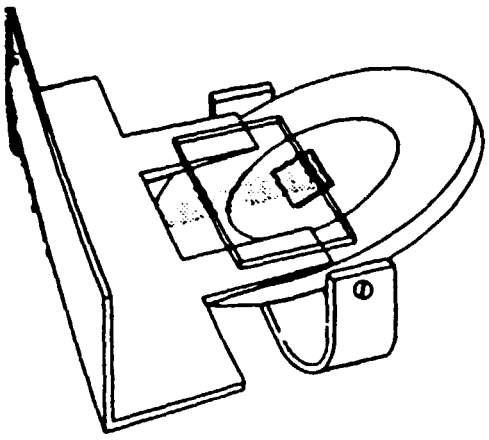

Figure 7. Camera for Berg-Barrett topography

Sample is mounted on a tilting stage (right), and the film plate is held close to the sample surface by a supporting plate that also screens the film plate from scattered incident radiation

A Berg-Barrett arrangement can also be used for topography of polycrystals. Only suitably oriented grains will diffract the incident X-rays and the shapes and intensities of the grain reflections are influenced by the inclination of the reflected rays relative to the photographic plate, the distance of each of the grains from the plate, and the particular crystallographic planes diffracting the incident rays. Nevertheless, the technique is useful in preliminary investigations of texture and of grain size and shape; special surface preparation is unnecessary.

Transmission topography. Figure 8(a) shows a transmission arrangement for a divergent beam. Parallel planes, each choosing incident rays with the appropriate wavelength for diffraction, focus the polychromatic rays impinging on the thin crystalline wafer. The existence of substructure featuring relatively perfect, polygonized domains tilted slightly relative to one another causes the focal points for the domains to be displaced from each other along the focusing circle. Figure 8(b) illustrates a transmission arrangement for the Berg-Barrett method.

In the Lang transmission arrangements, X-rays from a point focus source pass through a set of narrow slits before incidence on the sample at an angle that satisfies the Bragg diffraction for a particular set of transverse planes (figure 9(a)). For a thin crystal ($\mu t \lesssim 1$), the direct beam is prevented from intercepting the photographic plate while the reflected beam passes through an appropriately located slit on the back side of the sample. An exposure taken with the assembly held stationary (figure 9(b)) is a section topograph, in which the imaged area is confined to the width of the Borrmann fan. Synchronized translation of the sample crystal and photographic plate yields a projection, or traverse, topograph. Either Lang technique can be used to image defects.

Divergent beam method. Anomalous transmission is important to an arrangement that incorporates a divergent beam. In this experimental setup, a thin metal foil on the end of an evacuated tube is the target of an electron gun (figure 10). The foil is situated near the sample and bombarded with electrons to produce a divergent spray of characteristic radiation on the sample. An advantage of this method is that significant elastic strain can be tolerated, because the lattice planes always reflect some of the diverging rays and therefore produce the anomalous transmission pattern (R_o and R_h of nearly equal intensity). Translation of the sample past the X-ray source enables scanning of the crystal for regions with defects that interrupt the wave interactions responsible for anomalous transmission. The divergent beam arrangement also creates conditions under which deficiency and diffraction cones are recorded. Deficiency cones are caused by the removal of radiation from the original cone due to diffraction from oblique planes; diffraction cones, by diffraction in the direction of the film. Imperfection degrades the contrast inherent in these conical sections, known as pseudo-Kossel lines. Discontinuities in the lines and modifications of the shape of the patterns are useful for deducing the localized and uniform strain components, respectively.

(a) Using white radiation from a point source. (b) Using characteristic radiation from a line source.

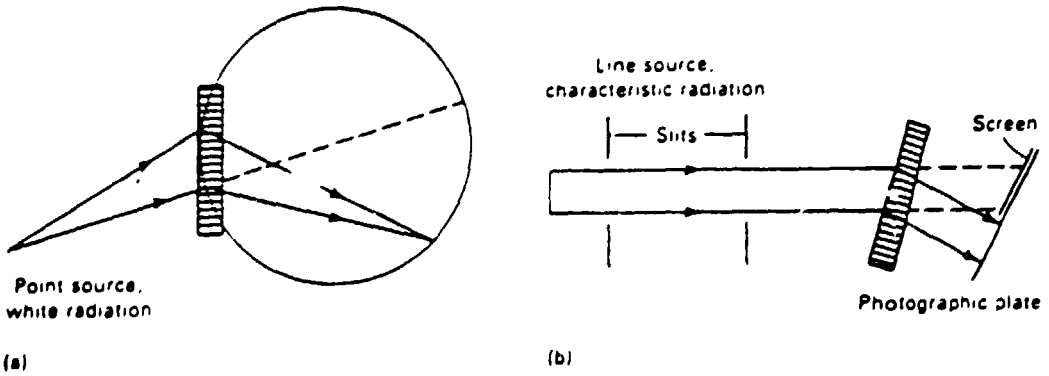

Figure 8. Configurations for transmission topography
(a) Using white radiation from a point source.
(b) Using characteristic radiation from a line source.

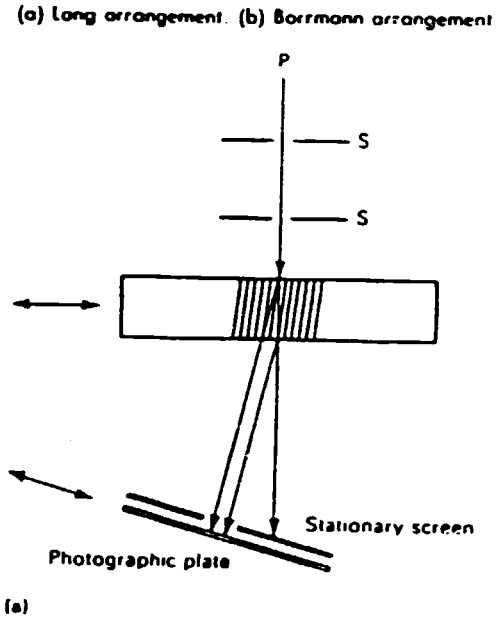

Figure 9. Defect imaging with transmission topography

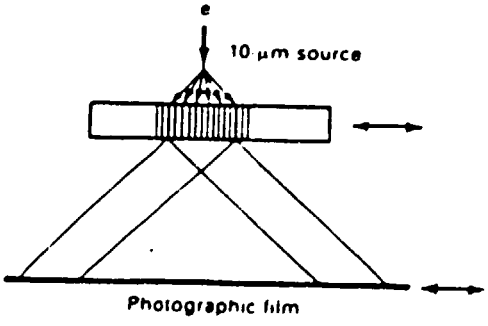

Figure 10. Divergent beam anomalous transmission method of X-ray topography

X-ray interferometry. Figure 11 shows an X-ray interferometer that exploits anomalous transmission. The interaction of the waves as they pass through and between the three crystals depends strongly on the perfection of the crystals. Distortions and displacements in the third (analyser) crystal as small as 0.001 seconds of arc and 0.01 nm respectively, are detectable. Other applications include observation of moiré fringes for edge dislocations, X-ray phase contrast microscopy, and precise measurement of X-ray refractive indices, X-ray scattering factors, and lattice constants.

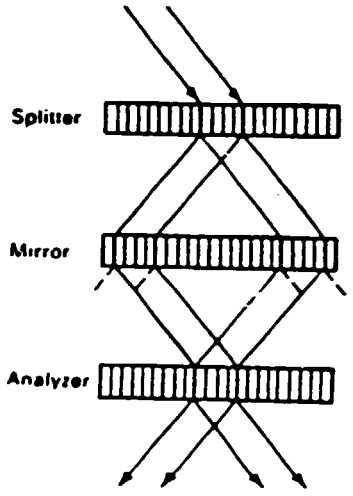

Figure 11. X-ray interferometer

Double-crystal spectrometry and polycrystal rocking curve analysis. The double-crystal spectrometer, or diffractometer, is used to determine precisely the degree of imperfection of crystalline samples. To achieve the desired sensitivity to small localized strains reflection from the first "perfect" crystal produces a monochromatic and highly parallel beam of X-rays used to probe the test crystal. Monitoring of the X-ray intensity diffracted by the test crystal as it is slowly rotated, or rocked, through the Bragg angle for the reflecting planes yields a rocking curve. Two settings for the first and second crystals are possible (figure 12 (a) and (b)). If the first and test crystals are identical in type and crystallographic orientation, the (+, -) setting has no dispersion effect, and the width of the rocking curve does not depend on the spectral spread of the incident radiation.

When the monochromator and test crystals are not identical, the arrangement is a nonparallel (+m, -n) setting, and the rocking curve is no longer independent of the spectral intensity distribution. This also holds for the (+, +) setting, for which all wavelengths reflected by the first crystal, that is, the small band of wavelengths the monochromator crystal accepts as a result of the inevitable horizontal divergence of the primary beam, will not be simultaneously reflected by the second crystal. Therefore, the breadth of the rocking curve is partly due to the extent of the spectrum of the incident radiation and therefore can be used to study the widths and fine structure of X-ray lines.

(a) (+,−) setting. (b) (+,+) setting.

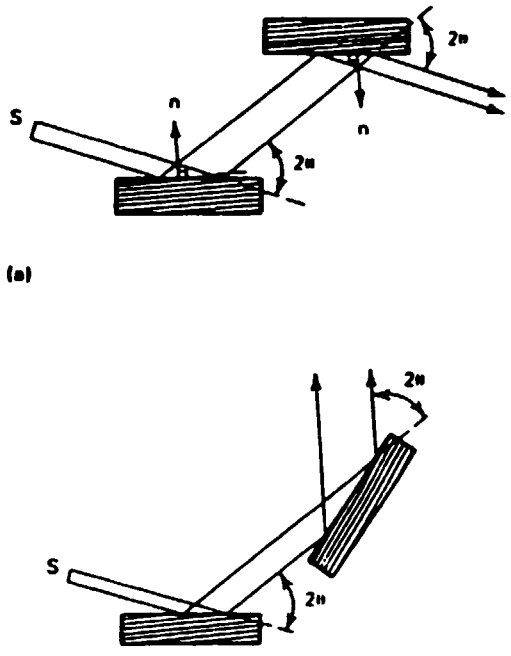

Figure 12. Double crystal diffractometer arrangements

The (+n, -n) arrangement typically provides narrow rocking curves for near-perfect crystals (a few second of arc) and is extremely sensitive to elastic deformations. If the crystal contains numerous defects, is plastically bent, or is composed of misaligned blocks, the rocking curve is broader (figure 13(a) and (b)). Under certain circumstances, the tilt angle between adjacent misoriented crystals may be accurately determined from a multimodal rocking curve (figure 13(c)).

The double-crystal arrangement becomes a true topographic technique if a film is interposed between the test crystal and the detector as in figure 14. Optimum resolution is obtained if the film is placed near the surface of the test crystal to prevent the rays emanating from distorted regions with different inclinations from crossing one another and deviating from their true spatial relationship on the surface. This is most conveniently accomplished by using asymmetric reflections. To eliminate the effect of dispersion, the $K\alpha_2$ component of the radiation reflected by the first crystal must be removed using a suitably positioned slit.

Adjustment of the second (test) crystal slightly off the maximum intensity position of the diffraction peak maximizes sensitivity to near-surface distortions and elastic strains. In highly perfect crystals, single dislocations may be resolved. For imperfect crystals, the physical origin of intensity fluctuations in the rocking curve profile can be conveniently determined by taking several topographs, each at a different angular position along the rocking curve (figure 15). Use of a position-sensitive detector parallel to the long dimension of the beam enables determination of the variation in rocking curve width along this direction on the sample. Similar measurements, made after incremental translation of the sample, allow generation of a two-dimensional mapping of the surface distortion.

To image larger areas of test crystals in a single exposure, an asymmetrically cut monochromator crystal can be used to expand the primary X-ray beam. By using two such crystals in succession, rotated 90° from one another about an axis parallel to the diffraction plane, the primary beam can be expanded and made parallel relative to the horizontal and vertical directions (see figure 14(b)).

(a) Bent crystal. (b) Crystal composed of misaligned independently reflecting domains. (c) Crystal containing a tilt boundary.

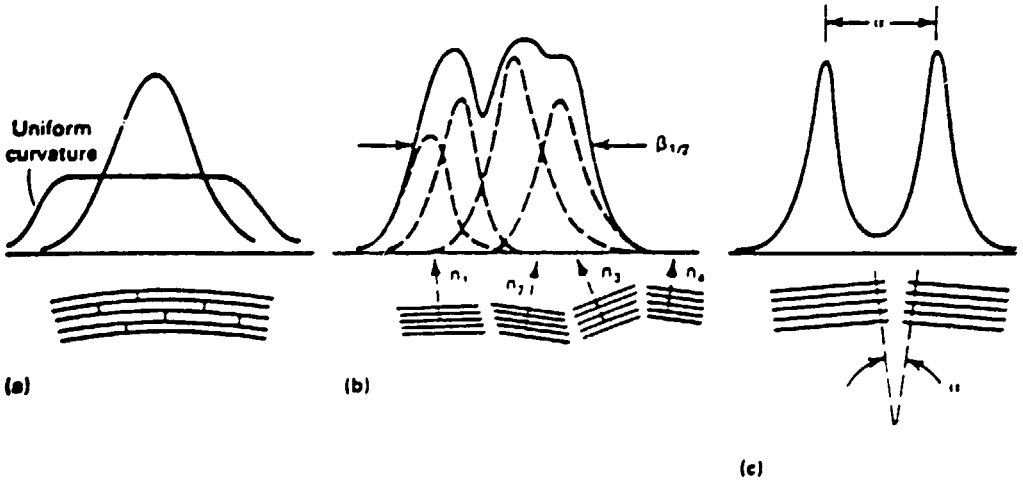

Figure 13. Intensity profiles (rocking curves)

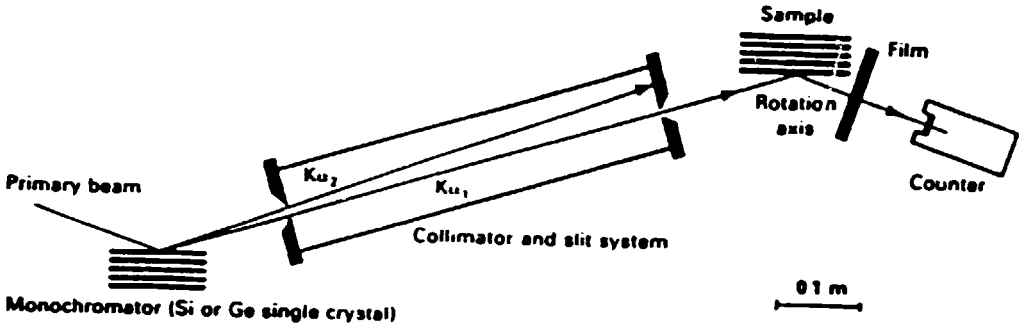

(a)

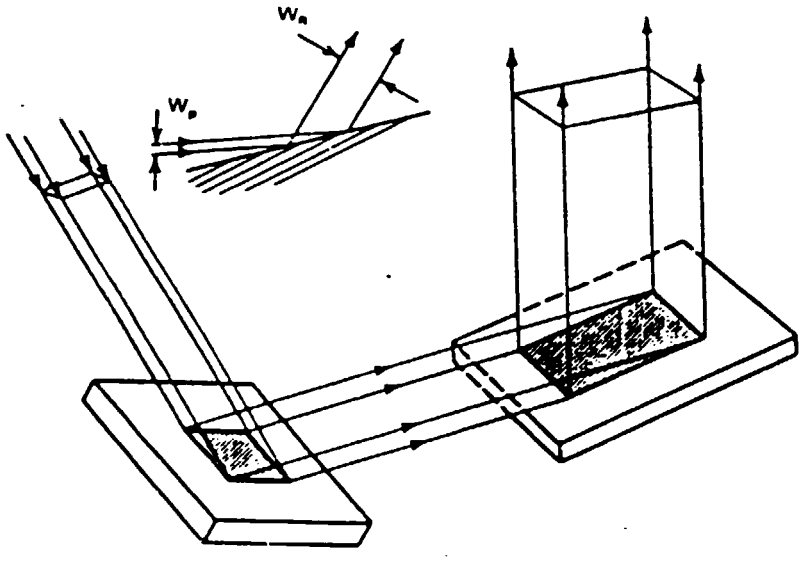

(b)

Figure 14. Double crystal diffractometer (a) and beam expansion by reflection from two asymmetrically cut crystals in succession (b)

(a) Rocking curve with (311)(123) orientation strained 5% in tension. (b) Topographs taken at angular positions 1 through 5

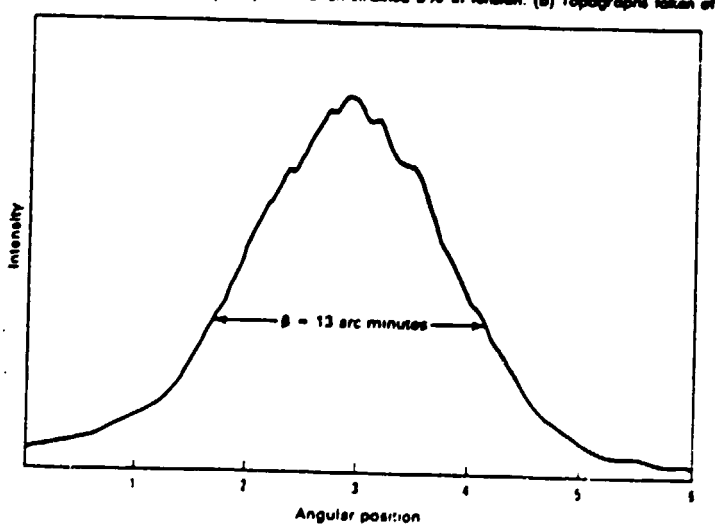

(a)

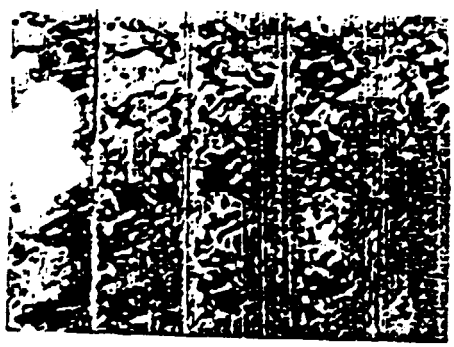

(b)

Figure 15. Rocking curve and topographs of a gold single crystal

The principles of double-crystal diffractometry have been successfully extended to study diverse polycrystalline materials. As shown in figure 16, an X-ray micrograph, or reflection topograph, can be obtained by intercepting the reflected rays from the sample material on a photographic plate positions close to and as nearly parallel as possible to the sample surface.

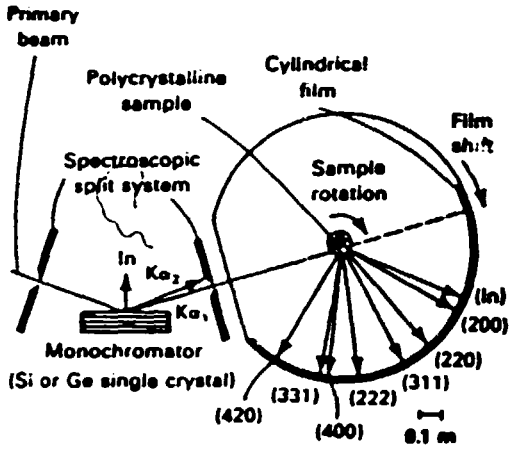

Figure 16. Double crystal diffractometer for polycrystalline samples.

Line broadening analysis and the microbeam method. Several methods for evaluating and imaging the substructure of polycrystalline materials use the typical Debye-Scherrer diffracted X-rays. These methods assist characterization of various types of strain, defect structures, and crystallographic orientation effects introduced or eliminated during material processing, treatment, or service. X-ray line broadening and integrated intensity measurements, for example, are widely used to determine microstrains, crystallite (particle) size, and fault densities. Because these methods do not provide information on the portion of the sample responsible for each component of the diffracted image, they are not topographic techniques.

The X-ray microbeam method is another approach for studying microstructural changes in polycrystalline materials. Like the double-crystal diffractometer method for polycrystalline materials, the microbeam technique allows resolution of the individual grains. Instead of using a highly parallel and monochromatic beam, the incident beam is simply restricted in size to control the number of resultant grain reflections. A microfocus generator is usually used with a 50 μm diameter, and the resolving power of the microbeam camera is approximately 1 μm. The site analysed is confined to a small area, for example, the crack initiation site in a sharp-notched fatigue specimen, but only a few grains can be imaged in a single exposure. Careful examination of the radial and tangential broadening of the reflection spot for each grain, that is, in directions normal to and along the diffraction ring, and the subdivision of the spot reveals the misorientation, lattice strain, and subgrain size within the grain.

Polycrystal scattering topography. The polycrystal scattering topographic (PST) methods sacrifice some of the resolving power of the methods described above for the capability to image considerably larger areas. Rather than exploiting variable absorption to produce an image, as is typical of radiographic techniques, these methods make use of elastic and inelastic scattering for image formation (figure 17). Therefore, the contrast does not rely on the presence of materials having large differences in X-ray absorption, but is derived from variations in crystal structure and material distribution. One of several Soller slit arrangements is used to maintain the spatial relationship of the scattered rays, providing a one-to-one correlation between the sample and the image of the emulsion plate (figure 18).

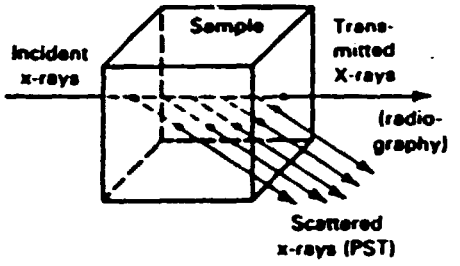

Figure 17. Basic principle of polycrystal scattering.

One geometry incorporates two Soller slits rotated 90° relative to each other and oscillated to prevent shadows from being visible. Oblique incidence of the beam on the sample, synchronous translation of the sample and slit/film cassette assembly, or expansion of the incident beam by reflection from an asymmetrically cut monochromator crystal can be used to increase the viewing area. Conventional sealed X-ray tubes are used, and a resolution of approximately 0.1 mm (0.004 in.) is obtained for transmission and reflection arrangements. Several methods implement white radiation incident on the sample: a thin pencil of rays may be used with a cone-shaped slit and x-y scanning or dual asymmetrically cut crystals may be arranged to intercept and resolve spatially diffracted rays at a selected range of azimuthal angles and to magnify the resultant image. Use of a position-sensitive detector, multichannel analyser, and CRT display allow more rapid and convenient image generation. Polycrystal scattering topography is particularly useful for evaluating the development and modification of deformation texture due to mechanical processing.

Synchrotron radiation. Synchrotron sources produce intense radiation, tunable to various wavelengths, that is advantageous for X-ray topography. A white beam used in the Laue setting allows analysis of curved crystals without compensation for the varying orientation (usually facilitated by instrumentation for automated Bragg angle control). Rapid characterization of the displacement vectors associated with various defects is possible using white beam topography. Coupled with position-sensitive or electro-optical detectors, synchrotron radiation affords the capability for monitoring dynamic processes, such as the movement of magnetic, ferroelectric, subgrain or twin domains and boundaries. Because the divergence of the incident beam is small, superior resolution is obtained even if the sample-to-detector distance is great. Therefore, ample space is available for locating furnaces, magnets, and other equipment about the sample.

Cross Soller slit method. (b) Soller slit oscillating method.

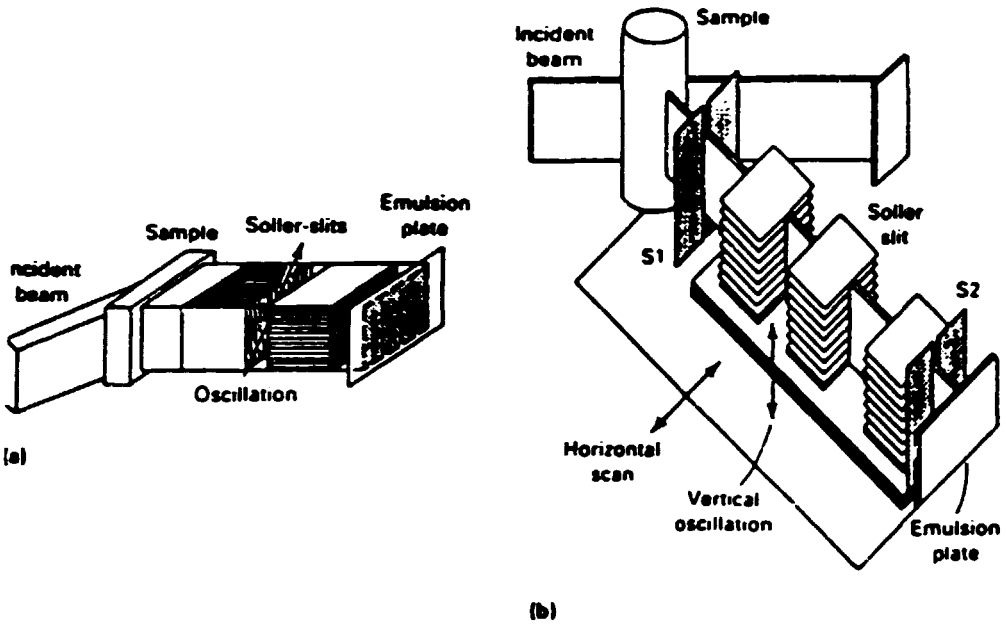

Figure 18. Two arrangements for polycrystal scattering topography

A high-intensity monochromatic beam from a synchrotron source also enhances the potential for probing small areas (approximately 1-μm spot sizes) in much the same way as electron microscopy, but non-destructively. Even thin layers produce sufficiently strong diffracted intensity, and there is less concern over intensity losses associated with attempts to expand the incident beam with a system of multiple asymmetrically cut monochromator crystals. In general, synchrotron radiation should be the next option considered when short exposure times or other special criteria demand intensities greater than those furnished by more conventional high-power laboratory generators, such as rotating anodes.

Applications

X-ray topography is well suited to three principal areas of research. The first is crystal growth and characterization of electronic device materials. Interest in single crystals is highest in the electronics industry, but single crystals - or at least highly oriented crystalline materials - are also of interest because of their favourable creep or corrosion resistance and high stiffness, for example, directionally solidified metals and alloys or fibre reinforcements in composites. In the electronics industry, an appropriate topographic method or combination of methods can reveal much about thin film and surface modified structures. The second area of research is material transformations and kinetics of crystal processes. Synchrotron radiation is particularly advantageous for these studies, because the bright beam allows the dynamic processes to be followed in situ. In the third field of application, materials deformation and fracture behaviour, the non-destructive nature of X-ray diffraction can be exploited to afford repetitive observations and measurements during deformation.

Crystal growth and electronic device material studies. X-ray topography has been used extensively to study defects produced during crystal growth. X-ray topography is useful for assessing all the microstructural features (growth bands, dislocations, faults, twins, point clusters, inclusions, and so on) that accompany crystal growth from solution or by melt, solid-state, or vapour techniques. The information gained through topographic studies enables modifications in technique, procedure, and operating conditions that enhance production of highly defect-free crystals.

The activity in electronic device development has prompted extensive application of X-ray topography. The perfection of the substrate material, the structure of any overlying films, and the defects in the interfacial region between them influence the behaviour and the performance of the device components. For example, dislocations and grain boundaries in the substrate result in device degradation by substantially reducing the minority carrier lifetime. X-ray topographic imaging and measurements of reflected intensities can be used to monitor their generation or prevalence during growth, cutting, surface preparation, and other processing/treatments of semiconductor substrates.

Rocking curve profiles obtained by double-crystal diffractometry, on the other hand, are most effective for characterizing thin films grown, deposited, or similarly produced on the surface of the substrates. Figure 19 illustrates the basic features of a diffraction scan from a sample with a thin (100 nm to several microns thick) epitaxial film. The information that can be extracted from the pattern includes (1) the misfit of the film and substrate lattices, determined from the angular separation of the diffraction peaks produced by the two lattices, (2) the composition of the film, calculated from the misfit, (3) the film

thickness, which controls the spacing and widths of the subsidiary peaks (the Pendellösung maxima located between the two primary peaks), (4) the local strain in the layer(s) is/are measured from the angular shifts of the primary peaks from the positions expected for known composition, and (5) the inherent nonuniform distortions of the layer(s) and substrate as evidenced by broadening of the respective diffraction peaks. The modification of surface layers by such processes as ion implantation affects the diffraction profiles in ways similar to those observed for newly deposited layers. For surface modification, emphasis is on evaluation of the damage, which includes atom displacements (defects, disorder, and/or amorphism) and macroscopic strains due to the ion distribution.

(a) Relatively thin film. (b) Relatively thick film. Peak positions and breadths, peak separations, number and spacing of subsidiary peaks, and interpeak intensities yield information useful in characterizing the junction.

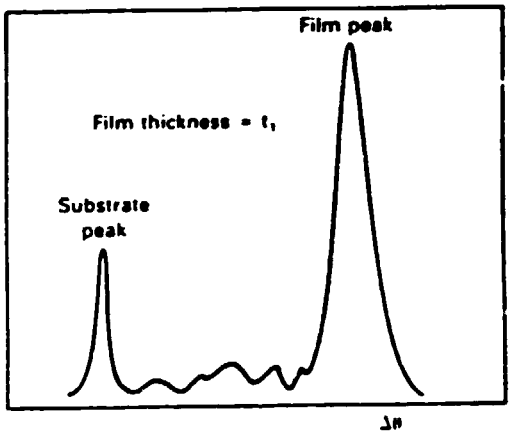

(a)

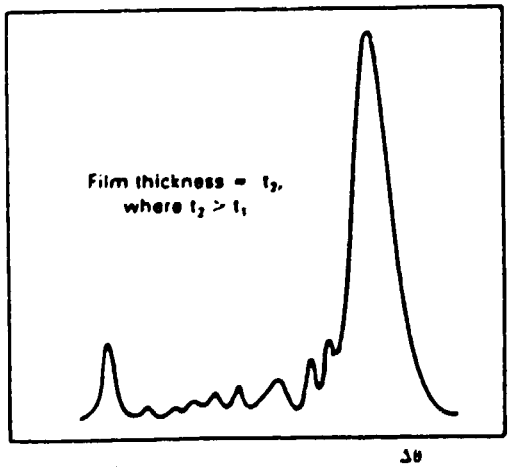

(b)

Figure 19. Illustration of rocking curve profiles for epitaxial films of different thicknesses

Topographic imaging techniques aid investigation of heterojunctions. Topographs can be taken of samples prepared with single or multiple films to reveal the misfit dislocations and other interfacial defects. The defect distribution can then be correlated with the quantitative information from rocking curve analysis and the measurements of electrical properties and behaviour. Damage due to implantation or the intentionally introduced defects on the backside of wafers, an industrial process for "gettering", can also be monitored using X-ray topography. In addition to its use in establishing the quality of the as-fabricated substrate and disclosing defects or strain due to subsequent processing, automated topographic scanning can be used to analyse completed devices rapidly.

Material transformations and crystal kinetics. Many recent studies involving X-ray topography, particularly the dynamic experiments conducted using synchrotron sources, have focused on material transformations and crystal processes. These include solidification/crystallization, ordering/disordering, recrystallization, precipitation, polymerization, and ferroelectric and magnetic domain formation.

Although considerable data have been generated to help model the kinetics of recrystallization, much remains to be learned about the mechanisms of solid-state nucleation and growth. X-ray topography can be used to probe bulk samples rapidly and non-destructively in order to monitor the structure of moving interfaces, including attendant defects, during recrystallization. Studies of aluminium demonstrated that the boundaries of the growing recrystallized grains were planar and became curved only when they encountered precipitates or impinged upon other recrystallized grains. In addition, the faces of the faceted grains exhibiting the lowest velocities corresponded to crystallographic planes with the densest packing of atoms. Finally, the dislocation density within the nucleated grains was found to be high immediately following nucleation to increase during coarsening.

Deformation and fracture behaviour. Topographic methods have been found to be extremely useful in studying deformation and fracture behaviour of various materials subjected to diverse loading and environmental conditions. Fracture surfaces, free surfaces, and small volumes featuring localized deformation, such as those near notches, crack tips, or sites of contact loading, can be examined.

Application of X-ray diffraction to evaluate deformations in polycrystalline materials of engineering importance is particularly effective in view of (1) its potential for non-destructive application so that multiple examinations can be conducted as the deformation progresses, (2) the large areas that may be scanned in comparison to some other techniques, (3) the subsurface information that can be obtained using penetrating radiation, and (4) the capability for dynamic processes using intense synchrotron sources and rapid detection systems. For example, fatigue deformation in diverse metal alloys has been studied using line broadening, microbeam techniques to probe the root of a starter notch, and the modified form of rocking curve analysis for polycrystalline materials. These techniques, along with polycrystal scattering topography, have great potential for

application in the field to evaluate cumulative damage in structural members and mechanical components. As portable X-ray generators, robotic manipulation, rapid and position-sensitive detection systems, and computer automation and data analysis are set to the task, non-destructive evaluation of the deformation state, before crack initiation and in the absence of other more microscopic flaws, will be possible outside the laboratory. (Extracted from an article written by Robert N. Pangborn, Department of Engineering Science and Mechanics, The Pennsylvania State University. Article courtesy Prof. L. Cartz)

5. DEFECT TYPES AND NON-DESTRUCTIVE TESTING TECHNIQUES FOR COMPOSITES AND BONDED JOINTS

P. Cawley, Department of Mechanical Engineering, Imperial College of Science and Technology, England
R. D. Adams, Department of Mechanical Engineering, University of Bristol, England.

OVERVIEW

In this paper, the main non-destructive techniques to identify defects are described and the sensitivity of each method to the different types of defect is indicated.

Non-destructive testing techniques

Developments in non-destructive testing of composites have been built on the experience gained with metals. However, of the five methods most frequently used with metals - ultrasonics, radiography, eddy current testing, magnetic particle inspection, and dye penetrants - only ultrasonics and radiography are often used with composites. Eddy currents have found limited application with composites containing a conducting material, but magnetic particle inspection cannot be used with non-magnetic materials. Dye penetrants can be used to find surface breaking defects, but it is difficult to remove the penetrant from the defects, which can interfere with subsequent repairs. Also, the defect most commonly found in composites is a delamination parallel to the surface of the structure, rather than a surface breaking transverse crack, so dye penetrants are less useful with composites than with metals. Since it is difficult to apply to composites some of the techniques used with metals, alternative methods such as low frequency vibration and thermography have been used. These are particularly suited to composites, since they are most sensitive to defects such as delaminations which run parallel to the surface of the structure.

There have been several comprehensive reviews of the range of techniques available for the NDT of composites and bonded joints and no attempt will be made to repeat such treatment here. Instead, the techniques that are commonly used to detect the defects mentioned above are described. The relative advantages of different methods, where several techniques may be used to detect a particular defect, and the problems posed by defects for which no satisfactory test is currently available are also discussed. Thus, techniques such as fibre optics, shearography, corona discharge, Raman spectroscopy, and dielectric measurements, which are still in the initial stages of development or which can only be used in a few specialist applications, are not mentioned here. The techniques commonly used to inspect composite and bonded joints and the types of defect which they can be used to detect are presented in Table 1. Acoustic emission has not been included in the table, because it is qualitatively different from the other testing techniques since it "listens" to damage growing and so is not strictly non-destructive. However, it is widely used with composites, particularly for proof testing.

Ultrasonic methods

Ultrasonic testing is the most widely used technique for the NDT of composites and bonded joints. The test may be carried out with either a single transducer in pulse-echo mode or two transducers in through-transmission mode. In either case, it is essential that the transducer(s) be coupled to the structure via a liquid or solid medium, because of the severe impedance mismatch between air and solid materials. This is usually achieved by immersion testing or, for large components, by the use of water jet probes. When testing is carried out manually, a thin layer of gel may be used as a couplant between the transducer and the structure, this technique being particularly suitable for field work. Some work at low ultrasonic frequencies has also been carried out using roller probes, where the ultrasonic transducer is held inside a wheel, the sound being propagated into the specimen via a soft rubber tyre. However, this method is not satisfactory for the detailed characterization of defects.

The large impedance mismatch between air and solid materials means that honeycomb constructions can be difficult to inspect using ultrasonics, because the ultrasound will not propagate through the structure except at the cell walls. Transmission down the walls is also difficult if they are made of an attenuative material such as Kevlar. Using a pulse-echo technique, only the bonding of the top face to the core can be tested reliably, but using through transmission both top and bottom bonds between the skins and the core can be inspected in a single test.

Using the same basic equipment with either water or gel coupling, several types of measurement are possible. The main types are discussed below. Various methods of displaying the test results are also available, the most commonly used being the well-known A, B, and C scans. The A scan is the display usually seen on the screen of the ultrasonic test set and gives the time history of the echoes received by the receiving transducer. In the B scan presentation, the vertical axis is the time axis of the A scan, the presence of echoes being indicated by intensity variations. The horizontal axis gives position information, so an image of the component cross-section is built up. If the amplitude of a particular echo is monitored at each point on the surface of the work, a C scan can be produced. Measurements at each point are taken using a scanning mechanism which produces a plan of the defect positions but gives no information about their depth.

Echo amplitude measurements at normal incidence

The usual method is to monitor the amplitude of the ultrasonic signal received in the time domain with the transducer(s) normal to the surface of the structure. In pulse-echo mode, the amplitude of the

Table 1 Types of defect and possible NDT techniques to test for their occurrence

Defect type	Inspection method										
	Ultrasonic methods										
	Echo amplitude (normal incidence)	Velocity	Back scattering	Spectroscopy	Acousto-ultrasonics	Bond testers	Radiography	Eddy currents	Thermography	Holography	Low frequency vibration
Composites											
Incorrect fibre type (e.g. HM/HT)	.	AL							...		AL
Porosity voids	D	AL	TD	.	TD	.	AL	SC	...	.	
Poor fibre-matrix bond strength	.	.	.	...		...	..	...	...	.	.
Poor matrix properties (e.g. due to poor cure or contamination)	AL	AL		TD		.			..	.	
Fibre misalignment			TD				AL	AL	..	.	AL
Incorrect volume fraction	SC	AL					AL	AL			AL
Incorrect lay up			TD		TD			AL	.		AL
Ply end discontinuities	AL		TD								
Foreign inclusions	D		TD				D	AL	D		
Translaminar cracks	AL		TD		TD		AL	AL	.	.	
Fibre breakage							AL	AL	..		
Delaminations	D			D	TD	D	AL	SC	D	D	D
Moisture ingress	SC	AL					AL		TD		
Adhesive joints											
Disbonds	D			D	TD	D	AL		D	D	D
Voids porosity	D		TD	TD			AL		..		
Poor cohesive strength				TD		SC		.	...		
Poor adhesion strength						.		.	...		
Poor filler in honeycomb construction	D						AL		...		

HM High modulus
HT High tensile
D Detectable using given technique (there may be limits on the size of defect that can be detected)
AL Application limited see text for discussion
TD Technique under development and showing promise
SC Some change in measured response caused but not sufficient to be useful
. Lack of reports in literature in most cases this means the technique is not applicable to the particular type of defect

echo received from the back face of the component will be reduced by defects in the structure. A delamination the plan dimensions of which exceed those of the ultrasonic beam will almost completely remove this echo, while porosity will cause attenuation of the signal as a result of scattering of the ultrasound by the small gas bubbles. Increased attenuation also arises from an increase in vibration damping of the material as a result of miscuring.

In the immersion testing of thin components, the echo from a reflector plate placed behind the component, rather than the echo from the back face of the component, is frequently monitored, because it is easier to separate this signal from those received from the front face of the structure and from any defects. Through-transmission testing, which involves monitoring the size of the transmitted pulse, is also used.

In pulse-echo testing, it is also possible to check for the presence of echoes between those from the front and back faces of the component, the presence of significant signals indicating the existence of defects or inclusions. The defect depth can also be found by comparing the transit time of the echo from the defect with that from the back face of the component.

Delaminations in composites, and disbonds in adhesive joints and between the top skin and the core in honeycomb constructions are easily detected by this type of test: foreign inclusions, provided that the material which forms them has a significantly different acoustic impedance from that of the composite, may also be detected in this way. Similarly, the absence of a fillet on the skin/core joints in a honeycomb structure affects the amplitude of the signal reflected from the back face of the skin and so can be detected. The extent of porosity can also be measured reliably, though careful calibration is needed and problems can be caused by changes in the signal amplitude because of surface roughness or inconsistent coupling. Overlapping plies may also be detected, since they give rise to an increase in porosity.

This method may detect changes in fibre volume fraction, but the effect on the received signal is small and can readily be masked by other changes. Incorrect cure of the matrix is likely to result in increased material damping and increased attenuation. Translaminar cracks may be detected by the use of high resolution probes and the signals produced by ply end discontinuities when attempting to butt two sheets of prepreg together are likely to be similar to those obtained from translaminar cracks.

When large areas are to be tested, it is often beneficial to use an automated testing system, the modern trend being for such systems to be computer controlled. For example, a computer based scanning system that automatically tests composite components for delaminations, porosity, ply slippage, and foreign inclusions has [illegible] developed.

Ultrasonic velocity measurements

The ultrasonic velocity in a material may readily be obtained from the transit time of a pulse through the test component, provided its thickness is known. The velocity of ultrasonic waves in the fibre plane is a function of fibre volume fraction and orientation, and measurements of in-plane velocity can also be used to distinguish between fibre types of significantly different moduli. However, it is usually most convenient to perform the test in a direction perpendicular to the plane of the fibres. The velocity of ultrasonic waves travelling normal to the fibre plane is a function of the extent of porosity and of the fibre volume fraction: by measuring the longitudinal and shear wave velocities, it is possible to calculate both quantities.

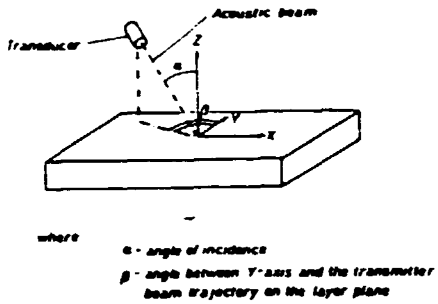

Figure 1. Schematic diagram of experimental system used to measure backscattering from composite samples

Ultrasonic backscattering

This technique involves inclining the ultrasonic transducer at an acute angle α to the normal to the test structure surface and then monitoring the echoes received by the transducer in pulse-echo mode as the component or transducer is rotated about an axis normal to the component surface, the angle α being kept constant (see figure 1). When the angle of rotation β is such that the transducer is normal to the fibre direction in any of the layers of the structure, the backscattered signal reaches a maximum. A plot of the signal intensity versus the angle of rotation may then be used to check whether the structure has been stacked correctly. If porosity is present, the backscattered signal is higher at all angles of rotation between the fibre directions than in a good structure. However, surface roughness can also produce an increase in the backscattered signal, so if small amounts of porosity are to be detected, it may be necessary to smooth the surface before testing. Local fibre waviness, translaminar cracks, and ply end discontinuities may also be detected.

There has recently been considerable interest in the use of leaky Lamb waves for the detection of defects such as porosity, translaminar cracks, and the delaminations in composites. Initial results on unidirectional material are very promising and the technique has now been extended to multidirectional laminates.

Ultrasonic spectroscopy

Originally, ultrasonic thickness gauges worked in the frequency rather than the time domain and used the first through thickness natural frequency of a plate f_n, which is given by

$$f_n = c/2t \quad . . . .$$

where c is the speed of sound in the matrial and t is the thickness. Hence, if the speed of sound is known and f_n is determined, the thickness may be obtained. This type of thickness gauge has now largely been superseded by instruments based on the measurement of the transit time of a pulse across the specimen, but the spectroscopic system does have advantages for thin structures where it can be difficult to resolve successive pulses in the time domain. A spectroscopic system can be used to determine delamination depths in a composite or disbond depths in a multilayer bonded structure. Spectroscopic measurements can also be used as an alternative to the time domain tests discussed above to detect the ultrasonic velocity changes produced by poor matrix curing.

Early work on ultrasonic spectroscopy was carried out using analogue spectrum analysers which give only coarse frequency resolution. However, high speed digital transient capture systems are now available, which can be coupled to Fast Fourier Transform processors to give much improved frequency resolution. This has led to the possibility of detecting poor cohesive properties of the adhesive layer in a joint, which has been one of the unsolved inspection problems in adhesive joints. Initial results also indicate that porosity in a joint can be detected by spectroscopy measurements.

Combined methods

If a composite is to be inspected for a variety of defects, it may be beneficial to process the ultrasonic test signal in several ways in both the time and frequency domains and to combine the results on the final display. This type of approach is described by Rose and co-workers who have developed a "feature mapping system" for the classification of defects in composites and bonded joints.

Acousto-ultrasonics

Acousto-ultrasonic testing involves the use of two ultrasonic transducers placed a fixed distance apart on the test structure surface, one acting as a transmitter and the other as a receiver. The received signal is then processed using the techniques commonly used with acoustic emission testing. There has been considerable interest in the technique for the inspection of composites and bonded joints and interesting correlations between the measured parameters and void content, stacking sequence, translaminar cracking, and delaminations in composites and disbonds in adhesive joints have been reported. However, the method does not always give satisfactory results and the reasons for this are not clear. Unfortunately, no reports detail the type of wave generated by the transmitting transducer and the mechanism by which changes in the received waveform occur. If this can be remedied the method may find wide application.

Ultrasonic bondtesters

A number of bondtesters operating in the frequency range between 100 kHz and 1 MHz are widely marketed. The Bondascope, manufactured by NDT Instruments, measures the magnitude and phase of the ultrasonic impedance of a bonded structure and displays the result as a "flying dot" on an oscilloscope screen. Changes in the magnitude and phase of the impedance can readily be related to the existence and depth of disbonds or delaminations. The Fokker Bond Tester Mk II uses a spectroscopic approach: frequency and amplitude changes are monitored in the first two modes of through-thickness vibration of a system comprising a transducer coupled to the structure. Changes in resonant frequency reveal the existence and depth of disbonds or delaminations. The manufacturer also claims that it can detect changes in the cohesive properties of a joint, but other authors report that this is difficult, and it has recently been shown that the instrument is not sensitive to changes in the cohesive properties of modern, high-strength adhesives.

Radiography

Conventional X-radiography

Conventional X-radiography of carbon fibre reinforced composites is difficult, because the absorption characteristics of the fibres and the matrix are very similar and the overall absorption is low. Therefore, it is not possible to determine the fibre volume fraction or the stacking sequence. The properties of glass or boron fibre reinforced composites are more suited to X-radiography, and in these materials the volume fraction and fibre alignment have been checked. Inspection of carbon fibre composites is made easier by incorporating lead glass tracer fibres in the material.

Detection of delaminations by radiography is difficult, because they tend to be normal to the X-ray beam and so make little difference to the overall absorption.

Disbonds in adhesive joints made with metal adherends cannot be detected by x-radiography, since absorption by the adherends is high and any lack of adhesive makes a negligible difference to the overall absorption. Disbonds in joints made with composite adherends act in the same way as delaminations.

Penetrant enhanced X-radiography

Introducing a radio-opaque penetrant into a defect such as a delamination can dramatically improve the contrast on the radiograph and can give very detailed pictures of, for example, impact damage, thus greatly assisting the study of its propagation. However, many penetrants are highly toxic and for the penetrant to be introduced the defect must be surface breaking. It is therefore likely that penetrant enhanced radiography will remain a laboratory tool, although some studies are being carried out to assess its use as a rapid means of checking the extent of lightning damage on composite aircraft panels.

Neutron radiography

The use of neutron radiography for the NDT of composites has been investigated. Neutron absorption is a function of the presence of elements such as hydrogen, and neutron radiography can be used to find voids, inclusions and transverse cracks. Gauging can be used to determine the resin content of a composite. X-rays are strongly absorbed by metals, so cannot be used to inspect an adhesive joint between metal adherends (unless the beam direction is parallel to the joint so that the X-rays passing through the adhesive layer do not pass through the adherends). As neutrons are absorbed more strongly by the adhesive, neutron

radiography can be used to inspect the adhesive joint between metal adherends. Neutron radiography should also be very sensitive to moisture in the composite. However, neutron sources are not usually practicable for use in large-scale NDT.

Eddy current testing

Eddy current inspection of composites is limited to those materials having a conducting phase and the measurements obtained are very sensitive to the volume fraction and integrity of that phase. Eddy current inspection can therefore be used to check the fibre volume fraction in a carbon fibre composite. However, this was not easy, particularly with cross-plied laminates. Defects such as fibre breakage and the presence of conducting inclusions can also be revealed.

Eddy current methods are relatively insensitive to porosity, non-conducting inclusions, and delaminations. Therefore, the method is complementary to ultrasonics in materials such as CFRP, since it is sensitive to those defects that are difficult to find using ultrasonics. Since the resistivity of carbon fibres is much greater than that of metals, lack of penetration depth is not usually a significant problem.

Thermography

Thermographic methods may be divided into two types: passive, in which the response of the test structure to an applied heating or cooling transient is monitored; and active, in which heating is produced by applying cyclic stress to the structure either in a fatigue machine or in resonant vibration. In both methods, the surface temperature of the structure is monitored, usually using an infrared camera, and anomalies in the temperature distribution reveal the presence of defects.

The passive method has been more widely applied than the active technique and its performance is strongly dependent on the heat source used, a flash gun generally being the most suitable. The conductivity and anisotropy of the composite are also very important; for example, in CFRP the conductivity in the laminate plane is about nine times that in the through-thickness direction, which tends to obscure defects that are not close to the surface.

The method is made more convenient by using a video recorder to store the rapidly changing temperature pattern after the structure surface is heated. In this manner, those defects in conducting materials that have only a transient effect on the temperature distribution may be detected. The method can be used with the heat source and camera on the same side of the structure (pulse-echo) or on opposite sides (through-transmission). The through-transmission method can detect deeper defects than the pulse-echo technique, but for defects close to the surface, pulse-echo is superior.

The method is attractive as a rapid means of inspecting large areas of structure. It can be used to find disbonds in adhesive joints, delaminations in composites, and inclusions having conductivity significantly different from that of the base material. Work at British Airways has shown that thermography is also a useful means of detecting moisture ingress in composities. However, equipment costs are high and the method is not as sensitive as ultrasonics for example, in detecting disbonds and delaminations.

Low frequency vibration

A variety of low frequency vibration techniques are used in NDT. The methods can be divided into global techniques, in which the integrity of the whole structure is assessed using excitation and measurment at a single point of the structure; and local techniques, in which measurements are taken at each point of the structure. The local methods may be further divided into those requiring only a single excitation point and those requiring excitation at each point of measurement.

Global methods offer the possibility of very rapid testing, but unfortunately they are not very sensitive. However, natural frequency measurements can be used to check quickly the volume fraction and winding angle of filament wound components; changes of around 1-1.5° in winding angle or 4 per cent in volume fraction can be detected. The stacking sequence of multilayer structures can be checked and fibre types of significantly different moduli can be distinguished. The method cannot be used to detect local defects such as delaminations at the production stage.

One of the methods involving single point excitation and multipoint measurement is optical holography, which detects anomalies produced by defects such as delaminations in the vibration mode shapes of a structure. The method is rapid, since a vibration exciter is attached to a single point of the structure, then a hologram of the complete structure is obtained. However, equipment costs are high and, unless a pulse system is used, the structure must be mounted on a table which is isolated from extraneous vibration. Active thermography may also be termed a local method involving single-point excitation and multipoint measurement.

The coin tap test, in which the region of structure to be tested is tapped with a coin, the operator listening to the resulting sound, is probably the best known local method. It is found that defective areas sound duller than good areas and the authors have carried out an extensive study of this technique. It was found that the difference between good and defective structures can be detected by tapping the structure using a small hammer with a force transducer incorporated in its head and monitoring the force input to the structure during the tap. This has led to the development of an instrument that will perform the test automatically and give an objective measure of the structural integrity.

The mechanical impedance method can also be used to detect delaminations in composites and disbonds in adhesive joints. The point impedance at a disbond or delamination is lower than that in good areas of structure so impedance measurements can be used to detect these defects. The impedance change produced by a given defect size reduces as the defect depth increases, so the test is most sensitive to defects close to the

surface. In figure 2 a graph is shown of the minimum defect diameter detectable using this method versus the defect depth in different materials. This graph relates only to relatively stiff structures and tests have shown that the method is less reliable for flexible structures. The sensitivity of the automated coin tap test is similar to that shown in figure 2, although tests indicate that it is more reliable than the impedance method for flexible structures.

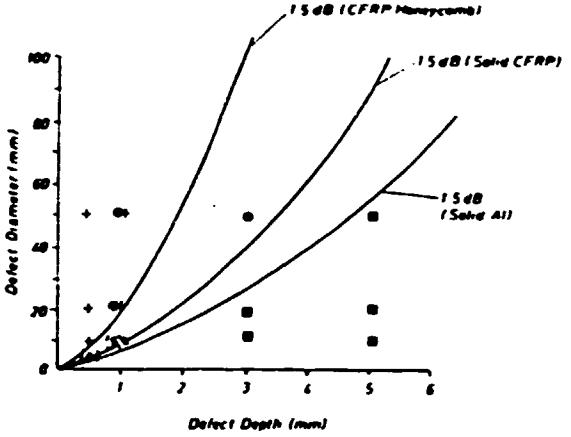

+ Detectable defect in honeycomb structure with CFRP skins

▲ Non detectable defect in honeycomb structure with CFRP skins

● Detectable defect in solid aluminium

■ Non detectable defect in solid aluminium

( ) Marginal case

experimental points are taken from C scans of CFRP skinned honeycomb panels and solid aluminium plates. solid curves show relationship between defect diameter and depth which gives 15 dB difference between impedance measured above a defect and that measured over a good area in structures fabricated from different materials

Figure 2. Detectability of defects in different materials (these results apply only to stiff structures)

Discussion and conclusions

It can be seen from table 1 that many techniques are available to detect delaminations in composites and disbonds in adhesive joints, but that no methods detect poor adhesion in adhesive joints or fibre-matrix bonding problems in composites.

Fortunately, provided that the volume fraction of the composite and the lay-up are satisfactory, current aerospace design criteria mean that the only defect likely to be of structural significance in areas of uniform stress is a delamination greater than 20 mm in diameter. Once a delamination has been found, it may then be necessary to use sophisticated techniques to map its full extent and to detect any associated translaminar cracks and fibre-matrix bond failures.

The best technique initially to detect a delamination depends on the defect size which must be found, the size of the structure to be inspected, and the environment in which the tests are to be carried out. Ultrasonic methods are very sensitive, but have the disadvantage of requiring a couplant between the transducer and the test structure. Coupling is most reliably achieved either by immersing the component or by using a jet probe system, both of which add to the expense and inconvenience of testing. Manual inspection using a gel couplant is often used, but the reliability and speed of the test is reduced. Passive thermography may be used to inspect large areas rapidly, but the capital costs are high and the sensitivity of the test may not be adequate in all cases. No couplant is required in the coin tap and mechanical impedance tests and the equipment is portable and relatively cheap. They are therefore attractive for use in the field. However, the sensitivity of the tests may be insufficient, particularly if defects at significant depths are to be found.

Stacking sequence, fibre volume fraction, and matrix cure may be checked non-destructively after production, but the methods available have not been widely used and are not fully developed. These parameters are usually monitored by process quality control and by destructively testing specimens produced at the same time as the structure. Fibre-matrix bond problems, poor fibre wetting and matrix contamination are usually eliminated by careful control of the materials before fabrication. Current design specifications will often tolerate quite high levels of porosity (5 per cent would be typical) and this is relatively simple to detect by ultrasonics or radiography.

In the above discussion, the inspection of large areas of uniform composite has been considered. Testing corners and other areas of rapidly changing geometry is much more difficult and designers must ensure that these regions can tolerate larger defects.

In the present work, the detection of defects, rather than their significance has been discussed. Obviously, an understanding of defect significance is essential in order to interpret the results of non-destructive testing. However, defect detection is currently better developed than the understanding of the significance of what has been detected. This is partly because of the rapid development of composite materials, which means that engineers have less experience of their failure characteristics than those of metals.

The inspection of adhesive joints presents more severe problems than the testing of composites. Disbonds can be detected in the same way as composite delaminations and generally do not present a problem, although the influence of a disbond on the strength of a joint is dependent on its position within the joint. There is no technique available to detect poor adhesion, although recent work on ultrasonic spectroscopy, which has yet to be applied in industry, foreshadows a test for poor cohesion. The integrity of adhesive joints must therefore be ensured by tests carried out before bonding, to ensure that surface preparation is satisfactory, and by very careful process quality control. Since both the adhesion strength of a joint and its susceptibility to environmental attack are governed by the quality of the adhesive/adherend interface layer, it is vital that new techniques be developed which will enable this region to be inspected. (Extracted from Materials Science and Technology, May 1989, Vol. 5)

6. APPLICATION OF NON-DESTRUCTIVE INSPECTION METHODS TO COMPOSITES

The last few years have seen a rapid escalation in both the number and structural criticality of composites applications entering service. The falling price of composites has vastly increased the number of applications in non-aerospace industries, including automotive, sports, boating, and construction. New aircraft systems currently under development will continue the trend toward more extensive applications and more exotic materials. Although the service record for composites has been excellent, the composites are subject to damage from overload, hail, lightning, bird strike, runway debris, ballistic rounds, and moisture intrusion. Low-strain designs, coupled with less critical applications, have made for relatively large acceptable flaw sizes and lax inspection criteria. As composite structures representing more aggressive design criteria begin to accumulate service hours, we will begin to see a new level of demands placed on non-destructive inspection (NDI) techniques to support the in-service maintenance and repair requirements for composites.

Visual inspection

All exposed aircraft structures receive frequent "walk-around" visual inspections. These inspections certainly apply to much of the composite structure currently in use. Many of the more severe conditions associated with composites are visually detectable. Punctures, surface-ply delaminations, scratches, gouges, and heat damage can frequently be detected by visual inspection. Disbonds between a composite skin and some substructure may also be detectable in some cases as a blister in the skin or an edge separation. This inspection is clearly valuable, but one cannot expect to detect all of the forms of damage that may be present in a composite structure. Further, if damage is detected, it is important that other tools are used to assess the extent of the damage because the subsurface damage may drastically exceed the surface-detectable damage. One common example is low-velocity impact damage. Numerous studies on this form of damage, which may result from hail, runway debris, or ground-handling abuse, have shown that substantial subsurface damage can result with little or no surface-detectable condition.

Tap test

The tap-test method, using either a coin or a special tap hammer, continues to be a common in-service inspection tool despite the availability of less subjective inspection tools. The use of this method has persisted for several reasons. The most obvious is that it does not require sophisticated or expensive equipment. Another is that many of the composites in use today consist of thin laminates in low-strain designs. This combination yields critical flaw geometries that are fairly large and close to the surface - two conditions necessary to the successful use of the tap method. The tap-test method is sensitive only to laminar-type flaws, such as delaminations or unbonds, and relies on the different acoustic resonance of the loose upper layer compared to that of the surrounding material. The tap method suffers, however, from subjective interpretation (particularly with complex geometries), variable application, declining sensitivity with flaw depth, and an inability to calibrate effectively for either flaw size or depth. The more recent applications of composites in thicker laminates and more highly loaded designs make this approach inadequate in many cases.

Ultrasonic correlation

Ultrasonic correlation offers a novel approach to the ultrasonic inspection of highly attenuative materials. It has proven effective in the evaluation of some of these materials where conventional pulsed ultrasonic systems have experienced difficulties in penetrating the material. The correlation approach achieves this increased sensitivity using a continuous-wave, cross-correlation technique that enhances the sensitivity of the test but sacrifices inspection speed.

The principal advantage of the correlator is that it provides substantial enhancements in the signal-to-noise ratio (SNR) of the ultrasonic signals. This SNR enhancement is achieved through a modification of the time scale required to produce an A-scan trace. Because the correlator uses continuous generation and accumulation of the ultrasonic signals, the maximum possible efficiency of data accumulation can occur. The SNR enhancement allows the correlator to produce usable A-scan traces where conventional pulsed ultrasonic systems are unable to produce a recognizable pattern.

For example, the correlator has been used to characterize polytetrafluoroethylene (PTFE [Teflon™]), a material very difficult to penetrate with conventional ultrasonic techniques. The results have been obtained by measuring ultrasonic velocity as the temperature of the PTFE sample changed. Figure 1 shows a velocity vs temperature profile with an excellent indication of a change in the slope of the curve at the phase-transition temperature of 30°C. Thicknesses of PTFE as great as 7.5 cm have shown results with the correlator.

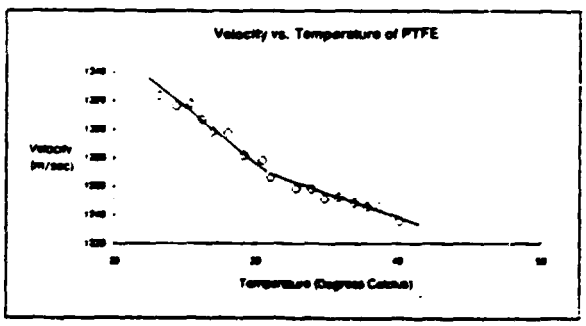

Figure 1. Ultrasonic velocity transition in PTFE measured with correlator

The correlator has also been successfully used on thick and highly attenuative composites.

X-radiography

X-ray imaging relies on the differential absorption or scattering of the X-ray photons as they pass through a material. Flaws that either allow more X-ray photons to pass or that absorb or scatter the photons can be imagined if the effect is

significant. X-ray inspection systems are usually sensitive to changes that result in an apparent change of at least 1 to 2 per cent of the material thickness or density. Composite flaws tend to lie between plies and present a very small apparent thickness change, particularly for thick laminates. However, the low density of most composite materials permits the use of low-energy X-rays, which help to enhance the sensitivity. X-rays can be used to detect porosity and matrix cracks as well as some foreign materials. More highly loaded applications and/or the use of more brittle matrix materials, both of which seem to be on the horizon, will make the detection of some of these conditions much more critical than it is today. Carbon fibres are not generally imaged by X-rays, but boron fibres are deposited on a tungsten filament and this filament can be imagined in x-radiographs. This allows detection of fibre fractures and determination of fibre orientations, so long as the number of plies does not get too large.

X-radiography is particularly useful for the detection of honeycomb-core defects in bonded sandwich assemblies. The low density and thin composite skins usually provide minimal interference for the X-rays to image the honeycomb-core materials. Core defects such as blown core; crushed core; condensed core; fatigued, corroded, or cut core; and foaming adhesive voids can be detected by radiographic methods. It is also frequently possible to detect water intrusion into the honeycomb core by using X-ray methods.

Significant progress has been made in recent years in the use of nonfilm electronic imaging systems for X-rays. These systems allow the real-time viewing of X-ray images and can drastically reduce the demand for expensive X-ray film. Although video imaging systems do not possess nearly the resolution of X-ray films, very small X-ray sources and geometric magnification techniques have been used to recover some of this sensitivity.

X-ray backscatter imaging

Conventional radiographic inspection techniques rely on the attenuation of a beam of penetrating radiation to form an image of a part. At low X-ray photon energies typically used with composites, a large portion of that attenuation is due to Compton scattering. Several approaches for taking advantage of the Compton scattered radiation to image the material have been proposed.

One approach, using a novel X-ray backscatter camera employing a slot instead of the traditional pin-hole approach, has been developed. This technique is illustrated in figure 2. The backscattered X-rays are detected by an array of scintillation detectors. The backscatter intensity information is obtained as a function of detector position; this, in turn, relates to different depths in the inspection object. One interrogates the entire object thickness at one time (composite structures as thick as 7 cm have been inspected). The inspection results provide indications of material-density changes by a change in intensity slope vs position and of voids or foreign material by an abrupt change in backscatter intensity. This method is particularly useful for the inspection of laminated structures such as pressure vessels and rocket motor cases. In some of these designs, ultrasonic inspection approaches are ineffective or impractical; the backscatter X-ray imaging approach offers a potential solution. Tight delaminations, with gaps less than 50 μm in width, can be detected.

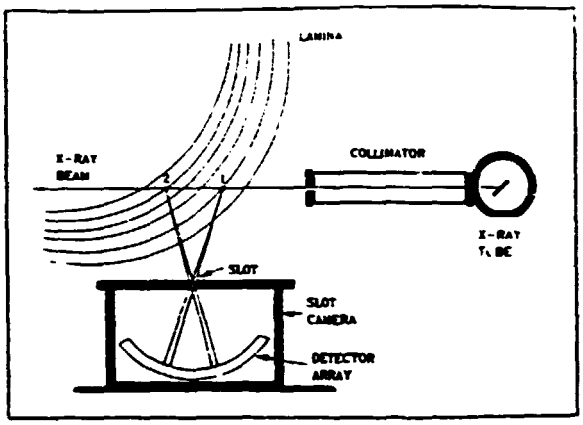

Figure 2. X-ray backscatter system geometry

Neutron radiography

X-rays are attenuated as a function of the density of the material through which they pass. If X-ray attenuation is plotted as a function of increasing atomic weight of the attenuating material, one finds a monotonically increasing function. The attenuation of thermal neutrons, plotted similarly, shows a generally random pattern in which there is high attenuation for several light materials - hydrogen, boron, and lithium in particular - and relatively low attenuation for most metals. For bonded structures, the high sensitivity of neutrons to hydrogen means that thermal neutron radiography can display adhesives, water, or corrosion in a metal bonded assembly more readily than can X-ray techniques. For composites, neutron techniques offer promise for the detection of variations in the organic matrix materials and moisture takeup

Laser holography

Laser interferometric holography techniques were evaluated for composites testing in the 1960s. In fact, several composites and bonded assembly testing systems were constructed. In spite of the use of massive optical benches and elaborate vibration isolation systems, however, the vibration problems of working in a production environment (much less an in-service environment) were not satisfactorily solved. The holographic inspection approach is sensitive to very small amounts of relative motion in the part surface. Typically, a part is tested by taking an image of the part at rest, then stressing the part surface, either with a small amount of heat or a mild vacuum. This light stressing causes the area of the surface over the flaw to deform slightly more than the surrounding material. Displacements as small as one quarter wavelength of the laser light being used cause a fringe to appear in the interference pattern. Unfortunately, unwanted test-object motion of an equally small amplitude will also cause fringes.

The development of phase-locked loop holographic systems has gone a long way to eliminate the problems associated with low-frequency vibration. Holographic inspection systems that use video imaging systems and "develop-in-place" reference holograms are currently being used in several applications.

Another development in the area of video holographic systems - electronic shearography has recently provided even greater immunity to test-object vibration and motion problems, making the rapid scanning of large areas of composites on the aircraft possible. Electronic shearography uses no film and compares a live video image with a stored video image to produce interference fringes.

Conventional interferometric holography interferes two holograms of a component to produce the interference pattern. Each hologram is produced by recording the speckle interference between a coherent reference beam and the coherent object beam that illuminates the surface of the test part. Deformations between the two exposures produce the interference fringes. Phase-locked holography uses the same basic technique, but uses the diffuse reflection of an unexpanded coherent beam shone on a small portion of the test object as the reference beam. These approaches are sensitive to any out-of-plane displacement on the part surface.

Shearography, on the other hand, uses no separate reference beam. Instead, the returning object beam is doubly imaged, with one of the images slightly shifted, or "sheared", relative to the unshifted image. Thus the interference pattern does not reveal bulk surface motion, but only the degree of differential motion of the surface along the direction of the shearing. This makes shearography particularly well suited to many production and depot environments because of its relative immunity to vibration problems.

Thermal infrared inspection

Infrared imaging systems have been investigated for quite a few years for applications with composite structures. Thermal monitoring has been effective in laboratory tests, but interpretation of the thermal patterns in actual structure has frequently been difficult. There have been many techniques evaluated which have variously made use of the loss in thermal conductivity at a flaw location and the generation of heat at flaws under cyclic loading. Thermal testing has suffered to a certain extent from the lack of a suitable, reproducible method for producing a thermal gradient in a composite structure and has had few applications for in-service inspection. Progress is being made, however, in the development of new thermal imaging systems with greater sensitivity and vastly improved image-analysis tools.

Thermal patterns can be produced by heating the inspection surface and monitoring the surface of the part for relatively hot spots caused by blockage of the thermal flow away from the surface by a laminar flaw. This method is particularly sensitive to flaws near the inspection surface; the sensitivity reduces rapidly with the flaw depth. The thermal images can also be produced by heating the far side and monitoring the surface for cold spots where the heat flow toward the inspection surface is impeded by the flaw. This "through-transmission" approach somewhat improves the depth sensitivity, but the method is still more sensitive to near-side flaws.

Impact damage often results in matrix damage near the surface of a composite material.

Thermal testing methods, such as vibrothermography, which cause the flaws themselves to become heat sources, have generally worked well in the laboratory with small test objects, but have been much less effective on full-scale structures.

Acoustic emission

Acoustic emission testing monitors the material under test for spontaneous noise generated under load. It has been used extensively in the proof-testing of fibreglass pressure vessels and beams. It has also been used to monitor and characterize damage-growth mechanisms in composites under cyclic loading. Acoustic emission testing is capable of detecting and characterizing matrix cracking, delamination, and fibre breakage. It is used extensively in the testing of composite pressure vessels and in the evaluation of some structures, such as "cherry-picker" booms; however, the method has not found particular application in the aircraft inspection arena for these flaws. This may be partly due to the need to have the component under load during testing. One area where acoustic emission testing has found acceptance is in the detection of moisture and corrosion in the honeycomb assemblies. If a honeycomb assembly containing water is locally heated in the vicinity of the water, the increased vapour pressure will force the water to move through the leakage path through which it entered the honeycomb cell. The motion of the water through the leakage path can be detected using acoustic emission equipment.

Acoustic-ultrasonics

The acousto-ultrasonic, or stress-wave factor, test method uses an ultrasonic transducer to inject a simulated acoustic emission pulse into the material under test. The wave form of the pulse is then monitored a fixed distance away with an acoustic emission transducer. Damage to the material will affect the manner in which the wave is transmitted through the material. The stress-wave factor will be affected most by discontinuities, which impede the motion of the stress wave through the material. The method can be applied in a through-transmission mode, but is generally used with both transducers on the same side of the part and monitors the transmission of signals parallel to the surface. In this mode, the method is most sensitive to matrix cracking and laminate porosity. It is also sensitive to fibre breakage and, particularly in the through-transmission mode, delamination. The method is relatively new and has suffered from problems in obtaining consistent results. Some of these problems have been solved or reduced, and the method shows some potential for evaluating the severity of matrix degradation in composites.

Eddy current testing

Eddy current testing depends on the injection of current loop paths in conductive materials. Although most matrix materials are very poor electrical conductors, some of the carbon fibres are relatively good. To form current loops, multiple

fibres must make electrical contact with one another at various places along the length. Fortunately, the use of carbon-fibre tows of 3,000 to 10,000 fibres or more cleary promotes tnis. Eddy currents can be used to monitor fibre orientation because the current loops are not circular but greatly elongated along the fibre direction. They can be used also to detect fibre breakage. Eddy current testing of composites has been investigated in laboratories for quite a few years, but has not received a great deal of attention to date for production or in-service inspection of composites.

Conclusions

The NDI methods most widely used in industry for composite inspection - ultrasonics and radiography - have much to recommend them in that many different types of discontinuities can be detected and characterized. Holographic and infrared inspection methods present the attractions of noncontact, large-area coverage and good sensitivity to discontinuities close to the inspected surface. Delaminations on the order of a centimetre in size can usually be detected by holographic interferometry; even smaller, near-surface discontinuities can be detected by infrared imaging. Both methods offer a television image display that provides straightforward interpretation.

New approaches include ultrasonic correlation and X-ray backscatter. The correlator offers the capability to inspect and characterize highly attenuative, multilayer composite structures. The X-ray backscatter camera is well suited to the inspection of laminated structures such as composites. The unit provides one-sided inspection and sensitivity to gaps, voids, foreign materials, and density change; discontinuity location can be displayd with this prompt-response system. (Extracted from Materials Evaluation, 47, April 1989, American Society for Nondestructive Testing, Columbus, OH, USA. Reprinted with permission.)

TABLE 1 Summary of Applicability of NDE Methods

Flaw Type	NDE Method*																	
	Visual	Tap Test	UT Through Transmission	UT Pulse Echo	UT Pulse Scatter	UT Resonance	UT Correlation	X-Radiography	X-Ray Backscatter	Neutron RT	Holography	Thermal IR	Acoustic Emission	Acoustic UT	Eddy Current
Porosity			1	1	2		1	1		1				2	
Foreign material	3		2	1			2	2	2	2		2			
Shallow delamination		2	1	1		1	1		1		1	1	3	2	
Deep delamination			1	1		3	2		1		3	2	3		
Matrix cracks	3				1		2	1					2	1	
Fiber breaks								2					2	2	1
Impact damage	3	2	1	1	2	2	1		3		1	1	3	3	2
Skin/skin disbond	3	2	1	2		2	1	2		2	1	1			
Skin/core disbond		3	2	2		3	3		2		2	1	3		
Crushed core			2				2	1			2	2			
Condensed core							2								
Blown core			2				1	2							
Core node disbonds								1							
Water intrusion			3	1			1	2		1	3	2	2		
Corroded core			2				2	2		1			3		
Fatigued core			2				2	1							
Foam adhesive voids							2	2		2					

*) 1 Good sensitivity and reliability. Good candidate for primary method
2 Less reliability or limited applicability. May be good supplementary method
3 Limited applicability. May provide some useful information

7. IMPROVING QUALITY THROUGH NON-DESTRUCTIVE TESTING

Non-destructive testing is critical during specification and procurement activities; it should also be part of preventive maintenance programmes. Non-destructive testing (NDT) involves measuring certain properties of materials without destroying or impairing the function of the material being tested. The measured parameters may be as simple as the reflective properties of a surface as it is struck by light, or as complicated as the emission of characteristic X-rays by a material after the absorption of energy.

There are many uses for NDT. By far, the major ones involve the location and measurement of discontinuities such as cracks, inclusions and porosity. A discontinuity in a material is simply any imperfection, or interruption in the material's continuity. Discontinuities can be as small as a few missing atoms, or as large as a crack several feet long. Applications of NDT also include thickness measurement, measurement of both thickness and density, alloy identification, measurement of clearances, and troubleshooting of process operations.

Non-destructive testing usually determines the desired property indirectly. The tests yield what is called an indication, which, in the case of discontinuities, may be the blackening of a radiographic film, the amplitude and travel time of an ultrasonic signal, or the phase of an eddy-current signal.

The desired property must then be inferred by interpreting the indication. For instance the appearance of a dark line in a radiograph must be interpreted to determine its source Is it caused by a crack or other type of discontinuity, or is it a nonrelevant or false indication whose cause has no bearing on the acceptability of the material? What is the correlation that identifies the cause? Is this deviation acceptable even though it may be caused by a discontinuity, or might it result in harm? These aspects of non-destructive testing will be covered in subsequent articles.

There are numerous non-destructive testing methods, as well as variations of their use, or techniques. Briefly, the types most applicable in the chemical process industries are:

Visual: One of the most common applications of visual NDT is evaluating the general condition of surfaces and welds. Visual aids may allow the tester to see inaccessible objects, or to enlarge or magnify the view. Such aids include fibre-optic borescopes, telescopes, microscopes and closed circuit television.

Leak testing: This is done by filling a vessel, tank, pipe or other device with a fluid (usually water) and placing it under pressure The pressurization simulates operational stresses, and any leakage may be a precursor to failure. Bubble solutions, or sonic or other sensors, are often used to help locate discontinuities that cause leaks.

Liquid-penetrant: First the item to be tested is thoroughly cleaned. Then a liquid (the penetrant) - typically a light oil with visible or fluorescent dyes suspended in it - is placed on the surface. This liquid makes its way into surface openings. After a certain amount of time (typically

10-15 minutes), the excess liquid is removed from the surface, and the liquid in any discontinuity reservoirs is drawn out. Dye stains that appear as the liquid spreads on the surface indicate possible defect locations.

Magnetic particle: This method is limited to use with ferromagnetic materials, such as iron and steel. A magnetic field is first established within the material; any surface or near-surface discontinuities will disrupt this field and produce leakage fields on the surface. The examination surface is then sprayed or coated with fine magnetic particles. These particles, which respond to the leakage fields much like the needle on a compass aligns with the Earth's magnetic field, line up to form patterns that indicate the locations of defects.

Eddy-current: Testing of this sort is performed using helical coils, through which a high-frequency electric current flows. This current induces a magnetic field, which in turn induces eddy currents (circular currents) within the material. Discontinuities and thickness changes will alter the flow of the eddy currents. Eddy-current methods can only be used on electrically conductive materials, and are most effective on discontinuities located on or close to the surface adjacent to the coil.

Penetrating radiation: Here, a source of radiation (either an X-ray tube or gamma-ray isotope) is placed on one side of the item being tested and a radiation detector (either an instrument or a radiographic film) is placed on the other side. The intensity of the radiation passing through to the detector is a function of the material thickness and density. The detector measures the radiation exiting the specimen. If the detector is a radiographic film, viewing the film with the aid of an illuminator allows one to see differences in the radiation transmitted through the specimen as dark and light areas.

Ultrasonics: In this method, a search unit with a transducer, or piezoelectric crystal, converts an electrical signal into a mechanical vibration, or ultrasound beam. As this beam passes through a material, it will be reflected and scattered by any discontinuities that may be present. The vibrations are reflected to a receiving unit (or to the original search unit), where they are reconverted to electric signals and amplified. These signals are then processed and displayed on an oscilloscope screen. The amplitude of the signal is related to the size and orientation of a discontinuity, while the travel time indicates the depth of the discontinuity.

Optical holography: This method uses coherent light (i.e. light of a single wavelength) to measure surface displacements. If a structure, vessel or other component is put under some type of load, it will respond (for example, by deflecting, expanding or contracting) in some predictable fashion. If discontinuities are present, the surface displacement will not be uniform. Changes on the order of a wavelength or smaller can be seen as changes in the amount of deflection. One of the ways of seeing these changes is to photograph the object illuminated with a laser (which is a source of coherent light) in an unloaded state and then reconstruct the picture (a hologram) and impose the image on the object. Imposing a load on the object will then produce nonuniform changes from this image if discontinuities are present.

Acoustic holography: This is really not a separate method, but type of ultrasonic testing. It combines the transmission of an ultrasonic beam through an object and the measurement of the vibrations (or displacements) in the object. This is done by making and analysing a hologram (a special photograph that reveals a three-dimensional image in space). In one variation of the method, an ultrasonic beam is transmitted through an object immersed in water. The beam causes displacements of the water surface, which vary in intensity based on discontinuities in the object being tested. An image of the transmitted intensities is formed by making a hologram of the water surface.

Another variation of the technique allows a reflected beam to be modulated electronically; with suitable processing, a hologram is formed. A picture of the discontinuity reveals the size and location of the discontinuity.

Acoustic emission testing: This can be used to monitor vessels, piping and other structures during operation to detect the propagation of discontinuities, which can result in catastrophic failure. When a structure is put under a load, stresses are created within the material. A discontinuity can result in a stress concentration, which causes the discontinuity to enlarge. Even though this enlargement may be very minute it results in the generation of a sound wave (vibrations) travelling from the discontinuity. These sounds can be picked up by sensors located along the structure's surface. By comparing the arrival times of various sensor locations, the emitting source can be located.

Evaluating materials

In evaluating materials, it is important to distinguish between a discontinuity and a defect. Some discontinuities are not serious, because they may or may not impair the material's function. On the other hand, if the stress concentration is high or the material's fracture toughness is poor, even a very small discontinuity can be serious.

When a discontinuity is detrimental to a particular material, it is termed a defect. Whether a discontinuity is, in fact, a defect typically depends on the material and its properties, the loads placed on the structure, the distribution of stresses within the material, and the size, location and type of discontinuity.

Different types of discontinuities are generated in various manufacturing processes. For instance, a cast part might have inclusions, cracks, porosity, voids due to shrinkage as the metal cools, and other types of casting discontinuities. Most welded parts are also castings, with the base metal acting as the mold. A weld can have many of the same types of discontinuities found in cast materials; welds can also contain incomplete fusion, incomplete penetration, burn-throughs or melt-throughs, and other types of discontinuities common to welds. Discontinuities are usually not considered defects until they reach a certain size, although some types, at any size, may not be permitted in a structure.

Various technical societies and government agencies that are responsible for designs and fabrication rules for such structures as boilers, pressure vessels, buildings, pipelines, ships and

aircraft publish acceptance criteria as part of their codes and standards. These acceptance standards typically specify the type and size of discontinuity permitted. They may say "no cracks allowed", or may give the dimensions for a particular type of discontinuity that is permitted, such as "3/32-in.-dia. porosity" or "1/4-in. long slag". Materials containing discontinuities that exceed these allowances must not be used unless they are repaired, if that is possible (e.g., jet-engine turbine blades often cannot be repaired).

A material containing a discontinuity that is not allowed by the applicable standard or code is said to be defective, but in actual fact may or may not be defective. This is because all standards and codes include safety factors. A discontinuity barely exceeding the size that is allowed will probably not be immediately detrimental to the function of the structure, unless for some reason another design consideration is compromised.

However, such discontinuities often become worse. For example, a crack can grow, through a process called fatigue, and reach a critical size, after which it will propagate very quickly. Or other problems may be present, such as corrosion or erosion. These conditions reduce the amount of material available to carry the forces, and increase the stress concentration, as well as continue to propagate discontinuities. Fracture mechanics is the field that evaluates whether a particular discontinuity may be detrimental to a structure based upon expected growth of the flaw, material properties and stresses in the material.

Monitoring process operations

In addition to evaluating materials, NDT can also be used to improve the operation of some processes. The efficiency of distillation and absorption columns depends upon the conditions of the vapours and liquids in the columns at various elevations. To optimize the operation of a column, the process engineer is concerned with the following conditions:

- Tray locations
- Extent and location of flooding
- Liquid levels on the trays
- Extent and location of weeping
- Location of foaming and foam density
- Functioning of mist eliminators
- Downcomer liquid levels

Non-destructive techniques are available to measure many of these variables on-line. Often, operational parameters can be varied during the test to determine the response of the column. In the hands of a process engineer who understands both the principles of the NDT method and the particular process, the results of such an analysis can be a powerful diagnostic tool.

One test of this type is based on the fact that the column walls, trays, packing, liquid, vapour and any foam present will absorb the radiation differently. In this test, a source of radiation is placed on one side of the column and a suitable detector on the other. Both are then raised along the column in unison, creating a density profile of the column and its contents. An analysis of the radiation absorption plot will reveal such problems as flooding, foaming, or missing trays or packing.

Another type of operational problem that can be identified by NDT is a blockage in process piping or a vessel. Such blockages may be due to scale, sludge, or accumulated process material. The blockage results in an increase in the mass of process material present. Radiation transmission techniques are particularly suited to measuring changes in mass (the higher the mass, the less radiation transmitted). Radiation gauges can locate blockages, since areas upstream of a blockage will have a higher mass, and thus lower transmission of X- or gamma-rays, than areas downstream of the blockage. (Source: Chemical Engineering, April 1989, article written by Frank J. Sattler)

8. ACOUSTIC MICROSCOPY IN MATERIALS RESEARCH

Acoustic microscopy is an advanced non-destructive sensor technology capable of revealing subsurface details. At a frequency of about 50 MHz acoustic waves can penetrate several millimeters into a sample, and this ability has given us the power to examine materials in depth.

Advanced materials can provide specialized properties or combinations of properties that cannot be obtained in conventional materials. However, such materials generally require unusual processing operations in order to achieve their unique microstructure and improved properties. These materials also tend to be expensive because of the complicated processing operations required to produce them. Because the relationships between the processing parameters, microstructure and resulting material properties are not always fully understood, and the microstructure is difficult to control, reproducibility in these advanced materials is often unsatisfactory. In order to improve the yield and the reliability of the manufacturing process and detect errors before significant value has been added to the product under fabrication, it thus becomes increasingly important to characterize and control each step of the fabrication process. Ideally, one would like to obtain this information on-line and non-destructively during the process cycle. To do this one requires advanced non-destructive evaluation sensor technology.

Acoustic microscopy is one such advanced non-destructive characterization tool. The unique ability of this technique to visualize subsurface detail beneath opaque layers in a non-destructive manner has led to its application in a wide range of fields from studying the properties of living cells and secreted structures in biological research to the characterization of microelectronic circuits, device packages and thin-film layered structures. Acoustic microscopy facilities have been established in several countries including China, the United States of America, the United Kingdom, Italy, Japan, the Netherlands, South Korea, France and the USSR. Companies as diverse as Digital Equipment (USA), Samsung (South Korea), IBM (USA) and Philips (Netherlands) now have acoustic microscopes in-house. Research activity in Ireland in acoustic microscopy is currently in progress at the National Microelectronics Research Centre in Cork where work is being carried out within the framework of an

ESPRIT II project. The objective of this article is to discuss the technique and outline several typical applications.

The principle of operation of a scanning acoustic microscope (SAM) can be described using the block diagram presented in figure 1. A train of electric pulses is sent from the transmitter to the lens via the circulator. The lens converts this electrical energy into an acoustic beam by means of a piezoelectric transducer which acts alternatively as a transmitter and receiver for the acoustic pulses. The reflections from the object are time dependent and the return acoustic pulse of interest (for example from a specific interface within a layered structure) is sent to the display memory. An image is constructed by scanning the lens in a raster fashion over the sample and recording the reflected signal from each point on/in the sample. For a given lens, the depth of penetration of the acoustic wave into the material depends on the frequency of the wave: the lower the frequency, the greater the depth of penetration. At a frequency of around 50 MHz acoustic waves are able to penetrate several millimetres into a sample. Deionised water is normally used as the coupling fluid between the lens and the sample due to its neglible contamination effect and reasonable acoustic energy transmission coefficient.

Depending on the scanning option chosen (x,y) or z, two different acoustic characterization techniques may be employed. An x,y scan (for a given depth z) yields the standard acoustic microscopy imaging mode of operation while a scan in the z direction yields a quantitative mode via the acoustic material signature of the sample. In the x,y scanning mode, the output signal of the acoustic lens depends directly upon the acoustic reflectance function of the structure and thus upon the mechanical and elastic properties of the sample examined. In the quantitative characterization mode, raster scanning (x,y) is not employed, but the sample is instead translated axially along the lens axis. In this mode the transducer voltage V(z) is periodic as the sample is translated from the focal plane towards the lens. The periodic minima observed are due to the interference of two waves: (a) a reflected axial wave and (b) a leaky surface wave (see figure 2) excited by a wave component obliquely incident on the sample at the Rayleigh critical angle Cr defined by $Cr = Sin^{-1}(Vc/Vr)$ where Vr is the velocity of the leaky surface wave and Vc is the acoustic velocity in the coupling fluid. This interaction gives rise to the so-called Acoustic Material Signature (AMS) or V(z) curve of the sample. This curve is characteristic of the material under investigation. An example of an experimentally recorded AMS for sputtered tungsten on Si(100) is presented in figure 3.

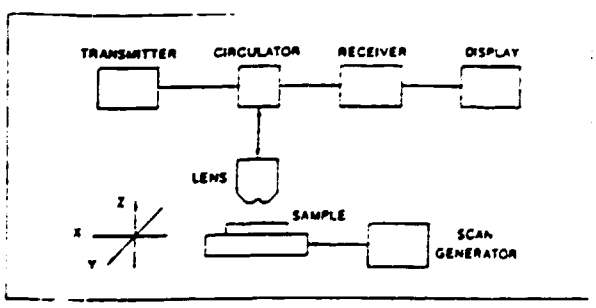

Figure 1. Basic elements of a reflection acoustic lens micro-probe

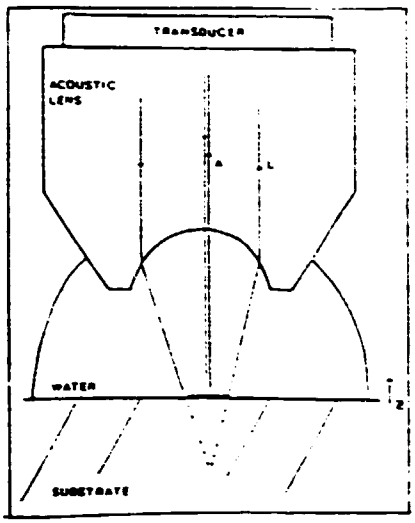

Figure 2. Schematic showing the two acoustic wave components responsible for the generation of the acoustic material signature

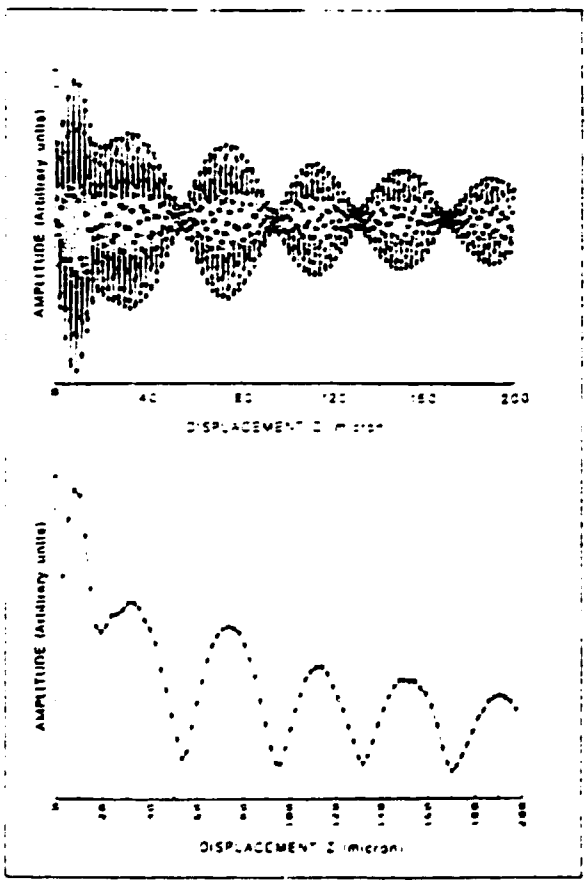

Figure 3. Raw and processed acoustic material signature curves for W/Si(100)

Quantitative analysis is possible due to the fact that the velocity of the leaky surface wave can be directly determined from the spacing Δz between the recorded minima of the AMS using the expression $Vr = Vc / [1-(1-Vc/(2f.\ \Delta z)^2]^{0.5}$ where f is the frequency of operation of the oscillator. Thus through an analysis of the AMS, we can observe and measure quantitatively variations of structural properties such as density and adhesion. This is possible because these structural properties modify the leaky surface wave velocity via their effect on the elastic constants of the sample.

The following sections specifically address the application of the acoustic microscopy techniques described previously to the characterization of microelectronic circuits, device packages and in particular thin-film layered structures. In the area of integrated circuit inspection, much work has already been performed. As the drive towards increased chip denisty continues, semiconductor manufacturers are turning to multiple interconnect levels and vertical structures (an example is the cross-section of a proposed four level metallisation structure shown in figure 4). It thus becomes increasingly important to verify if any interaction between the different layers (e.g. spiking, delamination etc.) has occurred during the process cycle. The analysis can be performed, in a non-destructive manner, uniquely by using acoustic microscopy.

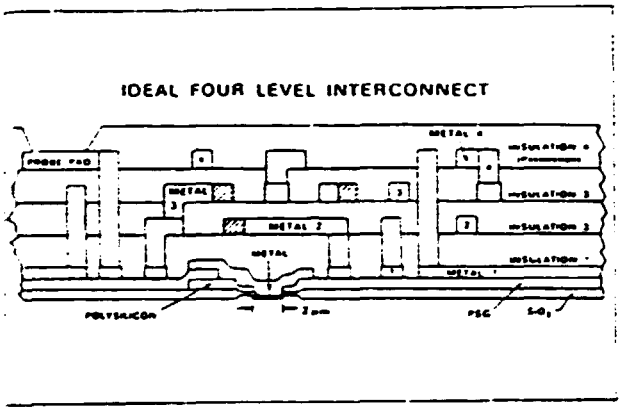

Figure 4. Vertical cross-section of a four-level interconnect structure

Applications reported in the literature include imaging of "pinhole defects" and photoresist inclusions, identification of delamination sites in a 450 nm thick SiO2 passivating layer on an IC test structure, alloying problems and spike defects at the edge of the LOCOS structures. At a higher level of fabrication another series of applications involve imaging of packaging related problems. Typical defects which can be detected include poor bonding between the chip and package, poor sealing of a hermetic package, voids and cracks. It demonstrates the utility of acoustic microscopy imaging for defect detection in silicon integrated circuits and device packages. In comparison with other techniques, the acoustic microscope is sensitive to defects beneath the surface of an opaque material that are inaccessible to optical and electron microscopy methods. Acoustic micrographs are also sensitive to partially cracked or delaminated conductors, defects which functional testing often fails to reveal. In addition the SAM can image dielectrics without the usual problems of charging. It can detect failures in these dielectric layers which often do not immediately manifest themselves in their electronic effects and which are difficult to detect with the scanning electron microscope: for example cracks in dielectrics which if undetected provide pathways for corrosion processes that can lead to eventual circuit failure. Concerning the imaging of semiconductor packages, the acoustic microscope, unlike the X-ray, shadowgraph (which is widely used in industry) is very sensitive to the presence of delaminations and can indicate the depth of a defect relative to other features of the package under examination.

The spectrum of possible applications of acoustic microscopy in a microelectronics research environment is further enlarged if we consider the possibilities offered by analysis of the acoustic material signature curve. One typical example of its application is on-line monitoring of the thickness of sputtered opaque metal conductors. This is an operation that has become important because of the necessity to control rigorously the lithography operations in silicon fabrication laboratories, which in turn demands strict process control of the thickness of the substrate and deposited layers (the thickness of thin films used for ion implantation masking influence manufacturing yields and IC performance; control of photoresist uniformity helps achieve identical die exposures over large diameter wafers). The thickness measurement can be separated into two parts: (a) the recording of the AMS signal and the evaluation of the associated Rayleigh surface wave velocity Vr, and (b) the use of velocity disperson curves to obtain the thickness (h) of the layer corresponding to the experimentally measured Vr. The use of this non-destructive AMS technique avoids the necessity of etching a test wafer to measure the thickness of the deposited opaque film using a mechanical profilometer, in addition it permits on-line rapid measurements to be made, thus enabling the process engineer to take corrective action if the measurement is out of specification, before significant value has been added to the wafer. The AMS method also appears to be a promising probe for the evaluation of the adhesion of thin films and the monitoring of the evolution of the mechanical properties of layers as a function of processing conditions and microstructure.

In conclusion this article has given but a limited view of the potential role for acoustic microscopy techniques applied to materials characterization in semiconductor technology development. However, the techniques are applicable for characterization and process control applications in all areas of materials processing, from the fabrication of steel to superconductors. Industry is becoming aware of the possible improvements in yield and reliability from using such techniques; in particular, those industries which carry out high value-added processing. Further evidence of the growing interest in the technique is reflected in the fact that acoustic microscopy projects have been sponsored by the CEC in both BRITE I and ESPRIT II. The future will find this non-destructive probe as familiar an instrument in both industrial and academic materials science laboratories as the ubiquitous scanning electron microscope. (Source: Technology Ireland, March 1989, article written by Dr. Gabriel Crean)

9. NON-DESTRUCTIVE VOLUMETRIC CT-SCAN EVALUATION OF MONOLITHIC CERAMIC TURBINE COMPONENTS

Introduction

The development of X-ray computed tomographic (CT) imaging for non-destructive evaluation (NDE) of structural ceramic material has been described. These techniques have the potential for mapping short-range (less than 5 mm) and long-range (greater than 5mm) density variations, detecting the sizing high- and low-density inclusions, and detecting and sizing (within limits) cracks in green-state and densified ceramics. CT imaging is capable of interrogating the full volume of a component and is noncontacting. It is also relatively insensitive to part geometry and thus can be used to inspect components with complex shapes such as turbocharged rotors, rotor shrouds, and large individual turbine blades.

This study concentrated on acquisition, quantitative evaluation, and display of CT-scan data in green-state ceramic turbocharger rotors. The work was accomplished using a medical CT imager (Siemens Somatom DR-H).

CT scans have been taken contiguously through green-ceramic objects to reveal their internal structure as a series of slices. If the slices are sufficiently thin (2 mm thickness is typical) and the object being inspected is sufficiently large (e.g., a 15 cm long turbine rotor), a very large number of slices may be produced (75 or more for a single specimen). The analysis of these CT-scan data sets presents a formidable obstacle to efficient interpretation.

Volumetric visualization

An emerging computer graphics technique called "volume visualization" has been applied to the NDE of structural ceramic objects. This technique displays a volume of data, such as a set of CT scans, rather than surfaces or edges of the objects. Traditional computer graphics uses lines or polygonal raster images to approximate the boundaries of an object or other data set. Lines or vectors yield so-called wire-frame representations. Polygons or surface patches in more sophisticated applications give so-called solids models. Volume visualization displays every point in a three-dimensional (3D) volume, without surface or edge approximations. Each point in a volume is called a volume element, or voxel for short. This is a generalization of the common pixel, or picture element.

Traditional computer graphics renders 3D surfaces into two dimensions by projecting them into a plane using standard perspective. The final brightness at a point on the display screen is determined by the brightness or colour of the surface in front of all others at that point. If the surface is partially transparent, then the brightness or colour is an average of all surfaces that show through to the point on the display.

Volume graphics takes the transparency concept one step further. Each voxel in the volume to be displayed is given an intensity value (brightness) or colour and a partial transparency (0-100 per cent). Then the brightness or colour displayed on a screen is the contribution at that point of all voxels lying along the line of sight to that point. If a ray is sent out from the eye, through the display screen, to the volume behind it, then the brightness or colour placed at the intersection point with the screen is an average of the intensities or colours of all voxels intersected by that ray. This averaging is weighted by the transparencies of the intersected voxels. Another way to state this is that all points along the line segment - the viewing rays obtained by the thickness of the object - contribute to the final brightness or colour of the display pixel intersected by the viewing ray. If this object is transparent, then points along other such intersecting line segments may also contribute to the display brightness or colour. The volume visualized may contain anything: gas, fluid, ceramic, binder/plasticizer, inclusions, etc.

Voxels as 3D generalizations of two-dimensional (2D) pixels were first mentioned in the literature in the 1970s, particularly in medical imaging based on CT-scanning devices. A great deal of effort has been expended on extracting surfaces from voxel collections because this was the only way of rendering views of them at that time. In the last several years, imaging techniques have emerged that represent the actual contents of a volume element - not at surfaces or edges, or the surfaces or edges of a connected set of voxels, but in the hardware and software to support those techniques.

The key technological change inspiring volume graphics is sufficient cost-reduction of the memory components to allow volume rasters of memory to be built, into which actual volumes of data can be rendered, as opposed to a 2D projection of a 3D volume into a plane of memory. It is equally important that processors to compute these large memories have also become affordable. One-dimensional display-list processors and calligraphic displays characterize vector graphics, and 2D frame buffers with video raster displays characterize surface graphics. Stereo, motion, and perhaps holography will, in conjunction with volume rasters, characterize volume graphics or volume visualization. Traditional frame buffers will be used in conjunction with newer volume buffers which may, in fact, simply be reconfigured frame buffers of sufficient capacity for volumes.

Much of the mathematical work already done on 3D integer grids is applicable to voxel data sets and can be used as the basis of new volume-graphics approaches.

Classification

Separation of the material types in each CT-scan slice and assignment of a brightness or colour to each voxel in a visualization is termed "classification". The most typical use of classification in conventional image-processing is in remote sensing. For example, Landsat earth-resources imaging is classified with the technique called "multispectral classification". These and similar satellites return data of the same land area as imaged through several different band-pass filters, which together cover the visible spectrum and more. Each pixel is classified by comparing its relative responses in the different spectral bands. This is equivalent to saying that the satellite approximates the spectral reflectance curve of each pixel imaged by an N-part approximation, for N-spectral bands. Then classification proceeds by matching each N-part approximate spectrum with known spectra of materials. If a pixel's approximate spectrum most nearly matches corn, then it is classified as corn

and assigned a colour. If it matches a spectrum of rock, then it is coloured accordingly. The resulting 2D visualization of earth-resources data is called a thematic map. These techniques have been applied to medical image-processing, especially for magnetic resonance imaging.

Pseudocolour has been used a great deal to simplify the interpretation of 2D classification, but many find it objectionable. Medical imaging applications rarely use pseudocolour because pseudocolour often contributes artifacts to the data. In particular, a pseudocolour table without smooth transitions between colours introduces aliasing between the areas of sharply distinct colours.

A generally useful classification technique that works for sampled scaler fields is a pseudocolour table lookup with carefully chosen colour changes. The general problem of classifying voxels in a volume containing multiple materials remains a difficult one.

The turbine rotor CT scans were classified into binder/plasticizer and Si_3N_4 components on a voxel-by-voxel basis according to the classification scheme shown in figure 1. The gray-scale histogram for each CT slice is a summation of the measured alternations for air, binder/plasticizer, and Si_3N_4. These material components may be classified for each voxel according to their respective per cent contribution to the measured alternation at each voxel. The presence of each material in a voxel, expressed as a percentage, may be found by a table lookup using the decision rule (figure 1). As a consequence, a voxel may contain air, binder/plasticizer, Si_3N_4, or some combination. In the overlap region noted in the figure, each voxel will contain fractions of both binder/plasticizer and Si_3N_4, which total 100 per cent. This scheme, originally described for medical imaging, may be extended for simultaneous classification of multiple materials.

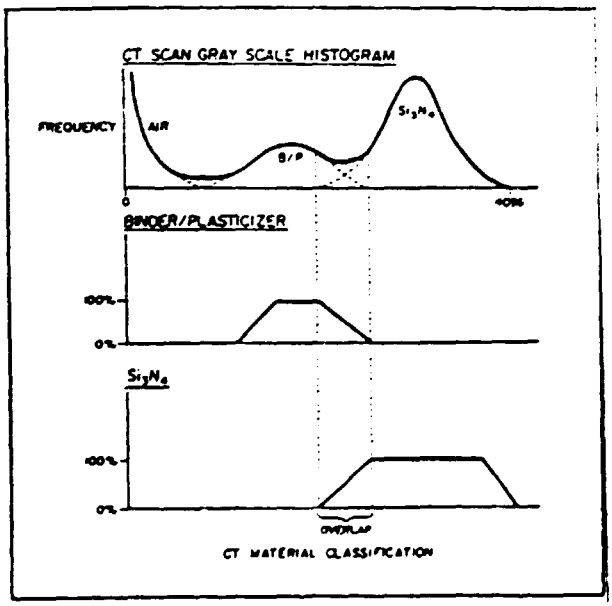

Figure 1. Material classification scheme used for colour and opacity assignments in volumetric-rendering technique

Materials and methods

The authors have recently undertaken the inspection of injection-moulded prototype turbocharger rotors of Si_3N_4, densified by the reaction-bonding process. Green-ceramic turbine rotors were evaluated using a medical CT scanner (Siemens Somatom DR-H). The feasibility of applying medical CT scanners to ceramic components, especially green silicon nitride (Si_3N_4) objects, has been reported. Typical applications include the localization of internal defects, inclusions, voids and inhomogeneities. The potential for quantitative evaluation of density variations and artifacts in these CT-scan data sets has been described elsewhere.

Two green Si_3N_4 ceramic rotors were made available to the Argonne National Laboratory. These two rotors were nominally 5 cm diameter, with shafts 1.4 cm diameter and 11 cm long. Significant differences in the defect contents of these two rotors were found on conventional industrial X-ray images.

Subsequently, the turbine rotors were examined with a digital radiography system, the Philips PCR. CT scans were obtained transaxially with a 512 by 512 matrix in these two components at a zoom of 10, yielding a pixel edge-length of 0.1 mm in the plane of section if 2 mm slice thickness and 1 mm table increments are used. Each slice was obtained in 7 seconds with 125 kVp and 410 mA. A total of 55 scans were required to examine each object. Before CT scanning, the turbine blades were numbered. There are a total of 11 blades in each rotor. Conventional X-radiography demonstrated defects in the turbine rotors, especially between blades 3 and 4.

CT scans were recorded on 2,400 ft (731 m) reels of nine-track 1,600 bpi magnetic tapes by using the standard archive utility program on the CT scanner. These data were input to the PICS-2000 radiology workstations, and sequences of rotating (spinning and tumbling) 3D images were produced.

The PICS-2000 workstation produces images that rotate about the x and y axes. Because the turbine blades were scanned axially, the study was concentrated on producing 3D spin images with rotation about the long axis of the rotors.

Images were reconstructed using surface and shaded volumetric-rendering methods with ceramic opacity set at 100 per cent and binder/plasticizer opacity set at 0 per cent.

Computed radiography

The turbine rotors were radiographed by use of a computed radiology system, the PCR. The PCR is an image-acquisition and processing system for filmless digital static-projection radiography. The system is a fully integrated unit and consists of an image reader, image processor, image recorder, and film-processing system. With the PCR, conventional radiography can be performed digitally, making digital image-processing techniques and digital storage possible.

The turbine rotors were radiographed by placing them on 10 by 12 in. (25 by 30 cm) image-processing (IP) plates in a conventional medical radiography facility with an automatic exposure calculator (Siemens Ionomat) and using 75 kVp X-ray tube accelerating potential. Each IP plate was loaded in

a specially built cassette similar in appearance to the standard film-screen cassette used in conventional medical radiography. The IP plate was coated with an X-ray energy storage phosphor-europium-doped barium fluoride bromide. The plates vary in size from 14 by 17 in. to 8 by 10 in. (36 by 43 cm to 20 by 25 cm), with the smaller sizes producing a higher spatial resolution. The 10 by 12 in cassette produces a pixel size of 0.15 by 0.15 mm.

When exposed to ionizing radiation, the phosphor of the image plates generates a large number of electrons, which are trapped in halogen vacancies (or holes) that exist in the phosphor crystals. This is proportional to the X-ray exposure and represents the latent image of the radiographed turbine blade. These phosphor crystals offer a greater dynamic range than the conventional film-screen combination.

The cassette containing the IP plate is inserted into the image reader of the PCR system. The IP plate is automatically removed and transferred to a reading stage. Here the trapped electrons on the IP plate are stimulated by a helium-neon (He-Ne) laser. The light signals are sampled and converted into a digital image. The digital image is then sent to the image processor, where image-enhancement techniques, such as gray-scale modification and edge enhancement, may be performed. Edge enhancement implemented as a convolution operation was applied to the turbine rotor images.

The image processor subsequently sends the processed digital image to the image recorder, where the image is converted to analog signals. These analog signals are imprinted on a single-emulsion, high-speed, fine-grain film (Fuji CR633), especially developed for use in computed radiology systems with a laser-beam recorder. A conventional wet-film processor is linked to the image recorder by a conveyor belt and the developed film can be obtained in approximately 2 minutes. The internally stored processed image can be displayed on a cathode-ray tube (CRT) console or digitally archieved to an optical disk.

Imaging workstation

A medical-imaging workstation (Philips Medical Systems/Pixar PICS-2000) was used for computer graphics display and reconstruction of the CT-scan data sets. The device consists of a dedicated microcomputer-based host (Sun 3) and computer graphics system (Pixar) with specialized software to produce volumetric visualizations from serial CT scans.

The PICS-2000 system implements volumetric imaging for the production of 3D image sequences. These may be recorded on hard copy or video tape. Volumetric imaging differs from the better known surface-image reconstruction in that internal structures within an object may be seen and that explicit edge or surface detection is not required. In surface rendering, thresholding image segmentation is typically used to detect object surfaces. With volumetric imaging-reconstruction techniques, one may see important features within objects as well as outside.

The PICS-2000 radiology workstation is a raster-based graphics computer that incorporates a Sun 3 160 workstation with a Unix operating system and the Musculoskeletal Software Package (MSP). This device is a joint development of Philips Medical Systems, Inc., and Pixar Corp. The Pixar image computer was originally developed by Lucasfilm for generation of special effects in the movie industry. It has a 1024 by 768 display attached to a 1204 by 4096 frame buffer, 48 bits per pixel (12 bits each red, green, blue and alpha channels), with both colour and monochrome display capabilities. The system disk is a 370-megabyte Fujitsu Eagle. The system configuration includes a Sun 3/180 workstation, with Sun Unix 4.2 BSD, a monochrome Sun text monitor, a Pixar image computer, a tape drive (1/2 in., nine-track 1,600 bpi), a video cassette recorder (standard NTSC compatible VHS), an NTSC RGB to composite video encoder, and Matrix Instruments model 4007 multiformat camera.

In the volumetric-imaging technique, each pixel from the reconstruction image will contain a fractional contribution of every material, such as ceramic, binder and air, encountered within the object. Volumetric imaging as implemented on our system uses CT density ranges and not thresholds to identify materials. Thresholds are used for materials classification to define ranges of CT densities that are characteristic of different materials such as ceramic, binder/plasticizer, or air.

A simple volume editor is implemented in the workstation. This facility allows the operator to specify a rectangular solid subregion within the volume to be displayed - all other components are invisible. Using this editor, it is possible to inspect part of a volume without display of either obscuring or overlapping adjacent structures. The image volume is edited manually using the optical mouse on the Sun 3 host computer by adjusting a region of interest on frontal and axial radiographic localization images that were precomputed from the volume.

Volumetric-rendering techniques

The system software implements volumetric imaging for production of 3D image sequences. These sequences consisting of 4-65 images in each set, may be displayed in real time, giving a spinning or tumbling appearance, and are recorded on hard copy or videotape. Volume imaging differs from better known surface imaging in that internal structures within an object contribute to the pictures and explicit edge or surface detection is not performed. In surface-rendering, thresholding is used to make a view of the surface of an object. Using volumetric imaging-reconstruction techniques, one can see important features within the object as well as outside. Each pixel will have a portion of every material, such as ceramic, binder, and air, encountered in the object. Three rendering methods are implemented in this system, shaded, volume and surface.

Shaded

"Shaded" reconstruction and rendering techniques generate surface views of objects contained in a sampled data volume, such as a set of contiguous CT slices. The 3D images produced are similar in many respects to those created by most surface-reconstruction imaging software operating on medical CT scanners or dedicated 3D imaging consoles. These images are similar to the "surface" images described below except that small surface details are enhanced by using gradient shading.

Shading refers to a process in which a simulated light source illuminates the object from an offscreen location. The effect is rather striking subjectively and adds considerable apparent detail, depth, and surface texture to the image.

Volume

Volume-rendering generates transparent views by computing ray sums through the sampled volume and projecting them onto the plane of a CRT display. The opacity of the volume image is based on the density values expressed as Hounsfield numbers in the CT scans. In the volume-rendering algorithm, each voxel contributes to the final image instead of only those on the sampled object's surface. For instance, when looking at a frontal view of an object, in this case a turbine rotor, each pixel in the displayed image will contain the sum of CT density values for ceramic, binder/plasticizer, or inclusions and any other material contained along rays that traverse the volume from a simulated viewing direction and intersect the plane of the CRT display screen.

This is the fastest of the volumetric-rendering methods because the algorithm involves almost a direct mapping of local CT density values according to final brightness, colour and opacity.

Surface

Surface images portray only the internal surfaces of objects being rendered and are used to give a depth-encoded view of the threshold-detected surface of the volumes under observation. The surface images are made by detecting the surface using the magnitude of the gradient produced with a simulated light source from voxel to voxel - not the direction, as do the shaded reconstruction images.

The computation of surfaces from CT volume data requires about four times longer than computation of the equivalent volume-type images.

Results

Newer digital radiographic techniques were applied to the inspection of complex ceramic components and verification of the CT volumetric 3D reconstructions with an image-receptor containing a photostimulable phosphor, used in place of film. Digital radiographic images of the two green Si_3N_4 turbine rotors were produced and have been used for comparison with CT scans and 3D reconstructions.

The shaded-rendering method produced gradient shaded views of the outer surface of the turbine blade and reproduced it as a solid object; consequently, no inner features were seen. Because of the complex blade curvature, artifacts were produced in the CT scans which appeared on the volumetric image reconstructions. These artifacts were seen as holes in the shaft at the bladed portion. The image editor was used to select only the base of the blade where defects were sought. The artifacts produced by the curved blade disappeared but the edited image still did not demonstrate the defect.

The surface-rendering method was then used to create visualization sequences. Images were reconstructed using a ceramic opacity of 50 per cent and a binder plasticizer opacity of 25 per cent. This created a transparent view of the turbine blade surface. A slight density was noted at the base of the blade, but it was unclear what it was. The image editor was used to select only the base of the blade. In retrospect, this enabled a slightly better view of the defect, but the defect was still obscured by a portion of the blades.

After the defect was plainly demonstrated on the edited image, the two previous surface images were reviewed. This time, the defect was obvious. In the nondefective turbine rotor, no serious artifacts or abnormalities were encountered. This was demonstrated on video tape recordings and still images.

This study serves to demonstrate the ability of computed tomography and 3D volumetric visualization to detect and display internal abnormalities in complex ceramic turbine components. The advantages of volumetric visualization for NDE include enhanced display capabilities for complex image data sets for improved localization and a means of illustrating NDE imaging test results.

The computer graphics workstation that performs the computations needed to produce these 3D image sequences currently costs more than $100,000. Advances in computer graphics technology will cause the cost of this functionality to decrease rapidly, and widespread use of these methods for many applications is anticipated in the future. (Extracted from Materials Evaluation 47, April 1989, American Society for Nondestructive Testing, Columbus, OH, USA. Reprinted with permission.)

10. COMPOSITE STIFFENER INSPECTION USING REDIRECTED LONGITUDINAL WAVES

Problem

Advanced composite materials have become important engineering materials in the modern aerospace industry. Their high performance characteristics and low weight make them ideal for aerospace applications. To further enhance performance, composite structures are often formed into C channels or include co-cured stiffeners that are T-, J-, and I-shaped. Although these stiffening methods differ in shape, they all possess a common feature of short vertical blades or flanges attached perpendicular to the skin (main body) of the structure. Figure 1 is an example of a C channel stiffened in a second direction by co-cured T stiffeners.

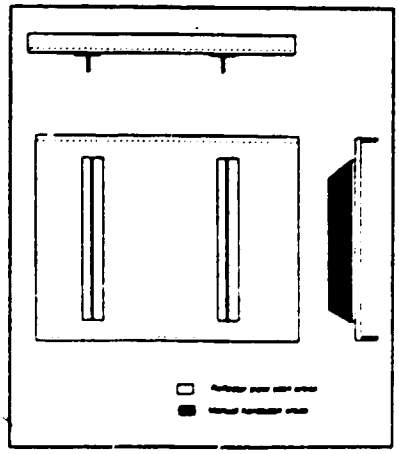

Figure 1. T-stiffened C channel

To verify structural integrity of composite structures, ultrasonic testing is commonly used. Automated ultrasonic techniques typically use immersion tanks or squirter systems to scan parts and display results in C-scan format. These methods are excellent for high-speed inspection of the large, relatively flat portions of composite structures but are not efficient for inspection of the stiffeners.

Some stiffeners can be inspected using the vertical axis in an immersion tank, but the setup to scan these relatively small areas can be time-consuming and difficult. Also, inspection of the entire stiffener may be obstructed by the size of the manipulator. For older immersion tanks without a vertical axis, parts must be stood on end - a process that is impractical in many cases.

An alternative inspection method is manual hand-scanning, which requires additional equipment and typically does not produce a permanent record. In general, there has been no simple way to make immersion C-scans of these angled structures.

Solution

A simple solution to this dilemma is depicted in figure 2. With a simple piece of angle stock, stiffeners can be scanned in an immersion tank by using transverse and longitudinal motion control and redirected longitudinal waves. By placing a 45° angle adjacent to the stiffener, the incoming L-wave is reflected 90° to strike the stiffener at normal incidence. The horizontal travel of the transducer is converted to an equivalent amount of vertical motion at the stiffener. If setup is correct, the stiffener can be scanned with a simple rectilinear scan pattern at normal incidence and constant water-path distance to the stiffener. If the reflecting surface is sufficiently smooth, energy loss will be minimal, and the stiffener can be inspected with the same basic technique used to inspect the skin.

A graphite-epoxy T-stiffened panel containing numerous Teflon® inserts as small as 0.25 in. (6.3 mm) was used for a test scan.

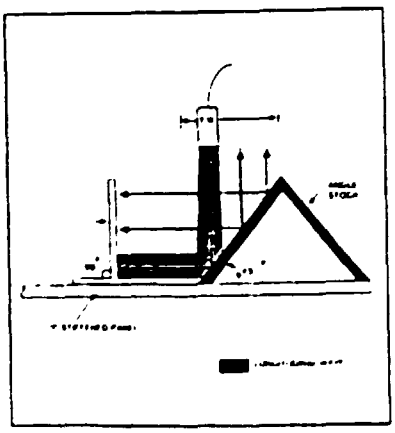

Figure 2. Composite stiffener inspection using redirected longitudinal waves

Conclusions

It is evident from the test scan that this technique can be effective for T stiffener blades or other similar stiffener configurations. By placing a 45° reflector adjacent to a stiffener and scanning normally, an undistorted and accurate permanent record is obtainable without additional equipment or part manipulations.

Some simple rules to consider are as follows: the height of the angle stock should be at least half the transducer diameter higher than the stiffener to ensure complete coverage; reflecting surface(s) should be as smooth as possible to minimize energy losses; and the long axis of the reflector must be parallel to the stiffener. Following these general guidelines makes it possible to inspect a variety of stiffener types as effectively as it would be to scan them directly.

This simple method is for inspecting stiffener configurations that are of uniform thickness and perpendicular to the skin. Although more complex stiffener configurations were not considered here, they too can be inspected with variations of this technique by applying a little ingenuity and a lot of common sense. (Source: Materials Evaluation, 47, April 1989, American Society for Nondestructive Testing, Columbus, OH, USA. Reprinted with permission.)

11. CURRENT AWARENESS

New devices, systems and their applications

METALS AND ALLOYS

Temperature-compensated conductivity monitor
(K. J. Law Engineers, Inc., Farmington Hills, MI, USA)

The Verimet M4900TC-I is a non-destructive production-speed instrument for testing aluminium, aluminium/lithium alloys, copper, bronze, and other non-ferrous metals at temperatures up to 400°F (204°C). The instrument uses eddy current principles to sort for alloy and temper, proper heat treatment, or hardness of ingots, casting, forgings, sheet stock, and processed parts. It features automatic temperature compensation, adjustable reject limits, and both digital and high-speed analogue output.

Conductivity measurements are adjusted automatically for temperature variation. Instrument accuracy is ± 0.5 per cent of the International Annealed Copper Standard when calibrated with standards or ± 1.0 per cent without standards. The system permits probe-to-part lift-off distances up to 0.025 in. (0.06 cm) for high-speed, non-contact measurements, sorting, or process control. (Source: Materials Evaluation/47, February 1989, Copyright 1989, American Society for Non-destructive Testing, Columbus, Ohio, USA. Reprinted with permission.)

• • • • •

Beta-backscatter thickness tester (CMI International, Elk Grove Village, IL, USA)

The Beta-Min 1700 beta-backscatter thickness-measurement system operates with any standard beta-probe system. The tabletop unit measures accurately the plating and coating thickness of gold, silver, palladium, tin-lead, tin-lead composition, and other precious metals. Three standard calibration techniques are offered, and measurements are given in microinches, mils, micrometers, angstroms, percentage composition, and counts per minute. Data are entered by pushing a button on the 24-character alphanumeric light-emitting diode display, eliminating the need for special key markings. Ten non-volatile storage locations allow quick entry of testing information, such as coating/base, probe type, aperture, and beta source. The system's storage capacity permits recalibration in seconds.

The unit's AG-1 probe guide, with its built-in magnifier, permits precise positioning of the beta probe, allowing accurate measurements of plating and coating thickness on printed circuit boards, of gold tabs, and of fine lines. (Source: Materials Evaluation/47, February 1989, Copyright 1989, American Society for Non-destructive Testing, Columbus, Ohio, USA. Reprinted with permission.)

* * * * *

A non-contact, non-destructive sensor system for online output of thin-film ceramic coatings on metals is being examined at the National Institute of Standards & Technology. The technique uses photothermal radiometry to monitor the surface uniformity of materials, exposing flaws and measuring the thermal resistance of ceramics applied to metal substrates. (Source: Metalweek, 26 September 1988)

* * * * *

Ultrasonic wall-thickness measuring instrument (Elcometer, Inc., Troy, MI, USA)

The Elcometer 202 hand-held, battery-powered ultrasonic wall-thickness measuring gauge is suited for use on steel structures. The instrument's design principle makes accuracy possible in measuring the effects of corrosion and erosion on wall thickness where only one surface is accessible. It has been pre-calibrated for steel, with no calibration controls to be adjusted, although materials such as aluminium, brass, copper, iron, and nickel can be measured with the conversion tables provided with the instrument.

The Elcometer 202 is available in either imperial or metric versions, and readings are displayed in either inches or millimetres. Digital circuitry and light-emitting diodes offer a clear, stable display. The unit is enclosed in an aluminium case with a wrist strap, making it suitable for on-site use. (Source: Materials Evaluation/47, February 1989, Copyright 1989, American Society for Non-destructive Testing, Columbus, Ohio, USA. Reprinted with permission.)

* * * * *

Hand-held tesla meter (F. W. Bell, Orlando, Fl, USA)

The Model 4048 gauss/tesla meter is suitable for magnetic field measurement during tests for the integrity of castings and weldments. Other applications including testing and sorting magnets, testing direct and alternating current motors, and loudspeaker testing.

The Model 4048 reads magnetic fields from 0.1 G to 20 kG (0.01 mT to 2T) with a resolution of 0.1 G (0.01 mT). (Source: Materials Evaluation/47, 1989, Copyright 1989, American Society for Non-destructive Testing, Columbus, Ohio, USA. Reprinted with permission.)

* * * * *

CERAMICS

Non-destructive strength measuring method for ceramics

A research group headed by Prof. H. Yanagida, Department of Industrial Chemistry, Faculty of Engineering, the University of Tokyo, has designed a method for measuring the mechanical strength of brittle materials such as ceramics by means of alternate evaluation of their electrical strength (dielectric strength). Prof. H. Yanagida and his associates discovered that when the distribution of mechanical and dielectric strength of a material is statistically studied, a clear interrelation exists between the two distributions. They have succeeded in demonstrating statistical distribution of mechanical strength without executing bending tests. In the past to evaluate the strength of a brittle material, many test pieces had to be subjected to bending tests. This new method saves waste of test pieces and greatly streamlines evaluation.

It is difficult to evaluate the mechanical strength of brittle ceramics and other like materials from their appearance as opposed to metal materials. Defective metals have visible flaws and their strength can be determined to a certain degree. In the case of brittle materials, as flaws are minute, measuring less than 100 microns, it is impossible to determine the strength visually.

Prof. H. Yanagida and his associates believed that there must be an interrelation between mechanical breakdown and dielectric breakdown because both are a breakdown phenomenon. They confirmed this by experiments.

Experiments were conducted using three kinds of thick ceramic films (200 microns thick) including barium titanate. In the first place, a three-point bending test was conducted to apply force to samples for the measurement of the mechanical strength of the materials. A direct electrical field was applied to an unstressed portion of the materials and dielectric breakdown was caused to measure their dielectric strength. After numerous tests, mechanical strength and dielectric strength were separately statistically treated by the Weibull statistical method.

In Weibull statistics, a strength distribution produces a rising straight line. The distribution of mechanical strength and that of dielectric strength were obtained separately and combined on the same graph. It was found that both distributions occupied nearly the same straight line.

If a dielectric strength test is made using one or two test pieces, alternate evaluation can be made of their mechanical strength. Detailed studies are

under consideration to clarify reasons for the interrelation between mechanical strength and dielectric strength. (Department of Industrial Chemistry, Faculty of Engineering, University of Tokyo 3-1, Hongo 7-chome, Bunkyo-ku, Tokyo) (Source: JETRO, November 1988)

* * * * *

COMPOSITES

RAJ Technology's (Morton Grove, IL) new method to test advanced composites non-destructively will soon be marketed industrially. The Insight-1000 acoustography method reportedly can expose such usual flaws as delaminations, inclusions, impact damage and porosity in graphite-epoxy composite laminates. Insight-1000 reportedly also offers the possible ability to supply real-time observation of damage growth during loading. RAJ said a full-field image is revealed in seconds. A "shadow" cast by a test piece struck by an ultrasound beam is transformed into a visual image via an acousto-optical display. A video camera shows the acousto-graphic image produced on the display and sends it as a video image to a capture board. This then digitizes the video image that is stored in the computer's memory and can be shown on a monitor. (Source: Metalweek News, 26 September 1988)

* * * * *

Fibre-to-resin ratio determination (The Expert System Technologies, Inc., San Diego, CA, USA)

The URA 2000 ultrasonic instrument determines precise fibre-to-resin ratios in composite materials, replacing destructive chemical analyses such as acid digestion, burnoff, and solvent wash.

A feature of the URA 2000 is its mapping capability, allowing manufacturers and researchers to analyse every inch of a composite material. A map is generated that shows variations in resin content across the surface of a part. Researchers are able to correlate the physical properties of the material with the mechanical behaviour of the part. A better understanding of this correlation allows designers to reduce design margins, thus enabling manufacturers to produce light, reliable parts and high-performance aircraft, rockets, satellites, and missiles.

The URA 2000 technology is being custom-developed for on-line, real-time monitoring as a statistical process-control tool. Fiberite Composite Materials recently completed a 90-day field trial of this instrument. (Source: Materials Evaluation/47, April 1989, Copyright 1989, American Society for Non-destructive Testing, Columbus, Ohio, USA. Reprinted with permission.)

* * * * *

Ultrasonic inspection systems (Custom Machine, Inc., Cleveland, OH, USA)

Model CM is part of a new generation of ultrasonic inspection systems for rapid inspection of a wide range of shapes and sizes of composite parts, computerized with the latest in data-acquisition packages and high-resolution colour graphics. The system is customized to the user's needs and sized to accommodate the parts to be inspected. The system may be squirter, immersion, reflector plate, or a combination of these types.

The Model CM is a combination squirter/immersion system with six pairs of squirters operating simultaneously, significantly reducing inspection time per composite panel. It also includes two long search-tube universal manipulators that can operate in any axis or plane (horizontal, vertical, inclined, compound inclined, and contoured) for inspection of standard or complex parts profiles. Contoured and ribbed panels can also be inspected. Ribs may be simple vertical webs or I-beam configuration.

Other options include recorders, precision readouts, multiple transducer manipulators, turntables, bar rotators, and part holding and conveying fixtures. (Source: Materials Evaluation/47, April 1989, Copyright 1989, American Society for Non-destructive Testing, Columbus, Ohio, USA. Reprinted with permission.)

Data-Acquisition system (Qualcorp Aerospace Systems, Staveley NDT Technologies, Bethel, CT, USA)

The US-980 data-acquisition system interfaces with a central computer so that much of the testing process is automated. The US-980's INTEL and IBM computers can analyse a part while acquiring data. Diferent modules can be used, depending on the testing need.

Data are acquired on a tape or optical disk, making possible the storing of information from manufacture to retirement of the equipment. A disk or tape distributed with the equipment can be used for comparisons during each subsequent inspection, so the life history of the part is maintained electronically. The system has both immediate display and manipulation and delayed display. It can also be used to plot a cathode-ray tube display.

The US-980 is used to acquire data from the top-of-the-line digital systems and from instruments such as the Qualcorp QC2000, which is used in aerospace applications to test carbon fibre-reinforced composite materials. (Source: Materials Evaluation/47, April 1989, Copyright 1989, American Society for Non-destructive Testing, Columbus, Ohio, USA. Reprinted with permission.)

* * * * *

Thermography (Inframetrics, Inc., No. Billerica, MA, USA)

Infrared radiometer systems see flaws in composite materials by temperature differences as small as 0.5°C transmitted to the surface. High-resolution thermal images in black-and-white or colour spot delamination, honeycomb flaws, and bonding. Model 445, for qualitative analysis only, delivers 445 real infrared lines for the highest black-and-white resolution available. Model 600, for measurement, gives 200 real infrared lines (400 interlaced) in colour or black-and-white and features built-in image processing and a host of absolute temperature capabilities. Special image-processing software provides engineers with everything needed for thermal decay (time vs. temperature) studies. (Source: Materials Evaluation/47, April 1989, Copyright 1989, American Society for Non-destructive Testing, Columbus, Ohio, USA. Reprinted with permission.)

* * * * *

PLASTICS

Ultrasonic flaw location slide

Edison Welding Institute, Colombus, OH, USA, offers the Mark II ultrasonic flaw location slide. This slide is a low-cost aid for plotting the size and location of flaws during ultrasonic testing of welded joints and is made of lightweight, sturdy, wipe-clean plastic. Readings for flaw range and associated probe standoff distance made during testing are rapidly transferred to the slide. The slide provides an accurate plot of flaw location and size within the weld cross-section. Each slide comes complete with a beam-plotting card and a protective plastic wallet. (Source: Materials Evaluation/47, March 1989, Copyright 1989, American Society for Non-destructive Testing, Columbus, Ohio, USA. Reprinted with permission.)

* * * * *

Dielectric analysis (Du Pont Co., Wilmington, DE, USA)

The Model 2970 dielectric analyser (DEA) is a thermal analysis instrument giving insight into the nature and behaviour of polymeric materials. It measures the chemical and rheological properties of a material as it is subjected to an electrical field. This produces quantitative data enabling the user to determine the capacitive and conductive nature of materials, characterize molecular relaxations, and monitor the flow and cure of resins.

A specialized sensor system, wider temperature, frequency ranges, and sophisticated software provide information on the chemistry, rheology, and molecular mobility of materials such as elastomers, thermoplastics, adhesives and coatings, and composites. This information is helpful in identifying the material's chemical structure and correlating it with processing behaviour and end-use performance. (Source: Materials Evaluation 47, April 1989, Copyright 1989, American Society for Non-destructive Testing, Columbus, Ohio, USA. Reprinted with permission.)

* * * * *

APPLICATIONS

Ultrasonic flaw detector (Hitachi Construction Machinery Co., Ltd., Tokyo, Japan)

The UT2000 and DT2000 portable ultrasonic flaw detectors make high-resolution measurements possible in a variety of applications. Both instruments are compact and feature built-in printers and sheet-type keypads for simple data entry.

The UT2000 makes measurements within the frequency range of 0.4 to 10 MHz and with the temperature range of 0°-45°C. Other features include a cathode-ray-tube screen and a liquid-crystal display with backlight illumination. Programming and data are stored on the unit s software cassette.

The UT2000 makes measurements within the frequency range of 0.2-15 MHz, and measures ambient temperatures from -10° to 45°C. Its features include rotary gain knob and cursor position knobs, adjustable gate and cursor widths, and simultaneous display of all recalibration values. Once recalibration values are set, a lock mechanism ensures measurement accuracy by preventing other keys from being pushed. (Source: Materials Evaluation/47, February 1989, Copyright 1989, American Society for Non-destructive Testing, Columbus, Ohio, USA. Reprinted with permission.)

* * * * *

Ultrasonic Pulser Receiver

Accu-Tron Inc., Millis, MA, USA, has made available the Model 1035 PR ultrasonic pulser receiver. Designed for ultrasonic testing material analysis, and industrial and medical research applications, this product is packaged in a stand-alone enclosure, uses a fast rise-time spike pulser, and has a receiver section featuring switchable 20 and 40 dB gain settings. The standard model provides signal attenuation adjustment in 2 dB steps from 0 to 68 dB; Model 1035PR-HR offers 1 dB steps over a range of 50 dB.

The ultrasonic pulser receiver is fully compatible with commercial oscilloscopes and transducers. Applications include ultrasonic flaw detection and thickness gauging, ultrasonic transducer and characterization, and research. (Source: Materials Evaluation/47, March 1989, Copyright 1989, American Society for Non-destructive Testing, Columbus, Ohio, USA. Reprinted with permission.)

* * * * *

Non-destructive testing with impulse radar

Years of pioneering work in radar systems technology by ERA has led to the successful development of a commercial impulse radar system for non-destructive testing.

The system includes a transmitter-receiver, associated antenna systems (transducers) and software for a broad range of surface and sub-surface applications.

Conventional techniques such as ultrasonics used for examining the structure of roads, bridges, buildings and earth materials, have limitations for detecting areas within the material where anomalies exist.

ERA's decision to produce its own impulse radar system follows a period in which the company's technical expertise has been sought by a number of large organizations needing to establish the feasibility of the technique for their specific requirements. These included: testing for defects in man-made structures; detecting buried objects such as pipes and cables; security applications; and assessing geological strata, particularly in borehole applications. The ERA system, which is under progressive development, is based on the detection of back-scattered impulses of microwave energy from features within the material being tested.

The next stage of development is planned to be a real-time signal processor unit for fast survey operation, capable of processing and displaying a colour image at the rate of one measurement every 200 mm at a survey speed of 50 kph.

This new technology has already been assessed as part of the first stage of a collaborative programme on the use of radar techniques for "strata prediction" for DTI's "Advanced Robotics for Tunnelling Initiative".

ERA's technical lead in the development of a commercially viable impulse radar system is paving the way for the application of this technology to routine non-destructive testing in a variety of industries. (Source: ERA Technology News, Cleeve Road, Leatherhead, Surrey KT22 7SA, UK)

Non-destructive PCB current test

An outstanding piece of electronics design has resulted in a non-destructive method of current measurement in a PCB track. An instrument based on the technique will measure current in the range 1 mA to 1 A without breaking a track or lifting a component leg as demanded by conventional measurement methods.

The Track Current Meter, designed by the small British company Laplace Instruments, uses a combination of special measurement probes, chopping differential amplification and current nulling to determine current flow irrespective of conductor thickness.

The meter comprises two basic circuit sections: a highly sensitive DC amplifier measuring the voltage drop along a section of PCB track due to the current flowing in the conductor under test; a reference current generator controlled by the output of the DC amplifier which injects a current of a magnitude and direction sufficient to cancel out exactly the voltage drop measured in the conductor. The instrument provides a readout of the mirror current which is equal and opposite to the current flowing in the track.

While the operating principle is as simple as it is novel, the measurement of DC potentials in the microvolt range has required some ingenuity on the part of the designer, David Mawdsley. The instrument requires twin contact electrode probes. An inner spring-loaded point measures potential while an outer fixed point provides the current injection. Successful measurement also requires a combination of polarity chopping followed by an averaging circuit. It is worth noting that the instrument allows equipment under test to remain fully operational and that current measurements are unaffected by current flowing in adjacent tracks. (Source: Electronics & Wireless World, July 1989)

* * * * *

Ultraviolet lamp (Spectronics Corp., Westbury, NY, USA)

The Spectroline® BIB-120 self-contained ultraviolet (UV) lamp is lightweight (2.5 lb [1.1 kg]) and versatile with an external transformer unit that produces high-intensity UV light and meets all specifications for fluorescent and red dye penetrant testing.

Suitable for MT, ultraviolet curing, leak detection, and other industrial applications, the BIB-120 uses a 120 w built-in ballast bulb. The device is available with a choice of two bulbs: concentrated spot or broad-beam spot. It features the Bulb-Saver™ (patent pending), which extends bulb life by reducing breakage due to shock damage.

The tough, dependable lamp head is housed in rugged aluminium with a special-tempered, crack-resistant filter that reduces replacement cost. It can be ordered with a standard 8 ft (2.4 m) power cord, an optional 20 ft (6.1 m) cord, or a 30 ft (9.1 m) retractable cord on a reel. (Source: Materials Evaluation/47, March 1989, Copyright 1989, American Society for Non-destructive Testing, Columbus, Ohio, USA. Reprinted with permission.)

* * * * *

Magnetic particle inspection system (Magnaflux, Chigaco, IL, USA)

A fully automated, user-friendly MT system for 155 mm projectiles provides fast and consistent part preparation, thus simplifying the inspection process. Parts are inspected after each part of a two-stage procedure - a coil process followed by a central conductor process. The coil station consists of two in-line coils with pole pieces in the centre to "control" the magnetic field path and find discontinuities in a circumferential direction. The central conductor processing station consists of a pair of air-cylinder-operated copper conductors which, when extended, pass through the inside diameter of the part. The magnetic field generated in the circular direction reveals longitudinal and radial discontinuities.

Automatic processing circuitry includes a current assurance feature with problem diagnosis assuring all parts are properly processed. A processing rate of 200 parts per hour should be readily attained. (Source: Materials Evaluation/47, March 1989, Copyright 1989, American Society for Non-destructive Testing, Columbus, Ohio USA. Reprinted with permission.)

Horizontal wet magnetic particle test benches (Penn Central Group, Auburn, Australia)

The Models 1571 and 1580 Lectroflux horizontal wet MT benches have applications in aerospace industries for the inspection of critical components and in general industry for quality assurance.

Features include low-voltage control circuits, solid-state controls, silicon rectifiers, digital amp meters for set and actual current, a separate oil-filled power pack for silent operation, dry sump operation for ease of cleaning, a heavy-duty stainless-steel tank, an ergonomically designed control panel with finger-tip control and light-illuminated function, and electric control that regulates accurately the magnetizing current to the predetermined value, especially important for small components. (Source: Materials Evaluation/47, March 1989, Copyright 1989, American Society for Non-destructive Testing, Columbus, Ohio, USA. Reprinted with permission.)

MISCELLANEOUS

Computerized ultrasonic inspection system

Krautkramer Branson, Lewistown, PA, USA, has announced a custom-computerized version of its KB 6000 ultrasonic testing and data-acquisition unit. The KB 6000PC system combines the KB 6000 with a specially designed software control system to provide increased materials inspection capabilities.

In addition to testing versatility and quality, the KB 6000PC increases quantity of inspection capability. Multichannel operation is as easy as single-channel. An unlimited number of test setups may be programmed and stored for instant recall, enabling fast, repeatable changeover from one test to another. One or more A-scans may be selected for presentation simultaneously. (Source: Materials Evaluation/47, March 1989, Copyright 1989, American Society for Non-destructive Testing, Columbus, Ohio, USA. Reprinted with permission.)

Ultrasonic flaw detector

The RG 21 ultrasonic flaw detection system from Gilardoni, Mandello Lario (Como), Italy, incorporates a large-screen monitor and a transmitter with a large spectrum and high-energy output for best excitation. The system offers two presetting possibilities: distance-amplitude correction and constant level. The damping control is adjustable from 25 to 1,000 Ω, with a default of 50 Ω.

The RG 21 can be powered from an outlet or by rechargeable batteries. Options include a software package for inspection of V-shaped welds and a plug-in device that calculates ultrasonic path for flaw location. (Source: Materials Evaluation/47, March 1989, Copyright 1989, American Society for Non-destructive Testing, Columbus, Ohio, USA. Reprinted with permission.)

* * * * *

Digital coating thickness gauge

Zorelco, Cleveland, OH, USA, has made available Model 717N, digital coating-thickness gauge for measuring dry, non-conductive coatings such as anodizing, paint, plastic, varnish, epoxy, glass fibre, porcelain enamel, etc., when applied to or placed on a non-ferrous substrate such as aluminium, brass, copper, etc. The constant-pressure measuring probe assures uniform contact pressure on flat, square, or round objects in any position. Options include nickel-cadmium battery, charger, and carrying case. A μm scale is available. (Source: Materials Evaluation/47, March 1989, Copyright 1989, American Society for Non-destructive Testing, Columbus, Ohio, USA. Reprinted with permission.)

* * * * *

Pinhole detector

Zorelco, Cleveland, OH, USA, has made available the 369/PHD and 370/PHD pinhole detectors for detecting pinholes, porosity, cracks, and flaws in thin, non-conductive coatings such as paint, plastic, asphalt, and varnish when applied to any conductive substrate. The 369 conforms to ASTM G6 specifications. The 370 conforms to NACE TM-03-84. Both are available in multiselectable and fixed voltage ranges. They operate on rechargeable nickel-cadmium batteries. (Source: Materials Evaluation/47, March 1989, Copyright 1989, American Society for Non-destructive Testing, Columbus, Ohio, USA. Reprinted with permission.)

* * * * *

Stress analysis system (Ometron, Herndon, VA, USA)

The Spate 9000 non-contact stress analyser is a modular system built around a unique scan unit that can detect stress changes down to 60 psi (414 kPa) for aluminium, with a spatial resolution as fine as 0.02 in. (0.5 mm). The system will work on almost any material, including metal, plastic, bone, human tissue, and composite materials such as graphite-epoxy, metal matrix, and ceramics.

The scan unit produces stress data by detecting the minute temperature changes resulting from the application of cyclic loading. Additionally, the system comprises an electronics console and dedicated software for data acquisition, processing, and display. This user-friendly system includes applications for design, durability testing, quality assurance, and research and development. Impact damage, delaminations, and the growth of damage due to fatigue can be measured.

A vibration measurement system can be added to the Spate 9000 scan unit to allow both stress and vibration data to be produced from the same experimental setup. (Source: Materials Evaluation/47, Copyright 1989, American Society for Non-destructive Testing, Columbus, Ohio, USA. Reprinted with permission.)

12. MARKETING

The first Brazilian patent in the field of non-destructive tests is granted

A new method to determine "in loco" the depth of surface cracks in metallic parts has been developed by COSIPA-Companhia Siderúrgica Paulista - and is now available in the market through a patent licence contract signed with Met-L-Chek do Brasil Indústria e Comércio Ltda, awarding exclusive rights for production and trade, in Brazil, of the instrument which enables its application.

The new method, with wide industrial utilization in non-destructive tests, mainly at production and maintenance phases of metallic parts, consists of a standard pentagonal shaped notched steel block (Pe) used for calibrating and gauging conventional ultrasound equipment, enabling it to determine the depth of surface cracks "in loco" through surface waves (Rayleigh).

Its practicability affords many advantages, especially in the area of industrial maintenance, reducing costs and time to solve problems of this nature when requiring ultrasound tests, since this is the only model which makes possible this test "in loco". Previously such a test was limited to laboratories, requiring the part or the equipment to be removed.

This situation, experienced by all professionals dealing with non-destructive tests, motivated COSIPA's technicians to promote research that led to the development of this new method. In order to accomplish it, it became essential to control the calibration of the surface wave. After overcoming the theoretical step the method was applied to several models of blocks, leading to the development of the ideal shape, the standard pentagonal shaped notched steel block (Pe), that permits calibration of conventional ultrasound equipment and to verify the surface wave behaviour. Laboratory tests were performed and further results were obtained in field tests that proved satisfactory, thus promoting the elaboration of this method, now patented by the company. (Source: Metalurgia Internacional, Vol. 1, No. 4, December 1988)

* * * * *

Materials research capabilities at Ocean Engineering Centre

The analysis and design of structures requires information regarding the various properties of the structural materials. With the latest advances in materials technology it is now possible to choose a material with the required properties or even to formulate a material for such specific properties. The materials research in the Ocean Engineering Centre is directed primarily to understand the behaviour of structural materials or composites in severe environments like the oceans. The facilities are specially designed to study both the short-term and long-term effects of the various Environments. Suitable accelerated and non-destructive tests have been formulated so that the various parameters controlling the behaviour of the structures can be established. The various activities are presented hereunder:

Concrete technology: Design and Development of Concretes for Special Applications; Mechanical, Physical and Chemical characteristics of Concrete; Shrinkage, Creep, Fatigue and Fracture parameters; Permeability, Porosity, Diffusion, Resistivity and Micro-structure; and Non-Destructive Testing.

Durability of Materials - Deterioration in Aggressive Environments like Oceans; Chemical Attack; Abrasion; Accelerated Testing and Long-Term Durability and Additional Non-Destructive Testing.

Corrosion - Corrosion of Structural Steels and Reinforcements in Concrete; Potential and Polarization Characteristics; and Corrosion Control.

The Laboratory also concentrates on the Development of Concretes with Admixtures; Polymer Concrete Composites (pc, pcc and pic); Ferrocement and Fibre-Reinforced Concretes. Based on the above experience it has also been active in the Evaluation of Damage in Structures; Relevant Repair Methodologies; and Specifications for Materials Specific to Particular Repairs. (Source: Research and Consultancy at Indian Institute of Technology, Madras, India)

13. PUBLICATIONS

Non-destructive testing

Krautkramer Branson, USA, has released a six-page, four-colour bulletin, number TG-310, on its DR 1 portable thickness Data Recorder for non-destructive testing. It describes the features of the unit and its use as a storage and management system.

* * * * *

Non-destructive testing volume

Fifteen research papers delivered at the Chicago Winter Annual Meeting of the American Society of Mechanical Engineers have been collected by J. L. Rose and A. A. Tseng into a volume called New Directions in the Nondestructive Evaluation of Advanced Materials.

More than half the papers deal with some form of ultrasonic evaluation applied to a range of materials, including ceramics, composites, and different types of bonds and joints. Other methodologies presented by the academic and industry researchers include neutron diffraction, micro-radiography and tomography, and accoustography.

The 110-page paper-bound volume, designated MD-Vol. 9, is available from ASME (New York City).

* * * * *

ASTM, Philadelphia, PA, has made available Testing Technology of Metal Matrix Composites (STP 964), ed. Di-Giovanni and Adsit, containing 28 peer-reviewed papers covering material systems from the continuous silicon carbon/titanium system to the particulate reinforced aluminium system. Material forms included range from precast block to braided pieces. Published in September 1988, the collection (472 pp) focuses on the need to obtain accurate and reliable test data. Current testing methodologies are defined and described, including elevated temperature tests, dynamic modulus tests, coefficient of expansion tests, and compression and buckling tests. The book is intended for composites researchers and designers, aerospace engineers, and materials scientists.

* * * * *

Report on non-destructive testing

A report on non-destructive testing (NDT) has been made available from World Business Publications Ltd., London, UK. The report (170 pp) describes the state of the art of the principal NDT techniques, reviews current research and development activities within companies, examines applications, and analyses the world market for NDT equipment. A directory of research laboratories, corporations, and associations involved in NDT is featured in the appendix. The report was prepared by Techtrends, Paris, France, in October 1988.

* * * * *

The second edition of the Handbook of Metal Treatments and Testing, by R. B. Ross, has been released by Routledge, Chapman, and Hall, New York, NY. The book (hardcover, 568 pp) is divided into three parts. Part One includes brief definitions and descriptions of metal treatment processes and techniques, arranged alphabetically. Part Two gives detailed information on blasting, electroplating, hardness testing, heat treatment, mechanical testing, non-destructive testing, painting, and welding. Part Three includes tables for identification and comparison of the processes discussed. Part Four is an appendix section providing standard physical data for ease of reference. Nine appendices provide useful information, including conversion tables for strength, hardness and tensile values, and gravity. A list of companies involved in metal treatments and testing is also featured. The purpose of this text is to provide engineers with detailed information about the treatment and testing of metals.

* * * * *

Electronics Reliability and Measurement Technology: Non-destructive Evaluation, ed. J. S. Heyman, is available from Noyes Data Corp, Park Ridge, NJ. The anthology (hardcover, 128 pp) examines electronics reliability and measurement technology and identifies advances in measurement

science and technology for non-destructive testing. The book is based on a workshop held at NASA Langley Research Centre, Hampton, VA, in 1986. Papers on specific topics are grouped within the book's 13 chapters. Several illustrations, photographs, graphs, and tables are included.

* * * * *

Adhesively Bonded Joints: Testing, Analysis, and Design (STP 981), ed. W. S. Johnson, is offered by ASTM, Philadelphia, PA. The collection (320 pp) features 21 peer-reviewed papers giving information about the mechanical behaviour of adhesives. The focus is on aircraft and naval applications, which are primarily concerned with bonding composite/metallic components. Techniques and specimen designs for determining tensile, shear, and mixed-mode properties of adhesives are discussed in the book's section on mechanical testing. Papers on stress analysis include both analytical and experimental methods to analyse the stress state in an adhesively bonded joint. A section on failure mechanism is included, and design and durability are discussed in the final section. The book is intended for use by aerospace and automotive designers and engineers, composite researchers, and adhesive manufacturers.

* * * * *

Ultrasonic Transducers for Non-destructive Testing. M. G. Silk, Bristol, UK: Adam Hilger Ltd., 1984. XIV, 162. Hardcover.

This book is a review of the theories and techniques used in designing and understanding ultrasonic transducers used for non-destructive testing (NDT).

The brief introduction into the basic considerations of wave modes and their application to NDT leads quickly into the nature of piezoelectric materials and their formulations. The common piezoelectric materials used for ultrasonic transducers are covered, including single crystal materials and ferroelectric cameras. Polymer materials such as polyvinylidene fluoride (PVDF) are discussed, and the less traditional wave-generation techniques based on electromagnetic-acoustic transducers and laser-generation and laser-reception techniques are covered late in the book.

* * * * *

Proceedings of the 12th World Conference on Non-destructive Testing - Amsterdam April 1989

The World Congress and Exhibition on Non-destructive Testing, which takes place every third year, was held in Holland during the last week of April 1989.

Steel applications

The sessions on applications in the steel industry reviewed developments in on-line inspection systems.

Automatic inspection of steel plate

The experience gained using on-line ultra-sonic inspection of wide heavy plate at AG der Sillinger Huttenwerk, FRG, since 1981 was described. Plate up to 4.8 m wide and 5 mm thick receives 100 per cent surface examination on an automatic line. Particular attention is paid to the edge regions as it is here that the most critical properties are required for welding. A 96 head probe is located below the roller table level, as are all the components of the inspection system, in order to avoid possible damage to the inspection equipment and also to maintain a clear top area for crane operations.

To improve sensitivity, small wide-beam probes are used each containing one transmitter and three receivers. Cleaned industrial water is used as the couplant and the probes can operate at temperatures up to 100°C.

Using the automatic inspection system has increased inspection from 30 per cent of total production achieved manually to 100 per cent today. Availability of the automatic system has proved excellent with a normal three-shift day being maintained.

The annual throughput of plate corresponds to examining an area of 660 acres each year.

Current developments include a prototype classification system known as Augur which aims to replace subjective manual decisions with objective machine functions. This is achieved by processing the ultrasonic amplitude and transit time signals by computer.

The basic inspection system is already operating at a number of plate mills throughout the world.

Development of an automatic eddy current rail tester

A system in operation at NKK's Fukuyama works is used to examine the head and base of railway rail during manufacture using an eddy current technique. The system is sensitive enough to detect cracks down to 0.5 mm in width, 0.4 mm deep and 30 mm long while the rail is travelling at up to 1 m/s. A total of 24 probes are used, eight of which are rotating (figure 1). These rotating probes assist in detecting cracks in the moving rail. A gap of 1 mm ± 0.3 must be maintained between the rail and the probes during examination. In practice, the tolerance achieved is better than ± 0.1 mm.

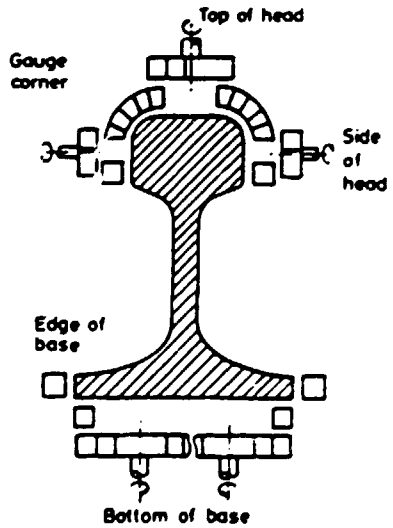

Figure 1. All areas of the rail except the web are examined on-line using 24 eddy current probes, some of which are rotating

The main advantages of the system are claimed to be that 100 per cent of all rails produced are inspected and that both longitudinal and transverse cracks can be detected

Automatic optical inspection of strip in a cold mill

An optical inspection system for steel strip installed at Sollac's Ste Agathe cold mill has been developed in joint collaboration with the Institut de Recherches de la Siderurgie Française (IRSID).

CCD line cameras and real-time digital signal processing enable strip to be examined at line speeds of up to 6 m/s. Signal processing allows pattern recognition to be achieved to enable classification of defects.

The inspection unit is installed on a linked pickling-cold rolling line immediately after the pickling line. An accumulator ensures a constant speed of strip as it passes the cameras. The 100 per cent examination achieved is valuable in maintaining continuous production as it enables hot rolling defects to be detected before they enter the cold rolling mill where they can result in damage to the rolls or a break in the strip feed. Folds, shelling holes and roll marks can all be detected by the cameras and action taken before they enter the cold mill. Both sides of the strip are inspected over their full width which can be up to 1.8 m wide.

To prevent image blur, a frame time of less than 400 μ s is used. If a defect is detected the image is stored and frozen for classification. Currently, classification is still at the development stage and is carried out off-line, but a prototype on-line system is being developed.

Alternating field leakage flux crack detection

Black, hot rolled products are difficult to examine for cracks because of the coating of scale present. The use of a high-power alternating-field leakage flux has been developed at the Institut Dr. Förster, FRG to examine black bar and seamless tubes.

The material to be tested passes through a high energy alternating field (figure 2) resulting in an induced magnetic field limited to the surface region of the bar or tube. 100 per cent examination of the surface is achieved by rotating the field yokes and sample. The presence of a crack distorts the field and this distortion is detected by a probe. Since an AC field is used, no residual magnetism results.

Cracks as shallow as 0.1 mm can now be detected. This is an improvement over earlier methods and has been achieved by ensuring complete magnetic saturation within the region examined and by limiting the sensor probe size to reduce the depth of penetration of its field. In this way, the signal-to-noise ratio is considerably improved.

Testing hot CC strand using eddy currents at Thyssen

A pilot eddy-current testing facility has been installed at Thyssen Stahl AG, Duisburg and is being jointly developed with AEG, Berlin. The system operates on the top surface of hot continuously cast

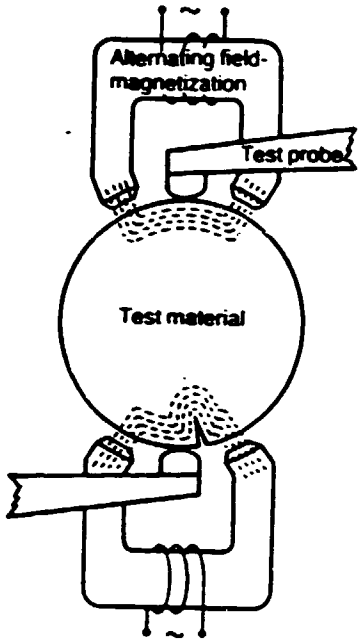

Figure 2- A high-energy alternating magnetic field saturates the surface regions of black bar or tube during its on-line inspection for surface cracks.

steel, above its Curie temperature. Flaws greater than 1 mm in depth can be detected, and the depth of those up to 6 mm recorded. The entire upper surface of the cast slab is examined using 10 probes each of which oscillates over 250 mm to enable the full surface to be covered. The probes can be parked in a safe position while casting dimensions are changed, or dummy bar passed.

Each of the 10 sensors consists of a crack detection sensor and a distance measuring sensor. The distance measuring sensor provides continuous automatic adjustment to the crack detection sensor support to ensure that it is kept at a constant distance from the slab surface.

Good discrimination is obtained between crack detection and surface irregularities, in particular casting oscillation marks, by electronic evaluation of the output signal and phase-sensitive rectification. The output analogue signals are digitized and relayed to a computer for processing and recording. The region where a crack is detected is automatically marked with an aluminium paint spray.

The surface of the slab is descaled using high-pressure water jets. Occasionally spurious results occur probably because of the presence of some remaining ferromagnetic scale. Likewise, the temperature at the slab edges sometimes drops below the Curie temperature resulting in invalid signals.

Correlation between crack depth measured using the automatic on-line device and determined on cold slab by grinding is high with about 80 per cent of the crack depths being correctly recorded by the automatic system.

Published proceedings

All oral presentations are available in a two volume hardback publication. Poster presentations, however, are not included. The Proceedings, edited by J. Boogaard and G. van Dijk, entitled Non-destructive testing (ISBN 0-444-87450 X) are published by Elsevier Science Publishers, P.O. Box 1991, 1000 BZ Amsterdam and costs Dfl 675 (approximately $193) inclusive of postage. (Extracted from Steel Times, June 1989, Vol. 217, No. 6)

14. MEETINGS

25-28 September 1989 Tallinn, USSR	EUROMECH 256: Non-destructive 3-D Experimental Stress Analysis (Institute of Cybernetics, Estonian Academy of Sciences, Akadeemia TEE 21, 200108 Tallinn, Estonia, USSR)
20-22 March 1990 Birmingham, UK	Engineering Integrity through Testing (Sponsor: Engineering Integrity Society, British Industry for Non-destructive Testing) (Contact: UKAEA, Springfields Northern Research Labs, Salwick, Preston PR 4 ORQ, UK)
October 1990 Japan	Non-destructive Testing (Sanpo Publication, Inc., Daiko Bldg, 2 Kanda-Hirakawacho, Chiyoda-ku, Tokyo 101, Japan)

Previous Issues

Issue No. 1	Steel
Issue No. 2	New Ceramics
Issue No. 3	Fibre Optics
Issue No. 4	Powder Metallurgy
Issue No. 5	Composites
Issue No. 6	Plastics
Issue No. 7	Aluminium Alloys
Issue No. 8	Materials Testing and Quality Control
Issue No. 9	Solar Cells Materials
Issue No. 10	Space-related Materials
Issue No. 11	High Temperature Superconductive Materials
Issue No. 12	Cutting Tools
Issue No. 13	Materials for Food Packaging, Storage and Transportation
Issue No. 14	Industrial Sensors

UNITED NATIONS INDUSTRIAL DEVELOPMENT ORGANIZATION

Price List for Advertisements in the Publication

Advances in Materials Technology: MONITOR

General provisions

1. UNIDO activities in the field of advertising are non-profit-making and are carried out to cover the cost of preparing, publishing and mailing its publications, which are sent to readers all over the world *free of charge*.

2. Requests for placing advertisements in the UNIDO *Advances in Materials Technology: Monitor* should be made in writing. They should be accompanied by a layout, illustrations and a text containing all necessary information.

3. Advertisements are printed in black and white and in English only.

4. UNIDO reserves the right to reject advertisements without giving reasons, to suggest amendments or to hold advertisements if space is not available.

5. UNIDO cannot guarantee to print advertisements on specific pages of the *Monitor*. Page proofs will not be provided to advertisers.

6. Payment of invoices is due immediately after receipt and should be made within 30 days in United States dollars or Austrian schillings to the UNIDO bank account (see below) or to the Treasurer, UNIDO, Vienna International Centre, P.O. Box 300, A-1400 Vienna, Austria (telegrams: UNIDO Vienna Austria; telex: 135612). Upon payment, please advise the Head, Development and Transfer of Technology Division, at the same address.

Bank accounts

For dollar payments:

"UNIDO dollar account" No. 29-05115
Creditanstalt Bankverein
Schottengasse 6, A-1010 Vienna, Austria

"UNIDO general account" No. 949-2-416434
The Chase Manhattan Bank
International Agencies Banking
380 Madison Avenue, New York, New York 10017
United States of America

For schilling payments:

"UNIDO schilling account" No. 29-05107
Creditanstalt Bankverein
Schottengasse 6, A-1010 Vienna, Austria

Prices

Size	Prices in Austrian schillings (AS) (or equivalent in US$)
Full page (255 mm × 178 mm)	AS 5,000
½ page (125 mm × 178 mm or 255 mm × 86 mm)	AS 3,700
¼ page (178 mm × 60 mm or 125 mm × 86 mm)	AS 2,500

The price for the publication of announcements of up to five lines under the rubric "Resources available" is AS 1,000. The text is subject to editing.

Resources available

Know-how, designs and licences offered to manufacture drilling machines for water wells of up to 2.5-m diameter and 80-m depth and for concrete-injected piles of up to 2-m diameter and 45-m depth. Claude Bourg, Drill-France, B.P. 15, Le Haillan 33160, France.

Know-how available to manufacture synthetic ceramic from mineral wastes, sand and a binding synthetic resin for use as sanitary ware, material for furniture, decorative items etc. L. Valette, Administrateur Gerant, Science, 98 avenue de Tervueren, 1040 Brussels, Belgium.

Manufacturers of various metal powders offer know-how for the production of electrolytic copper and iron powder, atomized aluminium powder and synthetic iron oxide. R. Devroy, Radar International, Post box No. 2014, Calcutta 700 001, India.

Technical know-how and complete turnkey plants available for the production of mono-crystalline and poly-crystalline solar photovoltaic cells and modules and integration of systems, such as photovoltaic powered pumping, refrigeration, communication and water purification systems. N. R. Jayaraman, Vice-President, TPK International Inc., 36 Bentley Avenue, Nepean, Ontario K2E 6T8, Canada.

Technology and licensing available for manufacturing polyurethane from saturated polyester polyols, polyether polyols, isocyanate intermediates, one- and two-component polyurethane systems. Capacity tailored to requirements, from 2,000 tonnes upwards. Application: flexible, semi-rigid polyurethane foams, industrial and domestic appliance insulation, shoe soling, coating and sealants. Synthesia Inter AG, Tigerbergstr. 2, CH-9000 St. Gallen, Switzerland.

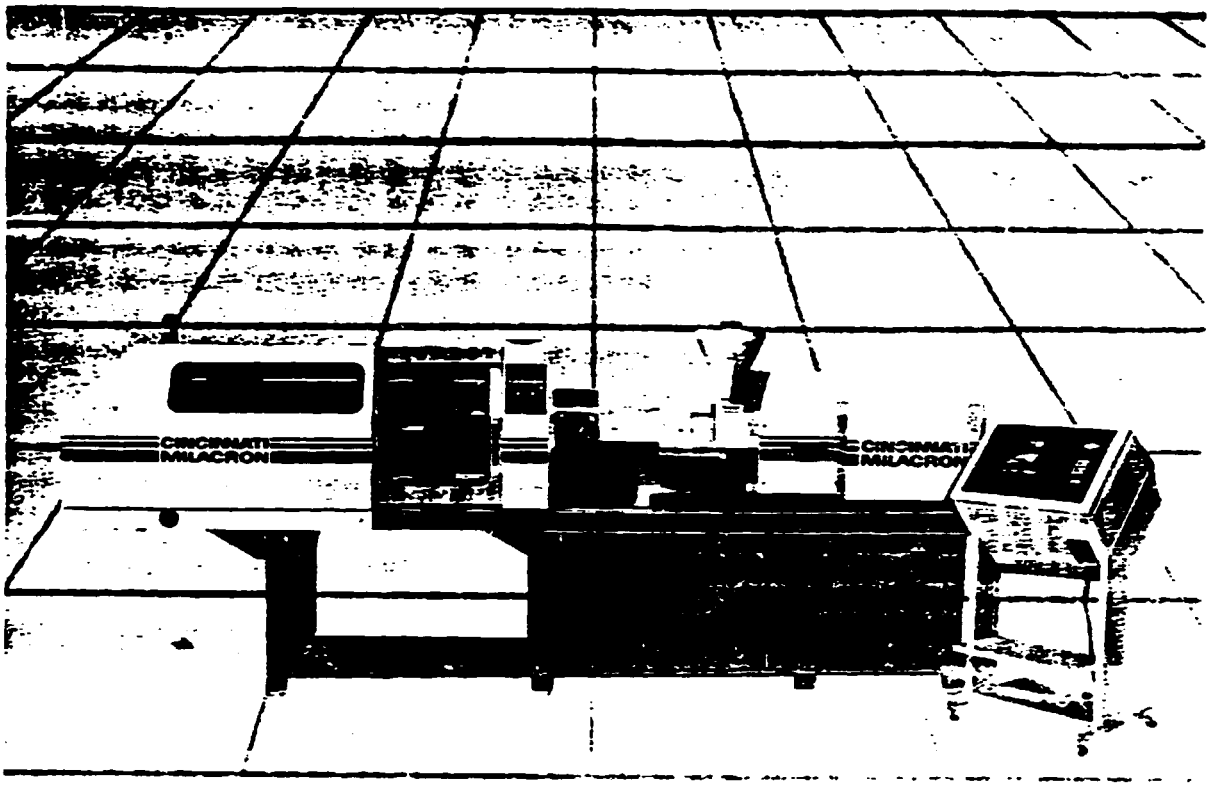

Fully electronic plastic injection molding machines "ACT" provide versatile, high-precision molding.

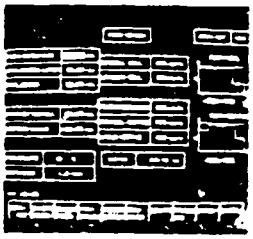

All "ACT" models come equipped with advanced CNC controllers as well as AC servo motors. Fast, easy setting of parameters using a versatile 14" colour graphic CRT. Without need for setting limit switches, valves and other mechanical adjustment. All molding parameters are recalled within seconds from the built-in memory. With additional external memory, capacity can be expended up to 240 molds. CNC controllers and AC servo motors provide high precision molding.

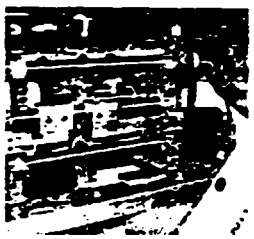

The "ACT" clamping unit features a double toggle design. It ensures high speed and repeatability. An AC servo motor is also used in the ejector mechanism. Programming from CRT, number of strokes, ejector speed and stamp position provides maximum flexibility. Each AC servo motor operates with a precision of 0.01 mm for each movement and also during movement. All AC servo motors are maintenance free and carbon brushes are not required.

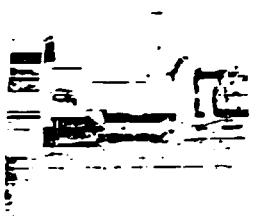

The ACT's come ned use of power fu AC servo motors and digital ba screw, barrel, and ejector control of injection screw positions and injection speeds. The ACT's extra-heavy duty AC servo motor features torque characteristics ideally suited to the injection molding machine's operation cycle. It provides full torque even in the lower speed range. In addition a pressure sensor is mounted at the base of the screw to provide pressure control accuracy.

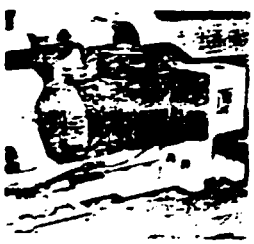

The AC servo motors, at rest in the off-cycle, eliminate energy loss due to friction, other needless, and only to the extent needed. They thereby result in a significant saving in energy. Overall, the use of AC servo motors and digital control in the ACT's also helps to achieve stable, molded products are kept free of ... and the work environment is kept extra clean. All "ACT" models from 150 t up to 3300 t, with direct drive by AC servo motor make for extremely quiet operation and a clean, pleasant work environment that [illegible] can appreciate.

Cincinnati Milacron Austria AG
[illegible]

Deutsche Niederlassung und technisches Zentrum
[illegible]

CINCINNATI
MILACRON

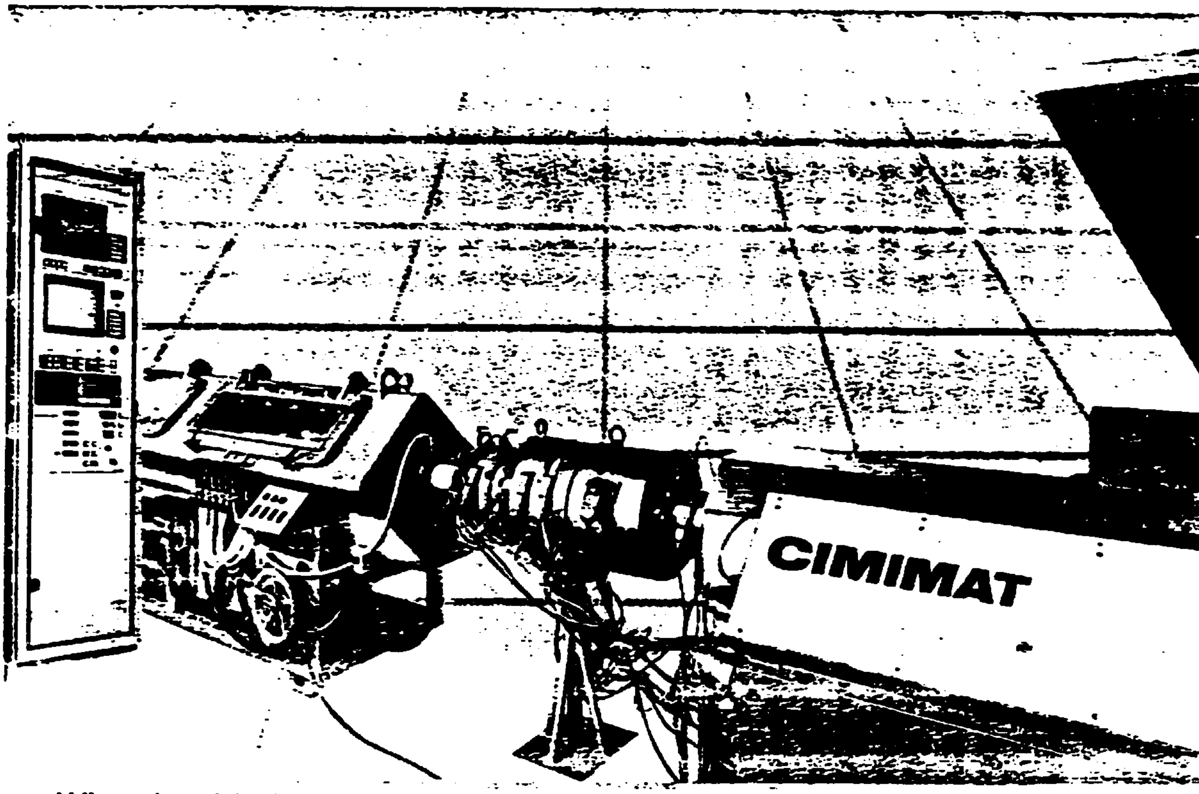

Why should pipe producers consider the new automatic pipe plant "CIMIMAT"?

Because:

This feature yields wall thick-

CIMIMAT is meant to increase the efficiency of your operation and helps you to reduce raw material costs ... at the same time producing better quality ...

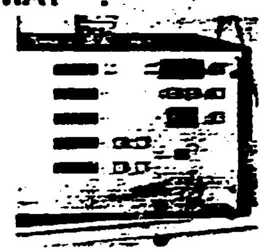

Because:

fluctuations in different raw material compounds.

The new weighing system SAVEOMAT controls the precise material consumption of the extruder. When employed ... the SAVEOMAT system makes for controlling haul-off speed so as to reach constant meter weights. And when employed in a CIMIMAT pipe line, the data acquired are used for automatic gauging in ultrasonic wall ... measuring.

Because:

sion line CIMIMAT is equipped with the thermal pipe centering system CIMICENT.

This is replacing a complicated and mechanically sensitive die-head construction.

The thermal pipe centering system CIMICENT works fault-free and is able to centralise thin or thick areas by equalising opposing sides.

With CIMIMAT you'll have an advantage in the very competitive pipe market.

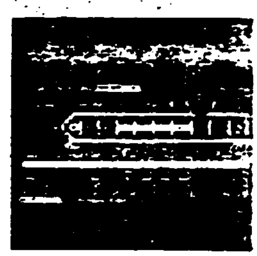

Because:

CIMIMAT means reliability to you.

Microprocessor control CIMICRON 9/16 guarantees pipe production within closest tolerances and it warrants moreover that once optimized process parameters are reliably reproducible.

Only the automatic pipe plant CIMIMAT from CINCINNATI MILACRON AUSTRIA offers you the combined advantages of the thermal pipe centering system CIMICENT and of automatic gauging of the wall thickness measuring.

Cincinnati Milacron Austria AG

Cincinnati Milacron U.K.

Finding better ways to more profit

CINCINNATI MILACRON AUSTRIA

UNITED NATIONS INDUSTRIAL DEVELOPMENT ORGANIZATION
Vienna International Centre, P.O. Box 300,
A-1400 Vienna, Austria

Advances in Materials Technology: Monitor Reader Survey

The Advances in Materials Technology: Monitor has now been published since 1983. Although its mailing list is continuously updated as new requests for inclusion are received and changes of address are made as soon as notifications of such changes are received, I would be grateful if readers could reconfirm their interest in receiving this newsletter. Kindly, therefore, answer the questions below and mail this form to: The Editor, Advances in Materials Technology: Monitor, UNIDO Technology Programme at the above address.

Computer access number of mailing list (see address label):

Name:

Position/title:

Address:

Do you wish to continue receiving issues of the Advances in Materials Technology: Monitor?

Is the present address as indicated on the address label correct?

How many issues of this newsletter have you read?

Optional

Which section in the Monitor is of particular interest to you?

Which additional subjects would you suggest be included?

Would you like to see any sections deleted?

Have you access to some/most of the journals from which the information contained in the Monitor is drawn?

Is your copy of the Monitor passed on to friends/colleagues etc.?

Please make any other comments or suggestions for improving the quality and usefulness of this newsletter.

FOR NEW SUBSCRIBERS:

Request for ADVANCES IN MATERIALS TECHNOLOGY: MONITOR

If you would like to receive issues of the Advances in Materials Technology: Monitor in the future, please complete the form below and return it to.

UNITED NATIONS NATIONS UNIES

UNIDO MAILING LIST QUESTIONNAIRE

Advances in Materials Technology: Monitor
(Code: 504)

	Type or print clearly (one letter per box) and leave a space between each word
NAME (underline family name)	
TITLE OR POSITION	
ORGANIZATION	
STREET AND No. (or P.O. Box)	
CITY AND STATE OR PROVINCE	
COUNTRY	

PLEASE DO NOT WRITE IN THESE SPACES

S/A	DISP. CODE	COUNTRY
CITY		

Readers' comments

We should appreciate it if readers could take the time to tell us in this space what they think of the 15th issue of Advances in Materials Technology: Monitor. Comments on the usefulness of the information and the way it has been organized will help us in preparing future issues of the Monitor. We thank you for your co-operation and look forward to hearing from you.